PROBABILISTIC RISK ASSESSMENT TOOL APPLIED IN FACILITY LAYOUT OPTIMIZATION

A Thesis

by

CASSIO BRUNORO AHUMADA

Submitted to the Office of Graduate and Professional Studies of
Texas A&M University
in partial fulfillment of the requirements for the degree of

MASTER OF SCIENCE

Chair of Committee,	M. Sam Mannan
Committee Members,	Mahmoud El-Halwagi
	Cesar O. Malave
Head of Department,	M. Nazmul Karim

August 2016

Major Subject: Chemical Engineering

ABSTRACT

The severity of several chemical incidents occurred in the recent past has been attributed to improper layout arrangement or proximity of a chemical facility to a densely populated area although this is not a new problem. To address this problem, researchers have been considering not just economic efficacy but also safety features in layout optimization. Therefore, there is still a need for a comprehensive risk assessment methodology in combination with the layout optimization formulation. Moreover, risk probability distributions should be employed to enhance understanding of overall risks and to support decision making during the design phase. The objective of this study is to incorporate a probabilistic risk assessment into the design optimization formulation. The methodology was divided in three main parts.

First, a risk assessment program has been developed in MATLAB to estimate risks associated with human life losses and structural damage in a chemical plant. Analytical models for fire and explosion scenarios and toxic chemical releases were included in the program. Monte Carlo simulation was then employed to propagate uncertainties attributed to environemtal conditions and release paramenters. The proposed program generates risk maps and risk distributions at a particular point of interest in a timely manner.

Second, domino effect concepts have been included in the resulting program to obtain minimal separation distances between process units necessary to prevent escalation events. These distances vary according the targeted unit type, escalation vector (overpressure or fire impigement) and the risk acceptability criteria.

In the last stage, risk maps and safety distances are included in a mixed-integer linear programming (MILP) for layout optimization. The objective function is set to minimize the total capital cost associated with structural damage risk, fatality risk, pipeline interconnection, and protective devices. Individual risk criteria was applied as an additional constraint for high occupancy buildings, meaning that the overall risk for buildings such as control room or lab may not exceed this criterion.

The proposed methodology has been demonstrated through a case study. It enhanced flexibility during the layout arrangement allowing the user not just include site-specific data but also the risk acceptance criteria, which reflects the company's safety culture.

DEDICATION

To my loved ones who make my life longer and meaningful

ACKNOWLEDGEMENTS

I would like to acknowledge my gratitude to many people who have supported me during the last two years. I was very lucky to find wonderful persons who have made my journey much more enjoyable and excited.

First of all, I would like to thank my advisor, Dr. M. Sam Mannan, for accepting me as a master's student. I am very proud of being part of the Mary Kay O'Connor Process Safety Center. The great atmosphere he has built at the Center was vital for me to complete this research. I also would like to thank my committee members, Dr. Mahmoud El-Halwagi, and Dr. Cesar O. Malave, for spending their time to serve on my committee.

Within the Center, I need to thank my team leader Dr. Noor Quddus for helping me out during all stages of my research, starting from the definition of the problem statement until the revision of my thesis. I also want to thank all the staff, especially Ms. Valerie Green, for the hard work taking a good care of us, and keeping the Center running

Thanks also to my friends for making my time at Texas A&M University an unforgettable experience. I hope our friendship last for many more years. I also want to extend gratitude to my sponsor the Coordination for the Improvement of Higher Education Personnel (CAPES) for providing me financial support to accomplish a dream.

Finally, thanks to all my family, especially my mother and sister, for always believing in me even when I question myself. I also want to thank my lovely girlfriend for encouraging me and being by my side every time I needed her support.

NOMENCLATURE

API	American Petroleum Institute
BLEVE	Boiling Liquid Expanding Vapor Explosion
BM	Britter and McQuaid Model
CCPS	Center of Chemical Process Safety
CFD	Computational Fluid Dynamics
DEGADIS	Dense Gas Dispersion Model
EPA	Environmental Protection Agency
GIS	Geographic Information Systems
GPM	Gaussian Passive Model
HSE	Health and Safety Executive
ISD	Inherently Safer Design
LFL	Lower Flammability Limit
LNG	Liquefied Natural Gas
LOC	Loss of Containment
MCE	Most Credible Events
MILP	Mixed-integer Linear Programming
MINLP	Mixed-integer Non-linear Programming
OGP	International Association of Oil & Gas Producers
OSHA	Occupational Safety and Health Administration
QRA	Quantitative Risk Analysis

RAC	Risk Acceptance Criteria
SD	Safety Distance
TC	Total Cost
TDC	Total Damage Cost
TNO	Netherlands Organization for Applied Scientific Research
TNT	Trinitrotoluene
UFL	Upper Flammability Limit
VCE	Vapor Cloud Explosion

TABLE OF CONTENTS

Page

Page

LIST OF FIGURES

Page

Page

LIST OF TABLES

Page

1. INTRODUCTION

1.1 Motivation

Facility siting and layout configuration are critical factors in the design and the expansion of an industrial installation. Determination of the relative position of units or process equipment is a complex task that requires a systematic analysis, which accounts not only economic efficiency but also other aspects such as operability, sustainability, and safety. In addition to the maintenance costs minimization, "optimal facility and layout" can build inherently safer designs and, consequently, reduce the "risk of losses" during plant operation [1].

During the last decades, there have been several chemical incidents of which severity can be attributed to improper layout arrangement or proximity of a chemical facility to a densely populated area (Table 1). One of the well-known incidents related to a poor layout is the Texas City Refinery explosion that happened on March of 2005, in which the high number of fatalities was caused due the inadequate distance between occupied portable trailers and the isomerization unit. At the moment of the incident, a flammable vapor cloud exploded destroying all trailers located within 121 feet from the release, and killing 15 workers; the blast waves also damaged a trailer 600 feet from the ISOM unit [2]. In response to this disaster, API released in 2007 the RP 753- Management of Hazards Associated with Location of Process Plant Portable Buildings [3] to address the siting of portable trailers, which was further incorporated as a standard practice under OSHA Process Safety Management guidelines.

Table 1: Accidents related to poor facility siting

Year	Location	Fatalities	Description
2013	West Fertilizer Company[4]	15	Ammonium nitrate storage
2011	Chemie-Pack, The Netherlands	0	Fire at chemical storage (resin and xylene)
2008	Imperial Sugar, GA[5]	14	Sugar dust explosion and fire
2006	Danvers, MA[6]	0	Heptane and alcohols
2005	Texas City, TX	15	Pentane/hexane release
2005	Buncefield, England[7]	0	Fire and explosion at oil storage
2005	Point Comfort, TX[6]	0	Propylene release
2001	Toulouse, France[8]	30	Ammonium Nitrate Storage explosion
1999	Allentown, PA[6]	5	Hydroxylamine decomposition
1998	Mustang, NV[6]	4	High explosives
1992	La Mede, France[9]	6	LPG leak
1989	Pasadena, TX [7]	23	Isobutane and ethylene release
1988	Norco, LA[9]	8	Explosion in the catalytic cracking unit
1984	Mexico City[6]	542	LPG line rupture
1984	Bhopal[10]	>2,000	Methylisocyanate release
1978	Texas City, TX[6]	7	Isobutane sphere failure
1976	Seveso[11]	0	Trichlorophenol release
1974	Flixborough, UK[7]	28	Cyclohexane release
1962	Brandenburg, KY[12]	1	Ethylene oxide explosion

Others high-consequence incidents have been related to poor facility siting and layout decisions. On March of 2004, a series of explosions and fires took place at Skikda LNG facility in Algeria claiming twenty-seven lives and injuring around eighty others [13]. The proximity of inhabited buildings such as control room, administrative office, and maintenance building to the hazardous unit was the major factor in the number of deaths and injuries, which were mostly caused by debris impact [14]. In a similar way, in 1989 at Phillips 66 facility, a massive vapor cloud ignited leading to a series of other

explosions killing twenty-three employees, many of whom were inside control rooms and other occupied buildings nearby the reactor unit [15].

Those mentioned incidents expose the importance of considering safety aspects during facility and layout decision. According to the Center of Chemical Process Safety (CCPS), there are three main types of siting analysis methodologies which are mostly used by industries to address safety features: consequence-based, lookup tables and risk-based [16]. Although many attention has been given to the risk-based design approach for several years, there is still a conflict of opinions regarding the benefits of this analysis among companies, contractors, and legislators [17]. As a result, its application is not as widespread as the others [17].

In consequence-based approach, the separation distances between units in the same facility and/or surroundings are established according to the effects of the maximum credible event (MCE) scenarios, characterized by the most likely scenarios with the greatest consequences that represent each possible type of hazard (*e.g.* explosion, fire, and toxic release) [4]. Besides the fact that this approach may have good results regarding the safety aspects, in most of the cases they are not economically viable [17].

Contrary to the consequence-based approach, the risk-based analysis considers the range of all possible scenarios. It requires a good understating of the frequency and the consequences associated with each potential event. In the end, the separation distance is obtained according to the risk acceptance criteria for the determined facility which can be related to individual or population risks. Besides the cost-benefit, it enhances more flexibility to the installation design by inserting the facility specificities with the use of

probabilistic methods. However, the number of variables grows exponentially with the system complexity and an extensive amount of time is required to perform this analysis.

Differing from the others methodologies, the lookup table is based on historical events and good engineering practice. The problem of using this approach is that it may not reflect the relative risk, and its efficacy in preventing or mitigating a dangerous event is not confirmed [4].

Therefore, the motivation of this study is to expand the usage of probabilistic risk methods earlier in the design stage of chemical installations in a timely manner, in other to minimize the risk of losses related to them, applying concepts that are believed to enhance safety but have been not widely used in this field.

1.2 Literature Review

1.2.1 Layout Optimization and Risk Analysis

Applying numerical methods to solve the layout problem is not a new subject of study. In the 70s, the "quadratic assignment problem" was used to allocate a number of production facilities based on the minimization of flow costs between facilities [18]. Since then, several different approaches have been applied to support plant layout decisions. Heuristic rules were suggested by many studies with no guarantee of the global optimality [19]. Additionally, graph partitioning problems were employed to determine the layout for single floor units.

Only after 1996 with the work published by Penteado and Ciric [20], safety considerations became part of reformulation problem. This method is formulated as

mixed-integer nonlinear programming (MINLP) to minimize the objective function composed of four factors- piping costs, land costs, the cost of protective devices, and financial risks associated with process safety incidents. These two last terms introduced the concept of process safety into layout optimization. Protective devices are used to prevent initiating events or minimize the effects on targeted units while financial risks include costs related to potential losses scaled by the frequency of occurrence [20].

Subsequently to the publication of Penteado and Ciric, this topic became very popular in the academia, and several different reformulations have been proposed to combine layout configuration and safety aspects. Patsiatzis and Papageorgiou incorporated the Dow Fire and Explosion Index into a mixed-integer linear programming (MILP) to consider probable damage losses and safety constraints [19]. The main advantage of using a linear model is the assurance of "global optimality" applying standard branch-and-bound solution techniques [19].

In recent years, quantitative risk assessment (QRA) started to be incorporated in the layout problem. Vázquez-Román *et al*. [21] and Díaz-Ovalle *et al*. [22] employed stochastic analysis such as Monte Carlo simulation with MINLP to account for uncertainties related to toxic release scenarios in an installed facility. However, structural damage costs were neglected, and safety was considered only due to fatality from toxic chemicals releases. In 2010, Jung *et al.*[9] adopted a MILP formulation in combination with probit functions to minimize total layout costs in a grid-based taking into account potential economic losses due to boiling liquid expansion vapor explosion (BLEVE) and vapor cloud explosion (VCE); later on, to overcome the limitations of grid-based

formulation, a new approach was proposed for continuous plane [7]. In this context, Medina-Herrera *et al.* [23] expanded the quantitative risk analysis to additional fire scenarios such as flash fire and jet fire into a MINLP formulation. In terms of risk reduction to the public and workers, Han *et al.* [24] imposed extras constraints on safety distances, delimiting what was called "risk zones" corresponding to areas where risk is above the acceptance criteria and should be avoided by the community and occupied buildings. Nevertheless, these methodologies have not accounted for uncertainties or low consequence events in a complete risk assessment, especially when it comes to fire and explosion scenarios.

Regarding domino effect prevention, a MINLP formulation was proposed by Lopez-Molina *et al*. [25] to optimize the facility layout based on the minimal probability of escalation events. In a distinct approach, Lira-Flores *et al.* [26] incorporated the Domino Hazard Index aiming the minimization of risk attributed to escalation events. Regarding the risk to the general public, Bernechea and Arnaldos [27] developed a method to support decision-making process during design stage employing inherently safer design (ISD) concepts and QRA. Domino effect was considered into QRA and plays an important role during the selection of possible facility layouts.

To conclude, the facility layout planning has been received much attention over the last years. However, in most of the studies, the risk is still calculated as a single value, and the uncertainties are not included in the formulation. Based on that, the use of the risk distributions should be incorporated in the design phase. It enhances the understanding of the overall risk and support the decision making during layout arrangement.

1.3 Objectives

Even though there are several reported studies incorporating safety into the layout optimization, there is a need for a method that combines layout optimization and a detailed risk assessment including uncertainties to estimate the risk. The main goal of this research is to apply a risk-based approach to the layout optimization of a chemical plant regarding the minimization of the total layout costs and risk. Specific objectives of the present work are summarized as:

- The first objective is to provide a tool that performs a probabilistic risk assessment in a chemical facility processing hazardous materials. The final program will propagate uncertainties associated with environmental conditions, failure data as well as release parameters. In the end, risk maps will be obtained representing the potential of human life losses and structural damage;
- the second objective, is to estimate inherently safety distances that prevent escalation events applying minimal threshold values;
- the third and last objective is to incorporate risk mapping and safety distances into design optimization problem. Additional safety constraints will be employed to account risk acceptance criteria (RAC) and mitigation systems into the facility arrangement.

1.4 Thesis Organization

Three stages were proposed and followed (see Figure 1) in order to achieve the main goals mentioned in the previous section.

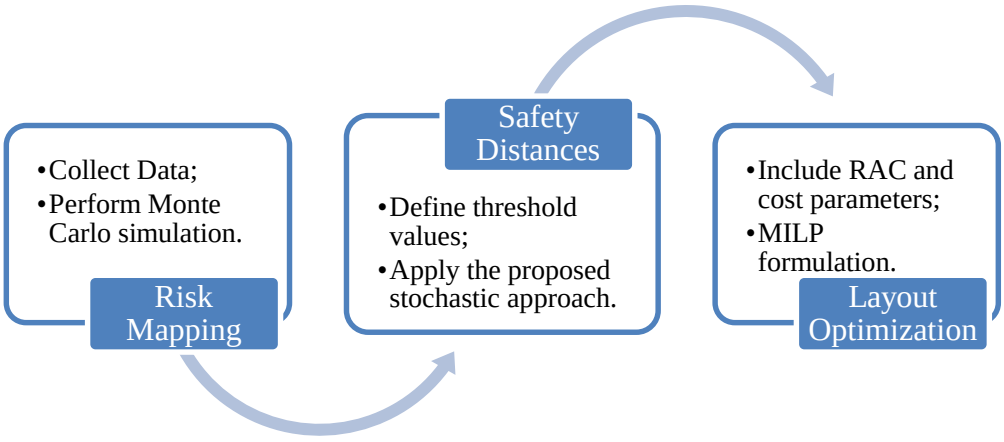

Figure 1: Global overview of proposed methodology

First, a literature review was conducted to understand all the steps of quantitative risk analysis. Since there was no available model implemented in Matlab, it was very challenging and time consuming for the authors to finalize this stage. In this context, Section 2 summarizes all models used for the initial phase of a QRA; it englobes source term modeling and gas dispersion models. An additional subsection describes how ignition probabilities are predicted in case of flammable materials. As part of risk assessment, Section 3 describes the consequence analysis fundamentals taking into account fire and explosion scenarios as well as toxic releases.

Section 4 introduces the proposed methodology to obtain risk maps, which consist in an extension of the studies performed by Alghamdi [28] and Ramirez *et al*.[29]. It is also described the procedures to estimate minimal separation distances for prevention of escalation events, which is part of the secondary stage of this study.

Section 5 demonstrates the layout formulation applied (third and last stage). A grid-based approach is used based on the work proposed by Jung *et al*. [9] with additional features to account for risk acceptance criteria and risk zones delimited by minimal separation distances.

Section 6 shows the applicability of the overall methodology in a case study involving a distillation unit that separates hexane and heptane.

Finally, Section 7 summarizes the conclusions and recommendations for the future work in this field.

2. SOURCE, GAS DISPERSION, AND IGNITION MODELING

2.1 Source Term Modeling

Source models are applied to estimate discharge rate, release duration, amount of released chemical, and fraction of vaporization from a fluid discharge [30]. These models are essential for risk assessment since their results determine the extension and size of vapor clouds and jet flames, which is necessary for consequence modeling. Several models are available, and their application may vary according to the material physical properties, discharge phase, and leakage source. For complex chemical plants, more than one source model may be required, and the most conservative results should be selected [31].

Release mechanisms are affected by the physical state of the material [30, 31]. If the material is stored as a gas or vapor, a jet of gas or vapor is formed during discharge. However, if the chemical is stored as a liquid, many outcomes are possible. For pressurized fluids at a temperature above its boiling point, the escaping fluid will partially flash into vapor when released to atmospheric pressure. A substantial amount of liquid may be entrained in gas as droplets. Part of the liquid may remain suspended as an aerosol and then evaporate while some may rainout onto the ground. A boiling liquid pool is likely to be formed by the remaining liquid which will result in extra vapor emission into the air. If a volatile fluid is kept under normal conditions, the release will first form a liquid pool which will subsequently evaporate.

For this work, flow through a hole was considered, and discharge rate was assumed constant to assure a conservative result. Additionally, three source models were applied

according to the phase of the material stored: gas/vapor, non-flashing liquid or flashing liquid. For flashing liquids, the fraction of aerosol formed was assumed to be the same amount as the liquid vaporized [31]. Details of each source model are explained in the following sections

2.1.1 Flow of Gas or Vapor Through Holes Modeling

According to CCPS, discharge models are governed by mechanical energy balance, which is typically represented as:

$$\int_{P_1}^{P_2} \frac{dP}{\rho} + \frac{g}{gc}(z_2 - z_1) + \frac{1}{2g_c}(v_2^2 - v_1^2) + \sum e_f + \frac{W_s}{\dot{m}} = 0 \qquad (2.1)$$

where P is the pressure (force/area), ρ is the density (mass/volume), g is the gravity acceleration (length/time^2), g_c is the gravitational constant (force/mass-acceleration), z is the vertical height (length), v is the fluid velocity (length/time), $\sum e_f$ is the frictional loss term (length^2/time^2) ,W_s is the shaft work (energy/time), and $\dot{m}$ is the mass flow rate (mass/time).

When gas discharges through a hole, the gas expands as pressure drops. Internal energy due to pressure is then converted into kinetic energy, and parameters such as density, pressure, and temperature change as the gas is being released.

If the mechanical energy balance is integrated along an isentropic path, the discharge rate can be determined by equation (2.2). This equation assumes ideal gas, adiabatic expansion, and no external work.

$$\dot{m} = C_0 A P_0 \sqrt{\frac{2gcM}{RT}\frac{\gamma}{\gamma-1}\left[\left(\frac{P}{P_0}\right)^{2/\gamma} - \left(\frac{P}{P_0}\right)^{(\gamma+1)/\gamma}\right]} \quad (2.2)$$

where C_0 is the discharge coefficient (dimensionless), A is the area of the hole (length^2), P_0 is the upstream pressure (force/area), γ is the heat capacity ratio (Cp/Cv), M is the molecular weight of the gas (mass/mole), R is the ideal gas constant (pressure-volume/mole-deg), T is the upstream temperature (deg), and P is the downstream pressure (force/area).

Typically in risk analysis, maximum flow rate is needed to assure conservative results. The maximum value is reached when the velocity of an escaping fluid is equivalent to sonic velocity. At this point, downstream pressure does not affect flow, which depends exclusively on upstream pressure [30]. The choked flow can be estimated by the following equation.

$$\dot{m} = C_0 A P_0 \sqrt{\frac{\gamma gcM}{RT}\left(\frac{2}{\gamma+1}\right)^{(\gamma+1)/(\gamma-1)}} \quad (2.3)$$

The maximum downstream pressure required to reach choke flow can be determined by:

$$\frac{P_{choked}}{P} = \left(\frac{2}{\gamma+1}\right)^{\gamma/(\gamma-1)} \quad (2.4)$$

If downstream pressure is below P_{choked}, resulted flow will be maximum, and equation (2.3) can be employed to estimate the release rate. Otherwise, equation (2.2) is used to calculate the discharge rate at the beginning of the release. For a conservative estimation, it is recommended a value of 1 for discharge coefficient.

2.1.2 Flowing of Liquid Through a Hole

Liquid discharges usually result from the pressure difference between stored fluid and atmospheric conditions. During the release, internal energy of fluid is converted into kinetic energy, which is then converted into thermal energy due to frictional forces between the escaping fluid and the equipment wall. Considering that density remains constant as fluid escapes through a small orifice, equation (2.1) can be directly integrated with the following result:

$$\dot{m} = \rho C_0 A \sqrt{2[g_c(P_0 - P_1) + g h_l]} \tag{2.5}$$

where h_l is the liquid height inside the tank.

The discharge coefficient represents the frictional loss term. For small orifices, it is recommended to use a value of 1 for discharge coefficient when Reynolds number exceeds 30,000 [30]. At these conditions, hole size does not influence exit velocity.

2.1.3 Flashing Liquids

Any pressurized liquid stored at a temperature above the boiling temperature will partially flash into vapor when released into atmospheric conditions resulting in two-phase flow. Vaporization happens so quickly that it can be considered adiabatic. The energy presented in the superheated liquid evaporates part of the fluid. Equation (2.6) represents the fraction of liquid vaporized.

$$f_v = \frac{m_v}{m} = \frac{C_p(T_0 - T_b)}{\Delta H_v} \tag{2.6}$$

where $C_p$the heat capacity of the fluid, ΔH_v is the heat of vaporization, T_0 is initial temperature of the fluid, and T_b is the boiling temperature.

Two-phase flows can be classified as either nonreactive or reactive. The second case occurs when exothermic chemical reactions take place, and, for the sake of simplification, it is not included in the model. Nonreactive two-phase flows occur when a liquid is discharged from processing equipment. For flashing liquid flowing through holes and pipes, two considerations should be accounted: subcooled liquid or liquid under saturation pressure. If the fluid is stored at a pressure higher than the saturation pressure (subcooled liquid), non-equilibrium conditions may exist if the fluid path length of the release is not long enough to allow the fluid flash within the hole. Therefore, the liquid will vaporize at the exterior of the equipment.

On the other side, equilibrium conditions are reached if the fluid path length is greater than 0.1 m, and the flow can be assumed choked [31]. For the model, it was assumed only equilibrium conditions and the mass flow rate is estimated by equation (2.7).

$$\dot{m} = AC_0\sqrt{2\rho g(P - Psat)} \tag{2.7}$$

For liquids stored at saturation conditions, Equation (2.7) is no longer applicable. A more detailed approach should be considered to account kinetic energy contribution [31]. Equation (2.8) estimates the mass flow rate for equilibrium conditions at saturation conditions and it is included in the model.

$$\dot{m} = \frac{\Delta H_v A}{v_{fg}}\sqrt{\frac{g_c}{TC_p}} \tag{2.8}$$

Fraction of aerosol formed was assumed to be the same as the liquid vaporized [31]. Therefore, if vaporization factor (f_v) exceeds 0.5, fluid escapes entirely as a vapor stream. Resulting discharge rates for both vapor $(\dot{m}_v)$ and liquid phase $(\dot{m}_l)$ can be estimated by following relations.

If $f_v < 0.5$,

$$\dot{m}_v = 2\dot{m}f_v \tag{2.9}$$

$$\dot{m}_l = \dot{m}(1 - 2f_v) \tag{2.10}$$

Else, if $f_v > 0.5$,

$$\dot{m}_v = \dot{m} \tag{2.11}$$

$$\dot{m}_l = 0 \tag{2.12}$$

Figure 2 shows the flowchart used to calculate mass flow rate for escaping fluids in the model. If discharging fluid is only in the liquid phase, then the next step consists in including the mass flow rate into a consequence modeling, which is described in Section 3. However, if the fluid escapes as vapor or two-phase, mass flow rate of the vapor phase is then fed into the dispersion model to predict vapor cloud size and concentration at a particular point. The dispersion models included in the model are described in the next section.

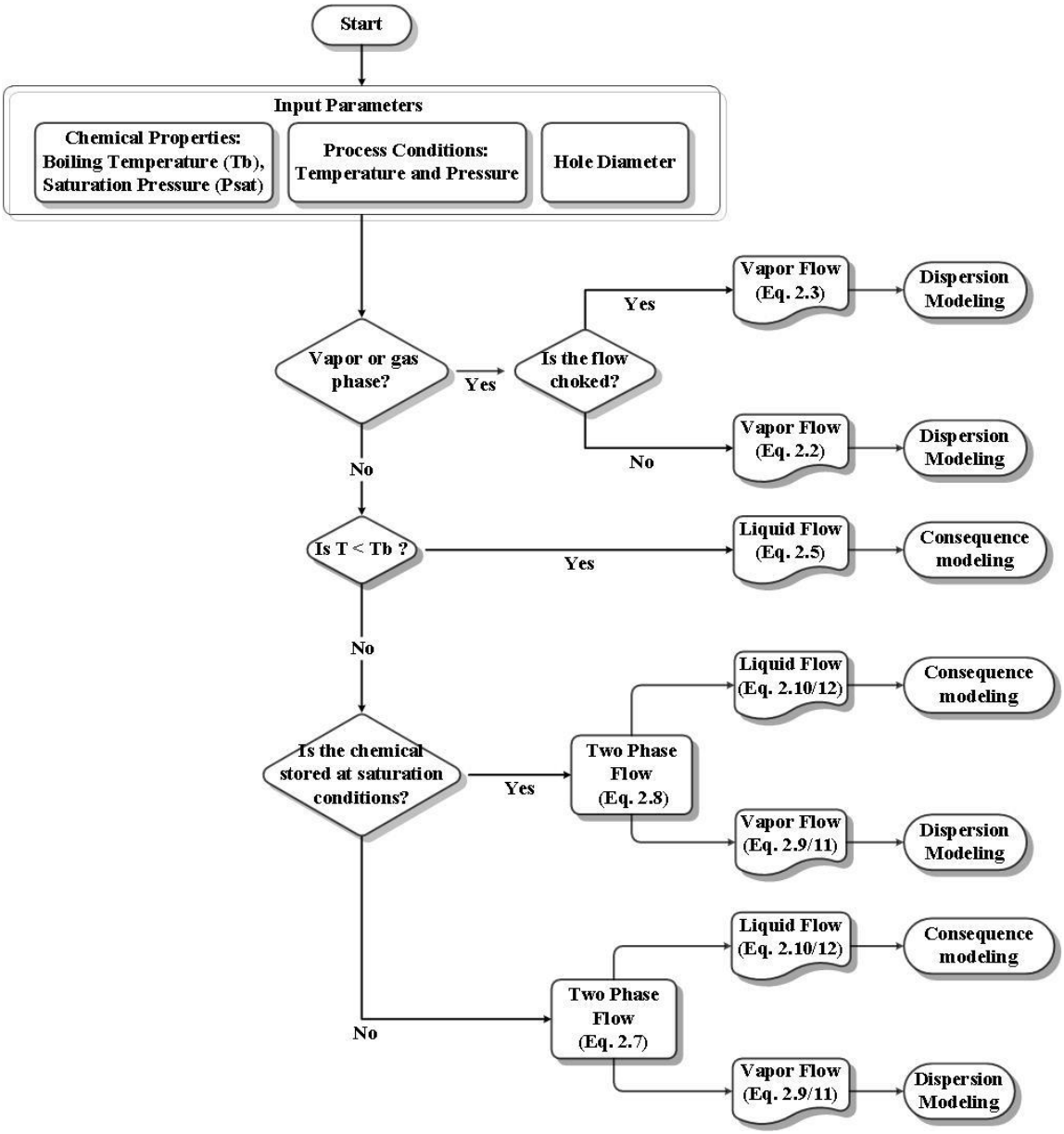

Figure 2: Flow chart of the source term models

2.2 Gas Dispersion Modeling

Hazardous materials, when released to the environment, are diluted and carried off by wind [32]. If the material is flammable and/or explosive, a vapor cloud may form and ignite causing damage due to the overpressure and/or irradiation. Additionally, if the

chemical has toxic effects, its concentration inside the cloud may cause deaths or permanent injuries to both employees and society. Thus, dispersion models should be employed to assess the risk of a chemical facility.

Choosing the proper dispersion model is not a straightforward task. It depends on several site-related parameters such as environmental conditions, level of obstruction, release direction, physical properties of the material, and discharge rate [33]. A large number of dispersion models is available in the public domain to perform dispersion analysis (*e.g.*, ALOHA, SLAB, DEGADIS, and INPUFF). They can be characterized mainly into two groups: dense gas models, and neutrally buoyant dispersion models. Most of these models are recommended by regulatory agencies such as US EPA. However, they are limited to open air releases and do not account for the effect of confinement and obstacles. In cases where confined and congested areas play an important role (*e.g.*, offshore facilities), more sophisticated models are required. Computational fluid dynamic (CFD) is a good alternative for those cases. However, it requires either long computation time and high level of expertise [34].

For the methodology proposed, two gas dispersion models were employed. The Gaussian plume model was used to simulate the neutrally buoyant dispersion of gases while the dispersion of heavier-than-air gases was predicted by the Britter and Mcquaid model [32]. Both methods were chosen due to their simplicity and robustness, which reduce the computation time while still give valid results.

2.2.1 Gaussian Plume Model

Passive dispersions occur when material dispersion (puff or vapor cloud) is mainly governed by atmospheric turbulence [32]. For constant atmospheric turbulence and wind velocity, the material concentration follows a Gaussian distribution in all directions. To predict passive dispersion, the Gaussian plume models (GPM) has been extensively used [32]. It can be employed for neutrally buoyant dispersions of gases at low concentrations, in the range of ppm [31].

Dispersion modeling expressions mentioned in equations (2.13) to (2.25) were obtained from the TNO "Yellow Book" [32]. At the first moment, it is shown equations to determine the variation of wind speed and mixing height. Then, the expression to estimate the concentration for both continuous and instantaneous release are mentioned. Finally, a procedure to calculate the flammability zone in case of a flammable material release is described.

Vertical variation of the wind speed can be calculated given the wind speed at a particular height, surface roughness length (z_0), and the Monin-Obukhov length, L. The vertical variation of the wind speed is then used in combination with the atmospheric stability and the Monin-Obukhov length to predict the mixing height, which is further applied to estimate the concentration of the released chemical.

Surface Friction Velocity

The surface friction velocity (u*) is assessed given the wind speed at a particular height (u_a) as follows.

$$u^* = k.\frac{u_a(z)}{f\left(\frac{z}{z_0}, L\right)} \qquad \left(\frac{m}{s}\right) \tag{2.13}$$

where parameter z can assume a maximum value of 100 m. In the model, z was fixed as 10 m, and wind speed was treated as a stochastic variable with values ranging from 1 to 5 m/s. The roughness length (z_0) was determined according to the terrain classification [32], and the Monin-Obukhov length (L) was obtained from the Pasquill-Gifford stability classes. Parameter *k* represents the Von Karman constant, which has a value of 0.4.

The Monin-Obukhov Length

The Monin-Obukhov length (L) is calculated numerically using the following expression.

$$\frac{1}{L} = \frac{1}{L_s}.\log_{10}\left(\frac{z_0}{z_s}\right) \tag{2.14}$$

where L_s and z_s are constansts that depend on the Pasquill-Gifford stability classes, as shown in Table 2 . In case of class D for the atmospheric stability, equation (2.14) results in $1/L = 0$. Finally, function $f\left(\frac{z}{z_0}, L\right)$ is defined below.

$$\begin{cases} f\left(\frac{z}{z_0}, L\right) = \ln\left(\frac{z}{z_0}\right) + 5\frac{(z - z_0)}{L}, & \text{for } 1/L > 0 \\ f\left(\frac{z}{z_0}, L\right) = \ln\left(\frac{z}{z_0}\right) - \varphi\left(\frac{z}{L}\right) + \varphi\left(\frac{z_0}{L}\right), & \text{for } 1/L \leq 0 \end{cases} \tag{2.15}$$

where,

$$\varphi\left(\frac{z}{L}\right) = 2\ln\left(\frac{1+\varphi^*}{2}\right) + \ln\left(\frac{1+\varphi^{*2}}{2}\right) - 2\arctan(\varphi^*) + \frac{\pi}{2}$$

$$\varphi^* = \left(1 - \frac{16z}{L}\right)^{1/4}$$

Table 2: Parameters to calculate the Monin-Obukhov length [32]

Pasquill-Gifford stability class	Ls (m)	z_s (m)
A	33.162	1117
B	32.258	11.46
C	51.787	1.324
D	∞	(not applicable)
E	-48.330	1.262
F	-31.325	19.36

Mixing Height

Mixing height is then obtained from the stability class and the Monin-Obukhov length as summarized in Table 3 . The Coriolis parameter is also included (f), which is defined as:

$$f = 2\Omega \sin\omega \tag{2.16}$$

where Ω is the earth's rotation ($7.27\ 10^{-5}\ s^{-1}$), and ω is the latitude on earth.

Dispersion Equations

After defining h_i and L, dispersion calculations can be performed. For a continuous released, concentration at any point is estimated by Equation (2.17).

$$c(x,y,z) = \frac{q}{u_a}.F_y(x,y).F_z(x,z) \qquad \left(\frac{kg}{m^3}\right) \tag{2.17}$$

where $c(x, y, z)$ is the concentration at position (x,y,and z), u_a is the wind speed (m/s), and q is the release rate (kg/s).

Corresponding equation for instantaneous release is obtained by Equation (2.18).

$$c(x, y, z) = Q.F_x(x, t).F_y(t.u_a, y).F_z(t.u_a, z) \quad \left(\frac{kg}{m^3}\right) \tag{2.18}$$

where t is the time after the release (s), Q is the total amount dischargerd (kg), and h is the height of the discharge (m).

Table 3: Mixing height estimation [32]

1/L	**Stability Class**	**Mixing Height h_i (m)**
>0	F,E,D	$0.4\sqrt{\frac{u^*}{f}L}$
0	D	Minimun value of 0.2 u*/f or 500 m
<0	C	1000
	B	1500
	A	1500

In both cases, functions Fy and Fz are equivalent. They are related to the horizontal and vertical dispersions respectively. Equation (2.18) has an additional term (Fx) to account for along-wind dispersion.

Expressions to calculate vertical dispersion are shown below. Source term was considered as a point source, which means that there are neither vertical nor horizontal dimensions.

If $\sigma_z(x) \leq 0.6.hi\sqrt{1-h/hi}$:

$$F_z(x,z) = \frac{1}{\sqrt{2\pi}\,\sigma_z(x)}\left\{\exp\left(-\frac{(z-h)^2}{2\sigma_z^2(x)}\right) + \exp\left(-\frac{(z+h)^2}{2\sigma_z^2(x)}\right)\right\} \quad (m^{-1}) \tag{2.19}$$

If $0.6.hi\sqrt{1-h/hi} < \sigma_z(x) \leq 1.6\,hi$:

$$\begin{aligned} F_z(x,z) &= \frac{1}{\sqrt{2\pi}\,\sigma_z(x)}\left\{\exp\left(-\frac{(2hi-h-z)^2}{2\sigma_z^2(x)}\right) + \exp\left(-\frac{(2hi-h+z)^2}{2\sigma_z^2(x)}\right)\right. \\ &+ \exp\left(-\frac{(z-h)^2}{2\sigma_z^2(x)}\right) + \exp\left(-\frac{(z+h)^2}{2\sigma_z^2(x)}\right) + \exp\left(-\frac{(2hi+h-z)^2}{2\sigma_z^2(x)}\right) \\ &\left. + \exp\left(-\frac{(2hi+h+z)^2}{2\sigma_z^2(x)}\right)\right\} \quad (m^{-1}) \end{aligned} \tag{2.20}$$

If $\sigma_z(x) > 1.6\,hi$:

$$F_z(x,z) = \frac{1}{hi} \quad (m^{-1}) \tag{2.21}$$

The lateral dispersion parameter, Fy, is defined by Equation (2.22).

$$F_y = \frac{1}{\sqrt{2\pi}\sigma_y(x)}.\exp\left(-\frac{y^2}{2\,\sigma_y^2(x)}\right) \quad (m^{-1}) \tag{2.22}$$

In the case of instantaneous or short duration releases, along-wind dispersion must be included. If the discharge is classified as instantaneous, Fx is calculated as follows:

$$F_x = \frac{1}{\sqrt{2\pi}\sigma_x(u_a t)}.\exp\left(-\frac{(x-u_a t)^2}{2\,\sigma_x^2(u_a t)}\right) \quad (m^{-1}) \tag{2.23}$$

However, if the material release is defined as short duration, the equation bellow must be applied to account release time (t_r).

$$F_x = \frac{1}{2u_a t_r}.\left\{\mathrm{erf}\left(-\frac{x-u_a(t-t_r)}{\sqrt{2}\sigma_x(u_a t)}\right)-\mathrm{erf}\left(-\frac{x-u_a t}{\sqrt{2}\sigma_x(u_a t)}\right)\right\}\ (m^{-1}) \qquad (2.24)$$

To calculate dispersion parameters, a practical approach was used [31, 32].

$$\sigma_y(x) = a.x^b$$

$$\sigma_z(x) = c.x^d$$

$$\sigma_x(x) = a.x^b$$

Constants a, b, c, d, e, and f differ according to the type of release (continuous or puff) and atmospheric stability class, as shown in Table 4.

Table 4: Recommended coefficients to calculate the dispersion parameters [31, 32]

Release Type	Atmospheric Stability	A	b	c	D
Continuous	A	0.54	0.86	0.28	0.90
	B	0.37	0.87	0.23	0.85
	C	0.21	0.87	0.22	0.80
	D	0.13	0.91	0.20	0.76
	E	0.098	0.90	0.15	0.73
	F	0.065	0.90	0.12	0.67
Puff	A	0.18	0.92	0.60	0.75
	B	0.14	0.92	0.53	0.73
	C	0.10	0.92	0.34	0.71
	D	0.06	0.92	0.15	0.70
	E	0.04	0.92	0.10	0.65
	F	0.02	0.89	0.05	0.61

Volume of the Cloud Between Lower and Upper Flammability Limit

The volume of a vapor cloud is required to estimate explosion impact due to a delay ignition. Even though most flammable materials are heavier than air, GPM is often used as an approximation [35]. A simplified approach was employed to calculate the cloud

size. For more precise solutions, partial equations should be solved analytically. For continuous release, volume was obtained integrating numerically the cross-sectional area over the center line from x_{ufl} to x_{lfl}, which represents the positions where concentration is equivalent to the upper and lower flammability limits, respectively. If the maximum concentration is bellow UFL, x_{ufl} is set as the first point from release source where concentration reaches the LFL. The cross-sectional area has an ellipse shape delimited by the cloud height (z_{lfl}) and width (y_{lfl}) as shown in Figure 3.

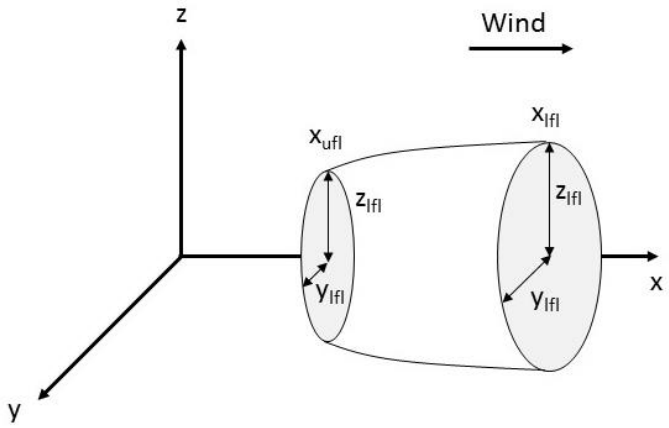

Figure 3: Flammable cloud from a continuous source

The cloud width and height are evaluated given the concentration profiles at the center line and dispersion parameters.

$$y_{lfl}(x) = \sigma_y(x)\sqrt{2\ln\left(\frac{c(x,0,0)}{c_{lfl}}\right)} \qquad (m) \tag{2.25}$$

A similar equation can be used for z_{lfl}. Vapor clouds that touch the ground are treated as half ellipsoid and the cross-sectional area is divided by 2.

The volume of a puff resulted from an instantaneous release was calculated applying the formula for a sphere**.**

$$V = \frac{4}{3}\pi\,(r_{lfl}^3 - r_{ufl}^3) \qquad (m^3) \tag{2.26}$$

where r_{ufl} and r_{lfl} are the distances from the center where concentration is equal to UFL and LFL, respectively. In this assumption, any point where concentration exceeds UFL will not ignite.

2.2.2 The Britter and Mcquaid Model

Many hazardous chemicals widely used in industry such as hydrocarbons, ammonia, hydrogen fluoride, and chlorine, can form vapor clouds that are heavier than air when released [36]. GPM already described is no longer applicable to this case, and a dense gas dispersion model must be employed to account negative buoyancy.

One of the simplest and fastest ways to modeling dense gas dispersion is to use top hat type models. It is assumed that instantaneous releases result in cylindrical clouds while continuous releases lead to wedge-shaped top hat profile. The cloud concentration is considered uniform, without any spatial variation, but it varies with time. The concentration outside the cloud boundaries is then considered zero.

The Britter and McQuaid model (BM) is a representative of top hat models, and it is broadly accepted for dense gas dispersion [32]. The model is composed of a collection of empirical correlations between parameters that affect gas dispersion process. The inputs are initial cloud size, initial discharge rate, release duration, and gas density. Wind speed and air density are also required.

Before proceeding with calculations for continuous and instantaneous releases, the cloud buoyancy must be estimated to be further applied.

$$g_o = g(\rho_o - \rho_a)/\rho_a \tag{2.27}$$

where g_o is the buoyancy factor (length/time^2), ρ_o is the density of the released chemical at initial conditions (mass/volume), and ρ_a is the air density (mass/volume).

2.2.3 Model for Continuous Release

For continuous discharges, BM model presents a collection of curves to estimate the downwind averaged concentrations (C_{mean}/C_o) ranged from 0.002 to 0.1. Equations presented in Table 5 consists of approximations of those curves and were used in the model; where q_o is the initial discharge rate (volume/time), u is the wind speed at 10 m height (length/time), and x is the distance from the release source (length).

To determine safe distances that prevent intoxication or ignition, the downwind distance (x_d) needs to be estimated given a safe concentration level. Then, an upwind extension of the plume (x_u) is calculated as follows.

$$x_u = 2L_b \tag{2.28}$$

where

$$L_b = q_o g_o / u^3 \tag{2.29}$$

Table 5: Approximation of the curves in the Britter-McQuaid Correlations [31]

Concentration ratio $\left(\frac{C_m}{C_0}\right)$	$\alpha = \log\left(\frac{g_0^2 q_0}{u^5}\right)$	$\beta = \log\left[x/\left(\frac{q_0}{u}\right)^{\frac{1}{2}}\right]$
0.1	$\alpha \leq -0.55$	1.75
	$-0.55 < \alpha \leq -0.14$	$0.24\alpha + 1.88$
	$-0.14 < \alpha \leq 1$	$0.50\alpha + 1.78$
0.05	$\alpha \leq -0.68$	1.92
	$-0.68 < \alpha \leq -0.29$	$0.36\alpha + 2.16$
	$-0.29 < \alpha \leq -0.18$	2.06
	$-0.18 < \alpha \leq 1$	$-0.56\alpha + 1.96$
0.02	$\alpha \leq -0.69$	2.08
	$-0.69 < \alpha \leq -0.31$	$0.45\alpha + 2.39$
	$-0.31 < \alpha \leq -0.16$	2.25
	$-0.16 < \alpha \leq 1$	$-0.54\alpha + 2.16$
0.01	$\alpha \leq -0.70$	2.25
	$-0.70 < \alpha \leq -0.29$	$0.49\alpha + 2.59$
	$-0.29 < \alpha \leq -0.20$	2.45
	$-0.20 < \alpha \leq 1$	$-0.52\alpha + 2.35$
0.005	$\alpha \leq -0.67$	2.40
	$-0.67 < \alpha \leq -0.28$	$0.59\alpha + 2.80$
	$-0.28 < \alpha \leq -0.15$	2.63
	$-0.15 < \alpha \leq 1$	$-0.49\alpha + 2.56$
0.002	$\alpha \leq -0.69$	2.60
	$-0.69 < \alpha \leq -0.25$	$0.39\alpha + 2.87$
	$-0.25 < \alpha \leq -0.13$	2.77
	$-0.13 < \alpha \leq 1$	$-0.50\alpha + 2.71$

Subsequently, the plume width b(x) is given by the following relation.

$$b(x) = 2b_o + 8L_b + 2.5L_b^{1/3}x^{2/3} \tag{2.30}$$

Vapor cloud height (b_z) is also a function of distance from release source. It can be calculated using the equation below.

$$b_z(x) = \frac{q_o}{2ub(x)} \tag{2.31}$$

Finally, the volume of the plume can be found using expressions for b and b_z.

$$V_p = \int_0^{x_d} b_z(x) \, . \, b(x) \, dx = \frac{q_o x_d}{2u} \tag{2.32}$$

2.2.4 Model for Instantaneous Release

Different from continuous discharges, curves applied for instantaneous releases give the down-wind maximum concentrations (C_{max}/C_o) in the range between 0.001 and 0.1. Equations presented in Table 6 consist of approximations of those curves used. To determine safe distances that prevent intoxication or ignition, it is necessary first to estimate the downwind distance (xd) given a safe concentration level. Then, the time a cloud reaches distance xd should be found by the following relation.

$$x_d = 0.4ut + b(t) \tag{2.33}$$

where term $0.4ut$ represents the advection velocity, and b is the cloud radius, which is a function of time (t), the initial volume (Vo), and the initial cloud radius (bo).

$$b(t) = \sqrt{b_o^2 + 1.2 . t \sqrt{g_o V_o}} \tag{2.34}$$

The mean height of the cloud is calculated by the equation below.

$$b_z(t) = c_o V_o / (\pi b^2 C_{max}) \tag{2.35}$$

Cloud height (bz) and cloud radius (b) are then employed to obtain the vapor cloud size.

$$V = \pi b^2 b_z \tag{2.36}$$

Table 6: Estimates of the curves from the Britter-McQuaid Workbook for instantaneous release[31]

Concentration ratio $\left(\frac{C_m}{C_0}\right)$	$\alpha = \log\left(g_o V_o^{\frac{1}{3}}/u^2\right)^{\frac{1}{2}}$	$\beta = \log\left(x/V_o^{\frac{1}{3}}\right)$
0.1	$\alpha \leq -0.44$	0.70
	$-0.44 < \alpha \leq -0.43$	$0.26\alpha + 0.81$
	$-0.43 < \alpha \leq 1$	0.93
0.05	$\alpha \leq -0.56$	0.85
	$-0.56 < \alpha \leq 0.31$	$0.26\alpha + 1.0$
	$0.31 < \alpha \leq 1.0$	$-0.12\alpha + 1.12$
0.02	$\alpha \leq -0.66$	1.15
	$-0.66 < \alpha \leq 0.32$	$0.34\alpha + 1.39$
	$0.32 < \alpha \leq 1$	$-0.26\alpha + 1.38$
0.01	$\alpha \leq -0.71$	1.15
	$-0.71 < \alpha \leq 0.37$	$0.34\alpha + 1.39$
	$0.37 < \alpha \leq 1$	$-0.38\alpha + 1.66$
0.005	$\alpha \leq -0.52$	1.48
	$-0.52 < \alpha \leq 0.24$	$0.26\alpha + 1.62$
	$0.24 < \alpha \leq 1$	$0.30\alpha + 1.75$
0.002	$\alpha \leq -0.10$	2.075
	$-0.10 < \alpha \leq 1$	$-0.27\alpha + 2.05$

*V_o is the total discharged volume.

In summary, if the gas is neutrally buoyant, GPM is applied. However, if the fluid escapes as vapor heavier-than-air, the Britter and McQuaid model is employed to predict vapor cloud size and safe distances given safe concentration of the material.

2.3 Ignition Probability Modeling

Models proposed by Moosemiller [37] were used to predict ignition probabilities for fire and explosion scenarios. Although default values for ignition probability are usually applied, such as 0.15 for immediate ignition and 0.3 for delayed ignition, they do not account for specific release conditions that may influence probability values such as temperature, release material, and an ignition source. Expressions used for ignition probability modeling are described in the following sections.

2.3.1 Immediate Ignition

Immediate ignition (prompt ignition) is ignition that occurs near the release source and early enough to prevent the formation of a large vapor cloud. The probability of this event occurring is a function of process conditions- temperature (T) and pressure (P)- as well as material properties- auto-ignition temperature (AIT) and minimum ignition energy (MIE).

$$P_{imm.ign.} = \left[1 - 5000e^{-9.5\left(\frac{T}{AIT}\right)}\right] + \left[\frac{0.0024P^{\frac{1}{3}}}{MIE^{\frac{2}{3}}}\right] \quad (2.33)$$

where the first term is equal to 0 if T/AIT < 0.9 and equal to 1 if T/AIT > 1; and $P_{imm.ign.}$ does not exceed 1.

2.3.2 Delayed Ignition

Delayed ignition takes place when a vapor cloud is formed before finding an ignition source. It may lead to a flash fire or a vapor cloud explosion depending on site

characteristics. The probability of delayed ignition is a function of "modifiers", which depends on flow rate (FR), minimum ignition energy (MIE) of the material, a "source factor" (S), and ignition time (t) [37]. Equation (2.38) is used to estimate delayed ignition probabilities; each term inside the brackets represent a specific modifier.

$$P_{\text{del.ign.}} = 1 - \frac{0.7}{[0.6 - 0.85\log(\text{MIE})][7e^{0.642\ln(\text{FR})-4.67}][1-(1-S^2)e^{-(0.015S)t}]} \tag{2.34}$$

If the product of all multipliers is less than 1, equation (2.39) must be used.

$$P_{\text{del.ign.}} = 0.3[0.6 - 0.85\log(\text{MIE})]\left[7e^{0.642\ln(\text{FR})-4.67}\right]\left[1-(1-S^2)e^{-(0.015S)t}\right] \tag{2.35}$$

The first modifier accounts for the tendency of released material to ignite, and it has a maximum value of 3 and a minimum value of 0.1. The second modifier represents the influence of the amount of released material; it has an upper limit of 2. The third and last modifier represents the release duration and the ignition type. Parameter S in this factor is based on the sources of ignition present in the area of the release. It can be replaced with either the fraction of the cloud within a process unit, or generic values based on equipment density from [37].

2.3.3 Delayed Explosion Probability

An explosion may occur given a delayed ignition of a vapor cloud. The probability of this event occurring depends on the flow rate of flammable material (FR) and a modifier factor (R) to account for the material reactivity.

$$P_{exp} = R * 0.024FR^{0.435} \tag{2.36}$$

where R is 0.3 for low reactivity materials (*e.g.* natural gas), 1 for medium reactivity materials (most materials), and 3 for high reactivity materials (*e.g.* hydrogen).

3. CONSEQUENCE MODELING

An overview of the consequence modeling is presented in this section . Given a release of a flammable or toxic material, many outcomes are possible including: vapor cloud explosion (VCE), boiling liquid expanding vapor concentration (BLEVE), physical explosions, fireballs, toxic exposure, flash fires, jet fire and pool fires. All outcome events implemented are shown in Figure 4 and Figure 5. They were selected based on common scenarios that may occur in a chemical facility as mentioned by the International Association of Oil & Gas Producers (OGP) and CCPS [30] to give a better understanding of the overall risk. All models included are discussed in the following sections.

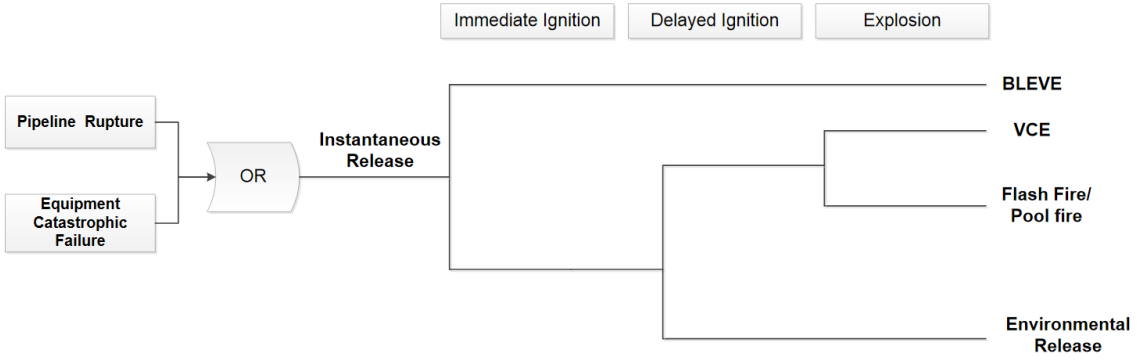

Figure 4: Bowtie analysis for instantaneous releases

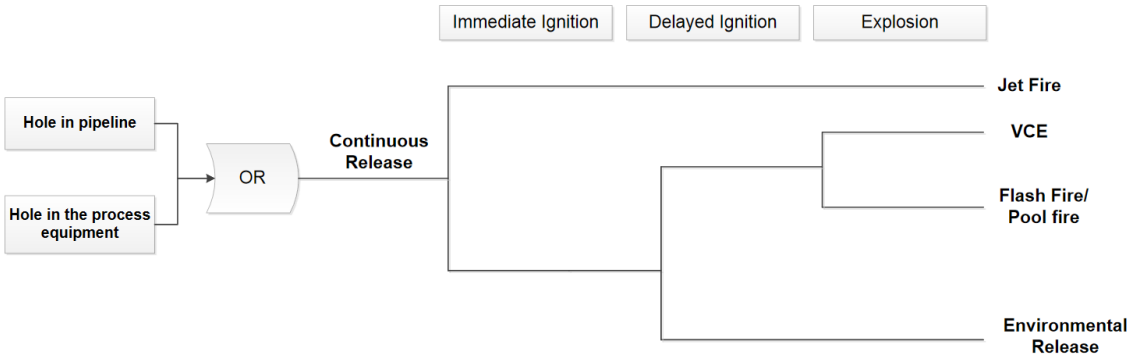

Figure 5: Bowtie analysis for continuous releases

3.1 Vapor Cloud Explosion Modeling

Vapor cloud explosion is characterized by a sudden pressure increase due to combustion of a premixed gas. Before a VCE takes place, some conditions must be met [38]. First, an accidental release of a flammable material must happen in an area that is partially confined and congested. Then, a delayed ignition must occur allowing the formation of a vapor cloud with concentrations between flammability limits. Third, ignition source must provide enough energy to ignite the fuel-air mixture.

In this work, VCE was modeled according to the TNO multi-energy method [32]. It is required knowledge of the chemical that ignites, its quantity, level of confinement and congestion in the area, and relative distance from the explosion center to predict overpressure and impulse at a particular point.

From the TNO chart, the scaled peak overpressure and positive phase duration relate with combustion energy scaled distance (r'), which is defined as the distance of a particular point of interested from explosion center, normalized by the amount of energy presented in the ignitable portion of the cloud.

$$r' = \frac{r}{[\frac{E}{p_{atm}}]^{1/3}} \tag{3.1}$$

where r is defined in meters, E is defined in joules, and pressure is defined in Pascals. The scaled overpressure is simply the overpressure generated by the explosion divided by the atmospheric pressure.

$$P_s' = \frac{P}{P_{atm}} \tag{3.2}$$

Overpressure is then applied to assess positive impulse (i_s).

$$i_s = \frac{1}{2} P\, t_p \tag{3.3}$$

This method starts with determining scaled distances of interested, followed by the definition of blast level curve to be used. Finally, scaled overpressures and scaled impulses must be read from the charts, and subsequently converted into to their real values. However, there are some limitations in applying graphical charts directly to the model, so mathematical expressions were employed to convert each curve and perform calculations continuously. Linear behavior is observed for all curves on a log-log scale at specific ranges of scaled distance, and was approached in the form:

$$y = cx^b \tag{3.4}$$

where b represents the slope, and c is the y –interception in log-log scale. The values for parameters c and b were used as suggested by Diaz Alonso *et al.* [39] and are listed in Appendix A. In terms of severity, there is still a lack of guidance regarding the choice of severity levels. However, the criteria proposed by Kinsella [40] can help the user during the selection of possible severity levels.

Substituting the expressions for scaled pressure, positive impulse, and relative distance into equations (3.2) and (3.3), we have:

$$P = \frac{c_o P_{atm} [\frac{E}{P_{atm}}]^{1/3}}{r} \tag{3.5}$$

$$i_s = \frac{1}{2} P c_I \left[\frac{r}{\left(\frac{E}{P_{atm}}\right)^{1/3}} \right]^{b_I} \tag{3.6}$$

Both equations are valid for scaled distances greater than 0.6 and explosion levels less than or equal to 6. Results are then fed into impact modeling to predict the probability of deaths and structural damage.

3.2 Flash Fire

Accidental releases of flammable materials may not explode. Flash fire is a nonexplosive combustion of a fuel/air mixture resulted from both continuous and instantaneous release [38]. If a prompt ignition takes place in case of an immediate release, the cloud may not be significant in size and affected area would be small, however if the cloud has enough time to spread among a facility before ignites, a major flash fire is likely to occur [36]. Based on that, only flash fire resulted from delayed ignition was considered in the model.

There are a few models available to predict thermal radiation effects from a flash fire. Usually, the area affected is assessed by first conducting a dispersion analysis and then defining the cloud burning zone from release source and half of lower flammability level [38].Then, it is assumed that people inside the burning zone are subjected to a fatal

injury while those outside does not suffer any adverse effect. The same assumption was applied for people inside buildings to give a conservative approach. Even though it is known that buildings can protect from flash fire, many uncertainties are raised to assess the probability the building catches fire and the likelihood of evacuation [41].

3.3 Boiling Liquid Expanding Vapor Explosion

According to CCPS [38], boiling liquid expanding vapor explosion (BLEVE) is 'a sudden release of a large mass of pressurized superheated liquid to the atmosphere'. This sudden release may occur when a pressurized vessel containing liquid "above is atmospheric conditions" is subject to a catastrophic failure, which can be caused by corrosion, fire engulfment, equipment defects, etc [38, 42]. The main hazards involved are the overpressure and the fragments created during explosion. This event is not limited to flammable liquids. However, if a flammable liquid is involved, an ignition will probably arise a fireball as a secondary effect. To assess the damage from BLEVEs, CCPS model [38] was used in combination with a methodology suggested by Cuchi *et al.* [43] to predict overpressure at a particular point. Then, TNO model for fireball [32] is applied to calculate heat fluxes in case of a flammable material discharge. Effects of fragments impact were not considered given the high complexity of current models and their lack of precision. All models are described in the following sections.

3.3.1 Overpressure Estimation

When a vessel fails catastrophically leading to a BLEVE, the mechanical energy stored in a fluid is released abruptly creating a blast strength [42]. At the moment of explosion, vapor phase increases in volume as pressure drops and the pressurized liquid flashes, strengthening pressure waves significantly. Based on that, some researchers define explosion energy as the work done by a fluid in expansion on the surrounding air following an isentropic path. Thus, this work can be estimated by internal energy variation from state 1 (initial state) to state 2, when the internal pressure is equivalent to ambient pressure. Therefore, the available energy to create a pressure wave given a fluid in expansion can be calculated as follows.

$$E_{ex} = m(u_2 - u_1) \tag{3.7}$$

where m is the total mass released, u_1 is the specific internal energy of the fluid at process conditions obtained from thermodynamic tables, and u_2 is the specific internal energy in expanded stated, which can be estimated considering an isentropic path.

$$u_2 = (1 - X)h_f + Xh_g - (1 - X)P_0v_f - XP_0v_g \tag{3.8}$$

where

$$X = (h_1 - h_f)/(h_g - h_f) \tag{3.9}$$

Here h is the specific entropy, v is the specific volume, P_0 is the atmospheric pressure, and X is the vaporization fraction. Subscript 1 refers to initial state while subscripts g and f refer to saturated vapor and saturated liquid at ambient pressure, respectively.

Then, available energy is converted into TNT equivalent mass to estimate pressure wave from the well-known plot of overpressure vs. scaled distance. However, in practice, burst power is not entirely used to generate pressure waves. Part is spent to propel vessel fragments while another portion is lost during vessel rupture. Consequently, a correction factor (β) must be applied to account this energy distribution. Cuchi *et al.* [43] propose the following expression to convert internal energy changes into TNT equivalent mass.

$$W_{TNT} = \beta\ (0.214)\ E_{ex} \tag{3.10}$$

where 0.214 is a conversion factor (0.2136 kg MJ^{-1}); E_{ex} is defined in (bar m^3); and β is the correction factor that might range from 0.4 to 0.8.

Once W_{TNT} is estimated, scaled overpressure is obtained from empirical correlation [31].

$$P_s = \frac{1616\left[1+\left(\frac{z_c}{4.5}\right)^2\right]}{\sqrt{1+\left(\frac{z_c}{0.0048}\right)^2}\sqrt{1+\left(\frac{z_c}{0.32}\right)^2}\sqrt{1+\left(\frac{z_c}{1.35}\right)^2}} \tag{3.11}$$

where z_c is the scaled distance defined as

$$z_c = \frac{r}{W_{TNT}^{\frac{1}{3}}} \tag{3.12}$$

Equivalent to VCE, results are included into impact modeling to predict the probability of deaths and structural damage.

3.3.2 Fireball

TNO [32] defines fireball as ‘a fire, burning sufficiently rapidly for the burning mass to rise into the air as cloud or ball’. As mentioned previously, if a vessel storing

flammable material is subjected to a BLEVE, fireball is inevitable due to auto-ignition of an immediate two-phase discharge. Vapor cloud explosions can also result in fireballs. However such fireball is influenced by buoyancy forces, differing from those from BLEVE, which is governed by momentum forces [42]. In this work, only fireballs from BLEVE was considered given its higher destruction power.

To predict the size, duration and radiation of a probable fireball from a BLEVE, following parameters must be defined [42]:

a) the total mass of flammable material stored,
b) the mass fraction contributing to fireball formation,
c) the fireball behavior with time,
d) the fireball duration and magnitude,
e) the heat generation,
f) the 'view factor', and
g) the impact modeling due to heat exposure.

A 14-step procedure is presented by TNO [32] to forecast the size and impact of a fireball from BLEVE. All steps relate to calculation of: (i) the likely amount of chemical that will be released in BLEVE; (ii) fireball radius, r_{fb}; (iii) duration time, t; (iv) fireball lift-off height, H_{bleve}; (v) the distance, X, from the fireball center; (vi) maximum view factor at a specific distance X, F_{view}; (vii) fraction of heat generated, F_s; (viii) the net available heat for combustion, ΔH; (ix) surface emissive power, SEP; (x) absorption factor for water vapor, α_w; (xi) absorption coefficient for carbon dioxide, α_w; (xiii) atmospheric

transmissivity, τ_a; and heat flux, q. Equations for each term mention above are summarized in Table 7

Table 7: Expressions for BLEVE parameters

Parameter	Equation	
Mass of material involved	$m = f\ x\ V\ x\ \rho_{mat}$	(3.13)
Fireball radius	$r_{fb} = 3.24m^{0.325}$	(3.14)
Duration of the fireball	$t = 0.852m^{0.26}$	(3.15)
Lift-off height	$H_{bleve} = 2r_{fb}$	(3.16)
Distance from the fireball center	$X = \left(x_{bleve}^2 + H_{bleve}^2\right)^{\frac{1}{2}}$	(3.17)
Maximum view factor	$F_{view} = (r_{fb}/X)^2$	(3.18)
Fraction of heat generated	$F_s = 0.00325\ P_{sv}{}^{0.32}$	(3.19)
Net available heat for combustion	$\Delta H = \Delta H_c - \Delta H_V - C_p.\Delta T$	(3.20)
Surface emissive power	$SEP = \Delta H\ x\ m\ x\ \frac{F_s}{4\pi.\ r_{fb}^2.\ t}$	(3.21)
Absorption factor of water vapor	$\alpha_w = 0.057 \log_{10}(P_{vw}\ X) - 0.148$	(3.22)
Absorption factor of carbon dioxide	$\alpha_c = 0.0085 \log_{10}(P_{vw}\ X) - 0.007$	(3.23)
Atmospheric transmissivity	$\tau_a = 1 - \alpha_w - \alpha_c$	(3.24)
Heat flux	$q'' = SEP\ x\ F_{view}\ x\ \tau_a$	(3.25)

where f is the volume fraction of the tank filled with flammable material; V is the tank volume (m^3); ρ_{mat} is the material density (m^3/kg); x_{bleve} is the ground distance from the tank center; P_{sv} is the vapor pressure of the material (N/m^2); ΔH_c is the heat of combustion at boiling point (J/kg); ΔH_V is the heat of vaporization at boiling point (J/kg); C_p is the specific heat capacity (J/kg K); ΔT is the difference between flame temperature and ambient temperature ($\Delta T = 1700$ K); and P_{vw} is the water partial vapor pressure (N/m^2).

Once heat flux is estimated, the likelihood of fatalities is obtained from impact modeling.

3.4 Jet Fire

Jet fire is ‘a turbulent diffusion flame’ resulted from combustion of a flammable material that is being ejected from process equipment such as pipes, vessels, and flanges [44]. The main hazard involved is fire engulfment that can lead to equipment failure, and further escalate to another event (i.e. domino effect). Jet fires can occur either vertically or horizontally; the last one has a higher probability of impingement on targets [44]. Based on that, a model proposed by Johnson *et al.* [36] was implemented to predict the flame size of horizontal jets, and delimitate fatal zones. As assumed for flash fire, people inside the flame area are subjected to fatal injuries while those outside does not suffer any adverse effect.

In horizontal jet models, the flame shape is treated as a conical frustum. Since large uncertainties and complex calculations are involved with surface emissive power (SEP) estimation, fatal zones were limited by the flame geometry instead of using threshold values for SEP. To predict the flame geometry, several parameters must be addressed: (i) the combustion effective source diameter; (ii) the Mach number; (ii) exit velocity of the expanding jet, (ii) the Richardson Number; (iii) the length of frustum; (iv) flame position, X,Y, and Z ; and (v) minimum and maximum flame diameters. All correlations are available in literature [36] and listed in Table 8.

Table 8: Correlations for jet fire parameters

Parameter	Equation	
Temperature of expanding jet	$T_j = T_0 \text{ x } \left(\frac{P_a}{P_0}\right)^{\frac{k-1}{k}}$	(3.26)
Exit velocity of the jet	$u_j = M_j \text{ x } \sqrt{k \text{ x } R \text{ x } T_j / w_g}$	(3.27)
Combustion effective diameter	$D_s = d_j \sqrt{\frac{\rho_j}{\rho_a}}$	(3.28)
Momentum flux	$G = \frac{\pi \rho_j u_j^2 d_j^2}{4}$	(3.29)
Momentum flux at x-direction	$\Omega_x = \left(\frac{\pi \rho_a}{4G}\right)^{1/2} L_{bo} u_a$	(3.30)
Momentum flux at z-direction	$\Omega_z = \left(\frac{\pi \rho_a}{4G}\right)^{1/2} L_{bo} w_a$	(3.31)
Richardson Number	$\varepsilon = \left(\frac{\pi \rho_a g}{4G}\right)^{1/3} L_{bo}$	(3.32)
X-position	$\frac{X}{L_{bo}} = f(\varepsilon)[1 + r(\varepsilon)\Omega_x]$	(3.33)
Y-position	$\frac{Y}{L_{bo}} = (1 + \varepsilon^{-1})^{-8.78}[1 + 0.002\varepsilon\Omega_x]$	(3.34)
Biggest diameter	$\frac{W_2}{L_{bo}} = -0.004 + 0.0396\varepsilon - \Omega_x(0.0094 + 9.5x\,10^{-7}\varepsilon^5)$	(3.35)
Lifted- high	$b = 0.141(G\rho_a)^{1/2}$	(3.36)
Smallest diameter	$\frac{W_1}{b} = -0.18 + 0.081\varepsilon$	(3.37)
Z-position	$\frac{Z}{X - b} = 0.178\Omega_z$	(3.38)

Effects of jet fires on equipment were not accounted given the high complexity to predict the time to failure. When jet fire flames engulf equipment, extreme heat fluxes occur on the impinged surface. It makes extremely difficult to estimate with accuracy the heat transfer rate, which varies according to flammable material, flame size, and turbulence, and the flame region [45]. Several values have been proposed for specific fuels

(e.g. propane and natural gas). However, there is no common agreement. Furthermore, equipment may be insulated by a fire resistant material; wich may range the time to failure from seconds to hours, depending on maintenance conditions.

3.5 Pool Fire

Pool fire is defined as "a turbulent diffusion fire burning" of the vaporizing flammable material from a horizontal pool with low or none initial momentum [32]. Several scenarios may lead to a fire pool; it usually starts with a non-flashing liquid discharge of flammable chemical from process equipment followed by ignition. If the liquid vaporizes while escaping (e.g. flashing liquids), only the remaining liquid will form a pool. Conditions for flashing discharges are discussed in section 2.1.3. Another important parameter to be considered during pool fire modeling is the geometry, even though pool fires are limited by surroundings (i.e. dikes), the occurrence of unconstrained pools is also possible in an "open, flat area" [30].

There are many pool fire models available, differing in degree of complexity. In this methodology, correlations proposed by CCPS [30] were included. It gives reasonable results for pool fires on land within a short period. To initiate a pool fire model, following parameters should be addressed:

- Mass released, m, in kilograms based on process conditions,
- Heat of combustion of the material, ΔH_c, in kJ/kg,
- Specific heat capacity, C_p, in kJ/kg. K, and
- The boiling point temperature, T_{bp}, in K.

From this information, the vertical rate of liquid level decrease (m/s) can be obtained as by

$$y_{max} = 1.27 * 10^{-6} \frac{\Delta H_C}{\Delta H^*} \tag{3.39}$$

where ΔH^* is the vaporization heat at boiling temperature.

$$\Delta H^* = \Delta H_V + Cp * (Tbp - Ta) \tag{3.40}$$

From these expressions, the mass burning rate can be found.

$$m'' = \rho y_{max} \tag{3.41}$$

And the steady-state diameter of the pool can be estimated employing the simplified model:

$$D = \left(\frac{4\dot{m}}{\pi \dot{m}''}\right)^{1/2} \tag{3.42}$$

The flame height can be found:

$$H = 42D \left(\frac{m''}{\rho_a \sqrt{gD}}\right)^{0.61} \tag{3.43}$$

And the burning time can be calculated:

$$t_b = \frac{m}{\dot{m}''A}, \text{for equipment}$$
$$t_b = 20 \text{ s}, \text{for employees} \tag{3.44}$$

Finally, the heat flux at any point of interest away from the center of the fire can be estimated by following point source model:

$$I_{s,k} = \frac{\tau_a * \eta * m'' * \Delta H_C}{16\pi (x/D)^2} \tag{3.45}$$

where η is the combustion fraction (typically between 0.15 and 0.35), and x is the distance from the center of the pool fire.

$$x^2 = \left(\frac{H}{2}\right)^2 + r^2 \tag{3.46}$$

Unlike a fireball or flash fire, pool fires can last longer than just a few seconds, causing damage due prolonged exposure. Thus, the burning time is required to scale the amount of heat dosage at any point from a pool fire. Subsequently, burning time and heat flux are fed into a probit function (see section 3.6).

3.6 Impact Modeling

The next step of proposed methodology is to assess the consequences of incidents outcomes mentioned above on workers and structures by employing impact models. It is known that overpressures, radiation levels, and toxic concentrations may cause damage according to the exposure levels, however, mathematical expressions are required to predict impacts and further calculate related risks. Dose-response curves are widely used, in combination with a probit equations, to assess a single-exposure effect [30].

Probit functions represent the linearization of a dose-response curve following a normal distribution. Once probit coefficients are correctly defined, probit variables can be obtained with any dosage and then converted to probability values. Although dose-response curves are usually employed in toxicology studies, this method can also be applied to predict the effects of any single exposure event, such as explosion overpressures or heat radiations from fire incidents.

Probit functions are usually in the form $Y = k_1 + k_2 \ln V$, where Y represents the probit value, and parameters k1 and k2 are obtained from best-fitting response data to dosage data. V is the causative factor whose definition changes according to associated

hazard. All probit functions included are summarized in table 10. Given the high complexity of assessing structural failure due to heat radiation, there is a limited (if any) number of models available. Consequently, it was not included in the model. Additionally, coefficients for common toxic chemicals are also listed in table 10. For toxic effects estimation, the time of exposure must be accounted and may vary according to dispersion model applied (e.g. 10 minutes for GPM).

Table 9: Probit correlations for different types of exposure [31]

Type of injury	Probit function	
Deaths from heat radiation	$Y = -14.9 + 2.56 \ln\left(\frac{tI_s^{4/3}}{10^4}\right)$	(3.47)
Deaths from lung hemorrhage (overpressure)	$Y = -77.1 + 6.91 \ln(P_s)$	(3.48)
Deaths from impact (overpressure)	$Y = -46.1 + 4.82 \ln(i_s)$	(3.49)
Structural damage (overpressure)	$Y = -23.8 + 2.92 \ln(P_s)$	(3.50)
Deaths from ammonia release	$Y = -35.9 + 1.85 \ln\left(\sum C^2 t\right)$	(3.51)
Deaths from chlorine releases	$Y = -8.29 + 0.92 \ln\left(\sum C^2 t\right)$	(3.52)

where time of exposure (t) is defined in seconds, heat flux (Is) is define in W/s, peak overpressure (Ps) is defined in pascals, impact (i_s) is defined in Ns/m^2, and concentrations (C) in ppm.

Once variable Y is known, it is converted to a probability of response by:

$$P = 50\left[1 + \frac{Y-5}{|Y-5|}\,\mathrm{erf}\left(\frac{|Y-5|}{\sqrt{2}}\right)\right] \tag{3.53}$$

where erf is the error function. This formulation is used to estimate the probability of a fatal incident and structural damage, which are fundamental to construct risk maps.

4. QUANTITATIVE RISK ASSESSMENT

This section describes the quantitative risk assessment (QRA) method developed for the layout optimization and facility siting. QRA is a probabilistic technique employed to estimate the risk from a particular process equipment or process unit [30]. Its aim is to support designers during layout modifications of existing or design of new facilities. Particular attention is given to on-site placement of high occupancy buildings such as control rooms or administrative buildings; however, this methodology can also be extended to far-field effects, helping decision makers in land use planning when combined with geographic information systems (GIS). Additionally, it provides a screening tool for possible events with major impacts, which should be further analyzed by more detailed techniques (*e.g.* CFD modeling) to account site specificities such as the degree of confinement or congestion, and geometry details.

This research provides a methodology to estimate overall risks from different possible undesirable incidents inside a chemical plant and a computer program has been developed. The program is able to assess the frequency of each outcome and its potential to cause deaths and structural damage given a set of equipment defined by the user. Then, for each set, individual risk curves are combined to obtain the overall risk. The results are then expressed as a plot of structural damage risk and individual risks varying with distances.

4.1 Overview of the Methodology

The proposed methodology starts with segregating all process equipment in different modules or process units with predefined locations. Then, a description of each unit or equipment is included specifying the module size (width and length), list of equipment and chemicals, process conditions, and the number of "virtual leak locations" [28].

The second step is to identify hazardous scenarios that either affect building occupants or escalate to another event. This analysis is conducted for each module separately. As discussed in Section 3, specific outcomes of concern are those involving fire, explosion, and toxic releases that may impact employees, buildings and equipment inside chemical plants. Hazards from runaway reactions, dust, and cryogenic materials are not considered, but it can be included in the model. Figure 6 illustrates the list of all possible undesired outcomes included given the process conditions and the chemicals involved. If a flammable material is present, then jet fires, flash fires, VCE, BLEVE followed by fireball, and pool fire may be possible depending of the process conditions. However, a BLEVE can also take place in case a pressurized tank storing non-flammable material catastrophically fails.

Once all hazardous events are known, the potential damage can be assessed and risks curves can be calculated for each module. Alghamdi [28] and Ramirez *et. al.*[29] proposed similar methodologies to calculate explosion risks from VCEs. Following the same direction, an approach was used to extend to other types of outcomes (see Figure 7). Given a specific equipment, hole leak sizes and their frequency of occurrence are obtained

from generic data [46, 47]. Then, the equipment type, hole size, and leak location are selected randomly by Monte Carlo simulation to calculate the discharge rate (see section 2.1), which is applied to estimate ignition probabilities (see section 2.3). Therefore, the frequency of each fire scenario is obtained combining leak frequency and ignition probabilities.

At the same time consequence modeling is performed. For scenarios that are not influenced by atmospheric conditions (*e.g*. BLEVE, jet fires, and pool fires), the affected area is estimated following equations listed in Section 3. Otherwise, a dispersion model (GPM or Britter and Mcquaid model) needs to be first employed to estimate gas cloud volumes, flammability zones and concentration isocontours using the release rate and leak location as well as randomly selected atmospheric conditions. Then, to predict damage from VCEs, the calculated cloud volume and the distances from the cloud center are included into the TNO multi-energy model to predict peak overpressures and positive impulses. As stated in Section 3, probit functions are applied to obtain the likelihood of fatalities and/or structural damage in case of VCEs, BLEVEs, pool fires, and toxic releases. For flash fires and jet fires, the flammability zone was considered as a fatal region- where the probability of fatality is equal to one. This process is repeated according to the number of iterations defined by the user. In each iteration, the risk curves are calculated and stored. Once all iterations are completed, the stored risk curves are used to obtain the risk distributions at particular points. The methodology has been implemented by developing a script program in Matlab. The program has been designed to calculate overall risk contours to support decision maker during the design phase. Even though it

does not take into account the effectiveness of mitigation systems, it can still be applied as a screening tool for comparison of potential layouts.

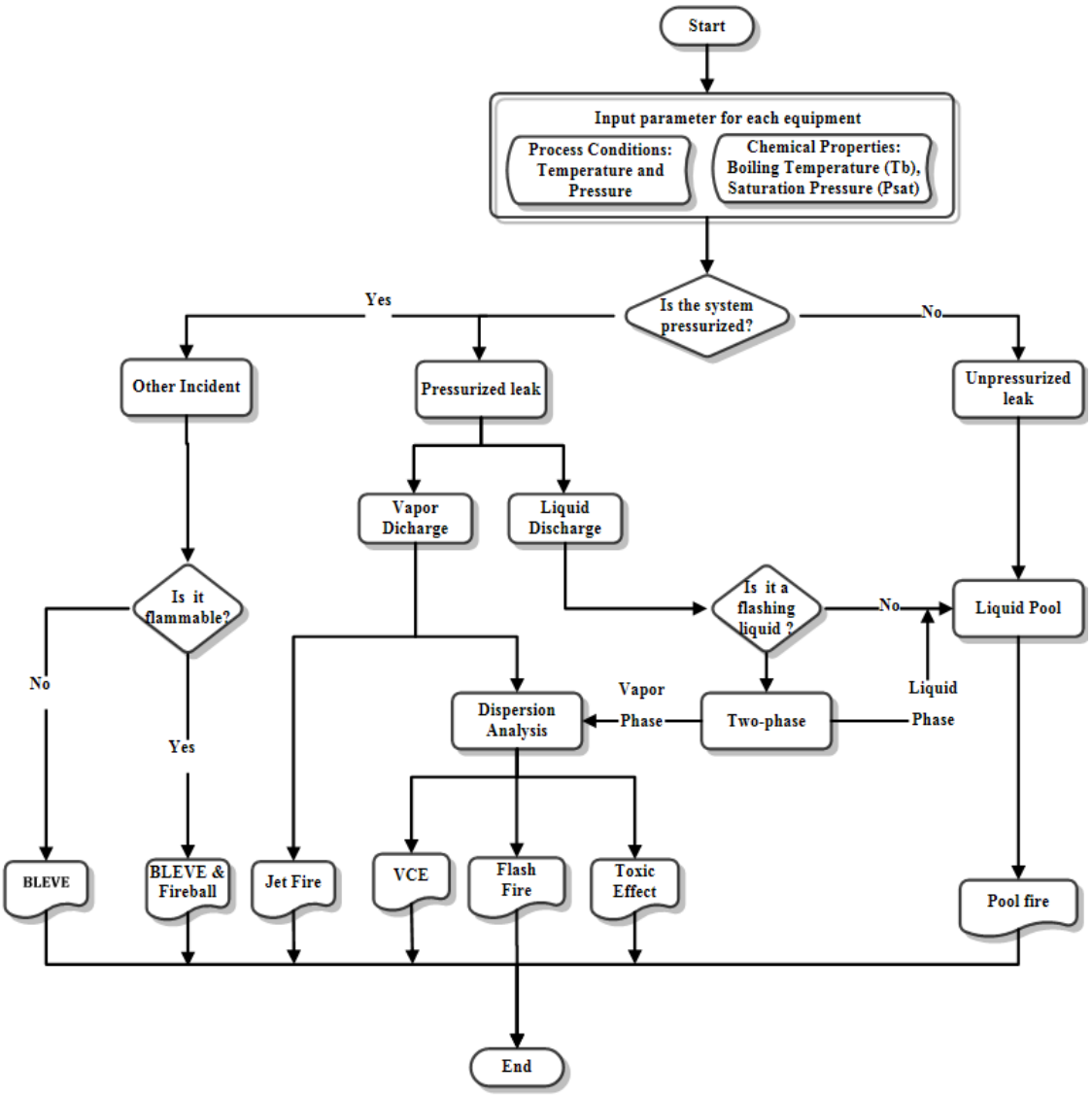

Figure 6: Possible outcomes scenarios based on process conditions (modified from [34])

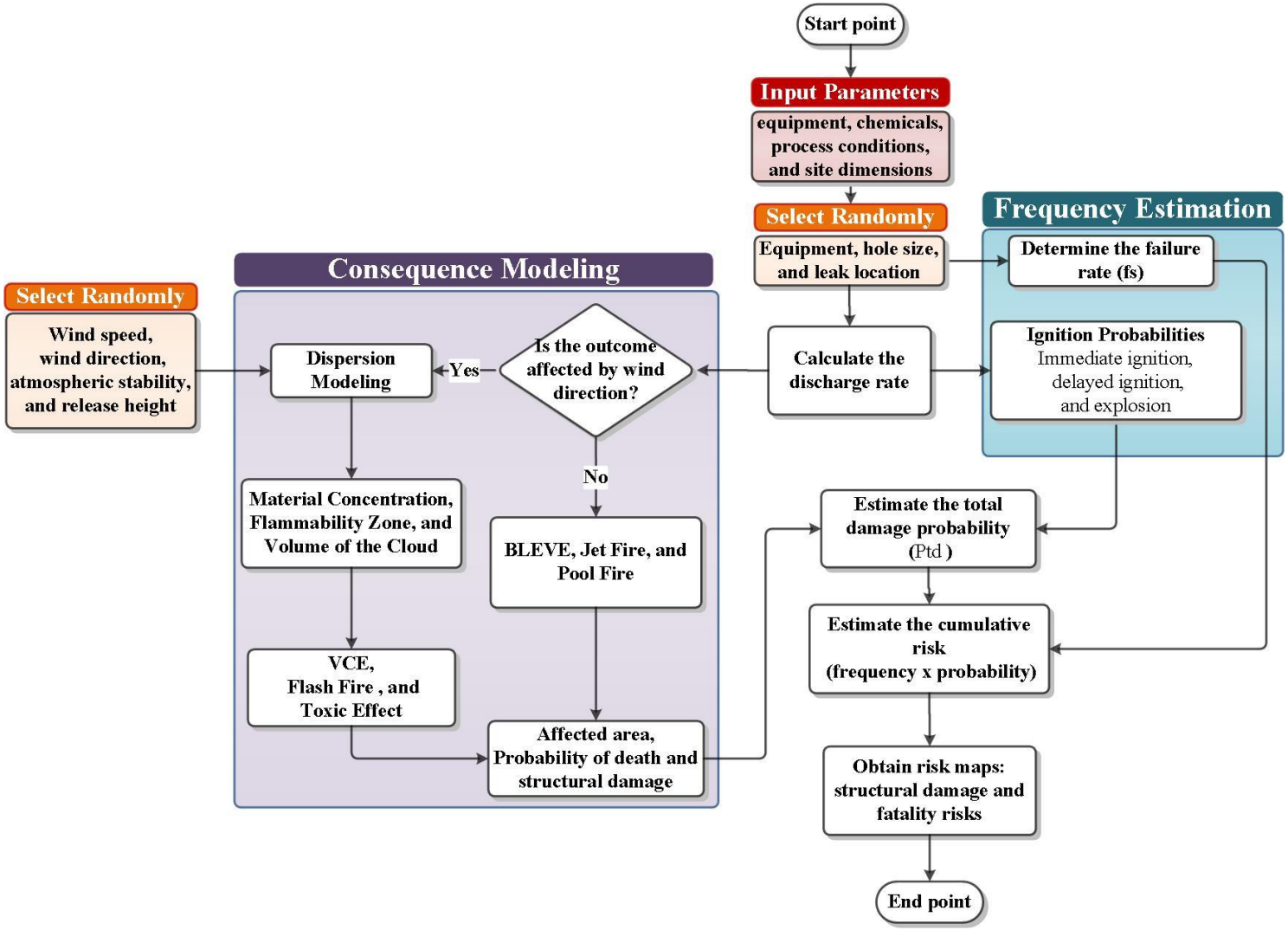

Figure 7: Methodology used for current research explaining how consequence model and frequency estimation are combined to estimate the risk of each outcome scenario

4.1.1 Scenario Frequencies

For this work, it is proposed to classify initiating events into two categories: continuous and catastrophic releases. Continuous releases are caused by the presence of holes in the process equipment resulting in small release rates while catastrophic events occur from equipment rupture leading to the discharge of the total containment within a short time. The primary objective of this distinction is to make sure that the worst-case scenario has been considered, and the risk has not been underestimated. The failure frequency of each initiating event can be obtained from generic data [46, 47]. Table 10 shows the release rates for steel process pipes with different diameters according to the initiating event.

Following the bowtie graphs showed in Section 3 (Fig. 3 and Fig. 4), the frequencies of each fire scenarios can be obtained combining initiating event frequencies and ignition probabilities (Table 12).

Table 10: Frequency release for steel process pipe [18]

Initiate Event	**Hole diameter range (mm)**	**Pipeline diameter**		
		50 mm	150mm	450 mm
Continuous	1 to 3	5.5 E-05	2.6 E-05	2.3E-05
	3 to 10	1.8E-05	8.5E-06	7.5E-06
	10 to 50	7.0E-06	2.7E-06	2.4E-06
	50 to 150	0.0E-06	6.0E-06	3.6E-07
	>150	0.0E-06	0.0E-06	1.7E-07
Catastrophic		7.0E-06	6.0E-06	1.7E-07

Table 11: Estimation of initiating events probability

Possible Scenario	Equation	
BLEVE	$P_{BLEVE} = P_{imm.ing}$	(4.1)
Jet Fire	$P_{JF} = P_{imm.ing}. P_{jet.dir}$	(4.2)
VCE	$P_{VCE} = (1 - P_{imm.ing}). P_{del.ign}. P_{exp\,\|del.ign}$	(4.3)
Flash Fire/ Pool Fire	$P_{ff/Pf} = (1 - P_{imm.ing}). P_{del.ign}. (1 - P_{exp\,\|del.ign})$	(4.4)
Environmental Release	$P_{ER} = (1 - P_{imm.ing}). (1 - P_{del.ign})$	(4.5)

where $P_{imm.ign}$, $P_{del.ign}$, and $P_{exp\,|del.ign}$ refer to the ignition probabilities for immediate ignition, delayed ignition, and explosion given a delayed ignition, respectively; and $P_{jet.dir}$ represents the probability of jet fire at certain direction.

4.1.2 Risk Estimation

The risk calculated in this methodology takes into account the frequency of initiating events, and the probability of occurrence multiplied by the damage likelihood of all possible outcomes that might occur in a specific module. The risk is evaluated for each scenario separately and further combined.

$$r_{i,j} = F_n * Pt_{i,j} \tag{4.6}$$

where

$$Pt_{i,j} = 1 - \prod_{k=1}^{K} (1 - P_k * Pdamage_{k,i,j}) \tag{4.7}$$

Here *k* represents each possible outcome; *i* and *j* are the Cartesian coordinates; P_k is the likelihood of scenario k; $Pdamage_{k,i,j}$ is the probability that event k causes damage at coordinates (i, j); and F is the frequency of each initiating event.

Equation (4.6) is used to estimate both fatality risks and structural damage risks. The frequencies of each scenario and its respective damage probability have already been discussed.

4.1.3 Monte Carlo Simulation

Since risk is a function of consequence and frequency, it is highly influenced by uncertain parameters such as failure rate, atmospheric conditions, release size, *etc* [29]. Large uncertain values for risk play an important role and may influence decision makers. Based on that, Monte Carlo simulation is conducted to propagate the uncertainties of each variable and calculate the range for the risk at a particular distance, instead of just point values. Each uncertain parameter was treat as a stochastic variable represented by probability distributions functions. For sake of simplicity, variations pertaining only to leak locations, leak source, hole size, release height, atmospheric stability, and wind speed and directions were included in the code. Constant values were assumed of the other factors.

4.1.4 Number of Leak Locations

The number of leak locations is defined by the user and it starts by specifying the length and width of the module as well as the distance between each element in the x and y directions. Then, the module area is divided in equally distributed grid points, which will be treated by the program as leak sources (see Figure 8). If the number of leak location is set to 1, then all releases are modeled as coming from the center point of the process module. Once the number of elements is defined, the leak position is selected randomly. It should be noted that it is role of the user to decide the optimum number of leak points which varies with module size and number equipment interconnections [28]. It is suggested as a rule of thumb to use grid size between 1 m^2 to 4 m^2 when considering the number of elements [28].

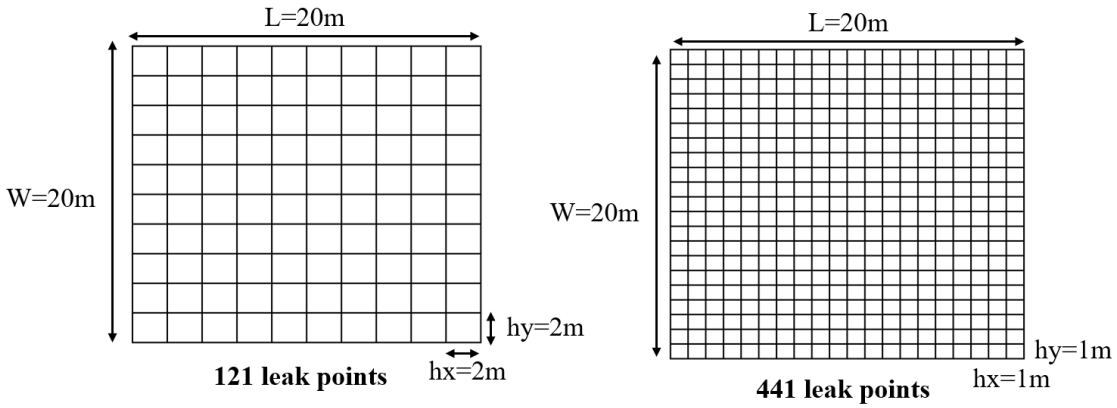

Figure 8: Different numbers of leak points according to the user specifications

4.2 Safety Distances to Prevent Domino Effect

Domino effect has been a major contributing factor for the severity of various industrial accidents. Although several works have been published to quantitatively assess domino effects [48-50], there is still divergent opinions among researchers regarding the proper definition of this term [51]. According to CCPS [30], the domino effect is "an incident which starts in one item and may affect nearby items by thermal, blast or fragment impact, causing an increase in consequence severity or in failure frequencies."

Thus, as suggested by Cozzani *et al.* [52], three elements must be in place in order to originate a domino effect:

i) The primary accident scenario, which leads to a domino effect;

ii) The escalation vector, which acts on secondary targets propagating the domino effect; and

iii) Secondary events due to the escalation vector, which may affect different plant units.

It should be clear that primary accidents alone do not characterize domino effects: an escalation event takes places if the severity of secondary scenarios is higher in respect to that of the initiating event [52].Thus, to assess the probability of escalation, it is crucial to first identify all primary scenarios with potential to damage secondary targets and further analyzes the consequences of secondary events. Modeling all possible domino scenarios is not a simple task and may be time-consuming since the number of secondary events grows exponentially as more equipment are added. Therefore, the complexity of domino effect assessment may vary according to the context and purpose of the analysis

[51]. A simple approach to address domino effect is to determine "inherent safe distances", which are the minimum separation distances between equipment necessary to prevent escalation events, early in the design stage [53].

Safe distances are based on threshold values that describe "the minimum intensity of primary scenarios able to trigger escalation"[26]. Even though those values can be adequately applied, there is still a lack of agreement among researchers and regulatory agencies regarding minimum values able to cause damage to equipment [26]. The large uncertainty in threshold values, which may differ in orders of magnitude, is related to the complexity of the escalation phenomena and depends on the characteristics of primary events, escalation vectors, and target units.

There are three main escalation vectors with potential to cause a domino effect: heat radiation or flame impingement, overpressure, and fragment projection [52]. Primary scenarios that have the potential to trigger those escalations vectors are listed in Table 12. Toxic release is not included since it does not lead to loss of containment (LOC) or any structural damage. In this research, effects of fragment projection are not included given the inaccuracy of current models. Additionally, safe distances were estimated based on threshold values recommended by Cozzani *et al.*[52], which depends mainly on primary scenarios.

Table 12: Escalation vector resulted from different primary events [52]

Primary event	Escalation Vector
Pool Fire	Radiation, fire impingement
Jet Fire	Radiation, fire impingement
Fireball	Radiation, fire impingement
Flash Fire	Fire impingement
BLEVE	Fragment projection, overpressure
VCE	Overpressure, fire impingement

Due to their short duration, flash fires are unlikely to cause damage to others equipment. However, if a potential source of fuels such as floating roof tanks storing flammable vapors is presented, the flammability zone extension should be considered as minimum distance [52]. Escalation due to fireball is not credible either for both atmospheric and pressurized tanks, unless fire directly contacts a nearby unit [53]. Therefore, safety distances are delimited by the fireball radius.

In the case of jet fires, the safety distance depends on the maximum flame length and the thermal radiation emitted. If equipment is engulfed by a fire or it is the proximity of a jet flame, the time to failure will depend on the type of equipment: atmospheric vessels can stand more than 15 min when located within 50m from the flame envelope while pressurized vessels this may stand up to 13 min before it fails [26]. However, since pressurized vessels are usually protected by both passive and active protective devices, an escalation event is not credible for long distances (greater than 25m) from the flame envelope [52].

For pool fires, LOC is considered if equipment is exposed to a certain heat radiation during a minimum exposure time; for this work, atmospheric vessels at distances

lower than 50m from pool limits will lead to escalation if the exposure time is greater than 15min [52, 54]. A conservative safety distance (20 m) is assumed for pressurized tanks.

For scenarios involving overpressure (*e.g.* BLEVE and VCE), threshold values for peak overpressure are applied to estimate the safe distances. All relations mentioned above, are summarized in Table 13. Finding inherently safe distances is the last stage of the QRA for this research and it includes all equipment with potential to cause primary accidents as well as all units that might be targeted. After deciding which unit or set of units (module) are likely to cause initiating events, all steps mentioned in Section 4.1 are followed to estimate the frequency (per year) of escalation events. However, in this particular case, escalation criterion (see Table 13) are employed instead of probit functions; thus, probability of having a propagation (Pd) is equal to 1 if the physical effects affecting a secondary unit exceeds the threshold values, otherwise Pd is equal to 0. Like risk maps, distributions for the risk of domino effect are obtained at specific position; then, decision makers may establish their criteria for safety distances. Once risk maps and safety distances are defined, we move forward for the layout optimization, which is described in the following chapter.

Table 13: Damage thresholds and safety distances to prevent escalation (adapted from [26])

Scenario	Escalation vector	Modality	Target unit	Escalation criteria	Safety Distance
Flash fire	Heat radiation	Fire impingement	All	Escalation unlikely	-
Fireball	Heat radiation	Flame engulfment	Atmospheric	I>100 kW/m^2	Maximum flame distance
			Pressurized	Escalation unlikely	-
Jet fire	Heat radiation	Fire impingement	All	Flame envelope	Maximum flame distance
Pool fire	Heat radiation	Flame engulfment	All	Flame envelope	Maximum flame distance
VCE and BLEVE	Overpressure	Blast wave interaction	Atmospheric	P>22 kPa	Respective scaled distance
			Pressurized	P>20 kPa	Respective scaled distance
			Elongated (toxic)	P>20 kPa	Respective scaled distance
			Elongated (flammable)	P>31 kPa	Respective scaled distance

Here *I* represents the heat flux, and P is the peak overpressure.

5. LAYOUT OPTIMIZATION FORMULATION

In this chapter the steps proposed to solve the layout optimization problem are presented. Once all risk mapping and safety distances are established (Chapter 4), a mathematical formulation using Mixed Integer Linear Programming (MILP) is applied to find the location of inhabited buildings and new equipment in order to minimize the total capital cost associated with structural damage risk, fatality risk, pipeline interconnection, and protective devices. Individual risk criteria were set as an additional constraint for high occupancy buildings, meaning that the overall risk for buildings such as control room or lab may not exceed this criterion. In the end, the final layout will be obtained based on minimal cost and the risk acceptance criteria (RAC).

5.1 General Description

Layout optimization can be formulated in two distinct manners: continuous plane and grid-based methods [55]. In the continuous plane method, different hazardous scenarios have been represented by non-linear equations which have been incorporated into the layout formulation [7, 21, 23]. The problem with this approach is that achieving global minimum becomes more challenging as the number of non-linear equations increases [7]. For grid-based methods, non-linear equations can be avoided and the optimal result is obtained more easily if the problem is feasible. In this case, each facility can either occupy one single grid with fixed size or multiple grids. In this study, both

assumptions are possible however, if multiple grids are occupied by at least one facility, additional constraints must be included.

As proposed by Jung *et al.*[9], the formulation starts dividing the plant area into a specific number of grids (n) with different coordinates, x_k and y_k. Then, each module (set of processing equipment) must be placed according to the recommendations provided by the standards such as API 752 and good engineering practices. Finally, new facilities (mainly inhabited buildings and storage tanks) are to be allocated in the remaining grids based on minimal costs and additional constraints. The optimization problem is solved by using CPLEX with GAMS software environment. The following sections provide the necessary information and constraints implemented in the model.

5.2 Sets, Scalars, and Parameters

All sets, scalars, and parameters used in the formulation are described as follows:

$\boldsymbol{e} \in \boldsymbol{E}$	set of possible escalation vectors (overpressure and fire impingement)
$\boldsymbol{f} \in \boldsymbol{F}$	set of all facilities to be allocated
$\boldsymbol{g} \in \boldsymbol{G}$	set of fixed modules
$\boldsymbol{i} \in \boldsymbol{I}$	set of units to be allocated
$\boldsymbol{j} \in \boldsymbol{J}$	set of high occupancy buildings to be allocated
$\boldsymbol{k} \in \boldsymbol{K}$	set of grids to be included in the plant site
$\mathbf{x_k}$	the x-position of each grid
$\mathbf{y_k}$	the y-position of each grid

$\mathbf{RD_{k,m}}$	the rectilinear distance of between the k-th grid and the m-th fixed module
$\mathbf{D_{m,f}}$	the minimum separation distances between units
$\mathbf{SD_{A,B,e}}$	the minimum distance between units A and B to prevent escalation event e
$\mathbf{UP_{f,m}}$	the interconnection cost between item f and m
$\mathbf{MCost_{p,e}}$	the cost of mitigation system p to protect from escalation vector e
RAC	the risk acceptance criteria
M	a big M scalar for non-overlap constraints
$\mathbf{Connect_{m,j}}$	the binary parameter that indicates interconnection between module m and unit j
$\mathbf{NP_f}$	the expected number of workers at a facility f
$\mathbf{SR_k}$	the risk of structural damage at a particular grid
$\mathbf{FR_k}$	the risk of fatality at a particular grid
$\mathbf{FC_f}$	the facility cost

5.3 Variables

The following variables are applied in this formulation:

$\mathbf{x_f}$	final values for x positions of each facility, f
$\mathbf{y_f}$	final values for y positions of each facility, f
$\mathbf{B_{f,k}}$	non-overlapping binary variable
Sep1 to Sep4	binary variables for separation distances constraints

$\mathbf{E1_{A,B,e}}$, $\mathbf{E2_{A,B,e}}$ binary variables for escalation zones constraints

$\mathbf{ProtDevice_{p,b,e}}$ binary variable that defines the assignment of passive mitigation systems to prevent escalation to a unit B (1 if protective device P is assigned to unit B, 0 otherwise)

5.4 Constraints

All constraints used in the formulation are detailed in the following sections.

5.4.1 Non-overlapping Constraints

A binary variable $B_{f,k}$ was implemented as suggested by Georgiadis and Macchietto [18] to ensure that all f facilities are allocated in different grids.

$$B_{f,k} = \begin{cases} 1, & \text{if facility f is placed at grid n} \\ 0, & \text{otherwise} \end{cases}, \quad \forall f \in F, \forall k \in L$$

$$\sum_{k=1}^{L} B_{f,k} = 1, \qquad \forall f \in F \tag{5.1}$$

$$\sum_{f=1}^{F} B_{f,k} = 1, \qquad \forall k \in K \tag{5.2}$$

The locations of pre-defined modules are fixed as follows:

$$B_{g,l} = 1, \qquad \forall g \in G, \forall l \in L \tag{5.3}$$

5.4.2 Facility Boundary Constraints

The facility boundary constraints operate assuring that all midpoints (x_f and y_f) do not assume any value different from the grid coordinates (x_k and y_k).

$$-\mathrm{M}\left(1-\mathrm{B}_{\mathrm{f,k}}\right) \leq \mathrm{x}_{\mathrm{k}}-\mathrm{x}_{\mathrm{f}} \leq \mathrm{M}(1-\mathrm{B}_{\mathrm{f,k}}) \tag{5.437}$$

$$-\mathrm{M}\left(1-\mathrm{B}_{\mathrm{f,k}}\right) \leq \mathrm{y}_{\mathrm{k}}-\mathrm{y}_{\mathrm{f}} \leq \mathrm{M}(1-\mathrm{B}_{\mathrm{f,k}}) \tag{5.5}$$

Once all midpoints are known, the distances between new facilities and fixed modules can be obtained. This procedure starts by estimating and storing rectilinear distances from an individual grid to fixed modules ($\mathrm{RD}_{\mathrm{k,m}}$). Then, as a facility is being allocated to a particular grid, it will be assigned to its respective $R\mathrm{D}_{\mathrm{k,m}}$. Using rectilinear distances rather than Euclidean distances approaches the piping costs estimation to the real industrial application [19].

5.4.3 Separation Distances Constraints

The minimum separation distance constraints determine how far away one facility should be from another. It can be applied in addition to Equation (5.2) to prevent overlaps in case a facility occupies multiple grids. Moreover it is also employed when safe distances should be maintained between process equipment and inhabited building. The general expression for minimum separation distances is given by

$$|\mathrm{x}_{\mathrm{m}}-x_{\mathrm{f}}|\ +|y_{\mathrm{m}}-y_{\mathrm{f}}| \geq \mathrm{D}_{\mathrm{m,f}} \tag{5.6}$$

where subscript m refers to the subset of new facilities. This general expression can be rewritten by using Big-M method.

$$(\mathrm{x}_{\mathrm{m}}-x_{\mathrm{f}})\ +(\mathrm{y}_{\mathrm{m}}-\mathrm{y}_{\mathrm{f}}) \geq \mathrm{D}_{\mathrm{m,f}}.\mathrm{Sep1}_{\mathrm{m,f}}-\mathrm{M}(1-\mathrm{Sep1}_{\mathrm{m,f}}) \tag{5.7}$$

$$(\mathrm{x}_{\mathrm{m}}-\mathrm{x}_{\mathrm{f}})-(\mathrm{y}_{\mathrm{m}}-\mathrm{y}_{\mathrm{f}}) \geq \mathrm{D}_{\mathrm{m,f}}.\mathrm{Sep2}_{\mathrm{m,f}}-\mathrm{M}(1-\mathrm{Sep2}_{\mathrm{m,f}}) \tag{5.8}$$

$$-(\mathrm{x}_{\mathrm{m}}-\mathrm{x}_{\mathrm{f}})\ +(\mathrm{y}_{\mathrm{m}}-\mathrm{y}_{\mathrm{f}}) \geq \mathrm{D}_{\mathrm{m,f}}.\mathrm{Sep3}_{\mathrm{m,f}}-\mathrm{M}(1-\mathrm{Sep3}_{\mathrm{m,f}}) \tag{5.9}$$

$$-(x_m - x_f) - (y_m - y_f) \geq D_{m,f}.\,Sep4_{m,f} - M(1 - Sep4_{m,f}) \quad (5.10)$$

$$Sep1_{m,f} + Sep2_{m,f} + Sep3_{m,f} + Sep4_{m,f} \geq 1 \quad (5.11)$$

Here, D_{mf} represents the minimum separation distance between m-th and f-th facilities; $Sep1_{m,f}$ to $Sep4_{m,f}$ are binary variables; and M is the proper upper bound.

5.5 Inherently Safety Zones and Mitigation Systems Constraints

The main purpose of including safety zones is to prevent domino effects. In Chapter 4, a methodology was presented to calculate inherently safe distances between process equipment. These distances are defined depending on the risk tolerance and, once estimated, they determine how far new process equipment should be from other new equipment and fixed modules. Two safety zones are defined: one to prevent escalation from overpressure and another to protect from fire impingement (see Figure 9).

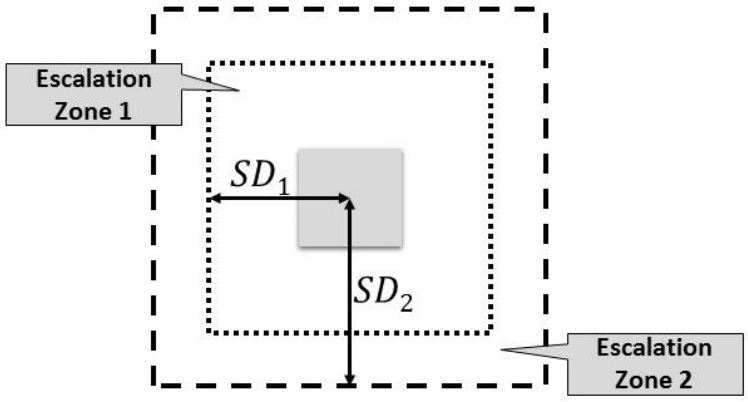

Figure 9: Visual representation of inherently safety zones (modified from [24])

Each hypothetical zone should not englobe any possible targeted unit, unless this unit is equipped with protective devices. To ensure that all safety distances are maintained, a set of constraints suggested by Hans *et al.* [24] were used.

$$(x_A - x_B) + M(E1_{A,B,e} + E2_{A,B,e}) \geq SD_{A,B,e} \tag{5.12}$$

$$(x_A - x_B) + M(1 - E1_{A,B,e} + E2_{A,B,e}) \geq SD_{A,B,e} \tag{5.13}$$

$$(y_A - y_B) + M(1 + E1_{A,B,e} - E2_{A,B,e}) \geq SD_{A,B,e} \tag{5.14}$$

$$(y_A - y_B) + M(2 - E1_{A,B,e} - E2_{A,B,e}) \geq SD_{A,B,e} \tag{5.15}$$

where subscripts A refers to the units with potential to cause initiating events; subscript B refers to possible targeted units; $SD_{A,B,e}$ represents the inherently safety distance given a specific escalation vector; and $E1_{A,B,e}$ and $E2_{A,B,e}$ are binary variables. This set of constraints is applied separately for each escalation zone individually, represented by subscript e.

When a targeted unit is protected by mitigation systems, the likelihood of escalation events is reduced [50]. Consequently, minimum separation distances are reduced by a factor ($RF_{p,e}$) depending on the protective device configuration employed. Therefore, the final safety distances are calculated as follows.

$$SD_{A,B,e} = SD_{A,B,e}^{initial}\left(1 - \sum_{P} RF_{p,e}.\, ProtDevice_{p,b,e}\right) \tag{5.16}$$

$$\sum_{P} ProtDevice_{p,b,e} \leq 1, \qquad \forall b \in B, \forall e \in E \tag{5.17}$$

Expression (5.17) limits one mitigation system configuration per unit, meaning that it can be either one protective device or a combination of multiples devices.

5.6 Risk Acceptance Criteria (RAC)

Individual risk criterion was used as an additional constraint for high occupancy buildings, which means that the overall risk for facilities such as control room or lab may not exceed this specific limit. This RAC is subjected to the organization's risk perceptions and risk attitudes (risk neutral, risk averse or risk seeking); however, the UK Health and Safety Executive (HSE) proposes a "tolerable criteria" (10^{-3} per annum) for employees working in harzadous areas [56]. Once RAC is defined, the following constraint is applied.

$$\sum_{k} B_{k,j}.\,\mathrm{FatalRisk}_{k} \leq \mathrm{RAC}, \qquad \forall j \in J \tag{5.18}$$

where j refers to inhabited buildings.

5.7 Objective Function

The objective function is a combination of total cost (TC) and total damage costs (TDC). The first term includes costs of interconnection between new facilities and fixed modules plus protective device configuration costs. TC ($) is expressed as follows:

$$\mathrm{TC} = \sum_{k=1}^{K}\sum_{f=1}^{F}\sum_{m=1}^{M} \mathrm{RD}_{m,k}.\,\mathrm{Connect}_{m,j}.\,\mathrm{IC}_{f,m}.\,B_{f,k} + \sum_{b=1}^{B}\sum_{p=1}^{P}\sum_{e=1}^{2} \mathrm{ProtDevice}_{p,b,e}.\,\mathrm{MCost}_{p,b,e} \tag{5.19}$$

where $\mathrm{Connect}_{m,j}$ is the parameter that indicates interconnection between item m and j; $\mathrm{IC}_{f,m}$ is the interconnection cost; and $\mathrm{MCost}_{p,e}$ is the purchase and maintenance cost of protective device configuration p in item b to prevent escalation e.

In addition to TC, costs due to the potential loss of life and structural damage are also included.

$$\mathrm{TDC} = \sum_{k=1}^{K} \sum_{f=1}^{F} (\mathrm{SR}_k . \mathrm{FC}_f + \mathrm{FR}_k . \mathrm{NP}_f . \mathrm{Comp}) . \mathrm{B}_{f,k} . L \tag{5.20}$$

where SR_k and FR_k are the structural damage and fatality risks at grid k, respectively; NP_f is the expected number of worker nearby facility f; Comp is the compensation cost due to fatality; and L is the expected life time of the facility.

The challenge here is to address economic value to human life; even though it is not possible to monetize one person's life, this analysis is crucial to evaluate monetary losses due to fatalities resulted from LOC incidents. Based on the United States Department of Labor [57], a compensation cost of $1.000.000 per occupational death was used. Finally, the objective function contains the sum of costs defined in equations (5.19) and (5.20).

$$\min z = \sum_{k=1}^{K}\sum_{f=1}^{F}\sum_{m=1}^{M} \mathrm{RD}_{m,k}.\,\mathrm{Connect}_{m,j}.\,\mathrm{IC}_{f,m}.\,\mathrm{B}_{f,k}$$

$$+ \sum_{b=1}^{B}\sum_{p=1}^{P}\sum_{e=1}^{2} \mathrm{ProtDevice}_{p,b,e}.\,\mathrm{MCost}_{p,b,e} \qquad (5.21)$$

$$+ \sum_{k=1}^{K}\sum_{f=1}^{F} (\mathrm{SR}_{k}.\,\mathrm{FC}_{f} + \mathrm{FR}_{k}.\,\mathrm{NP}_{f}.\,\mathrm{Comp}).\,\mathrm{B}_{f,k}.\,L$$

6. CASE STUDY

The proposed methodology was applied to a case study taken from CCPS [30] and Jung *et al.*[9] which is described in the following sections.

6.1 Case Description

This example case deals with a distillation column that separates hexane and heptane from a feed stream. It is assumed that there is single hazardous unit composed by a distillation tower, an accumulator, a steam reboilers, two pumps, one heat exchanger, three control valves, and steel pipes with three different diameters (0.10 m, 0.15 m, and 0.50 m). Figure 10 shows the process flow diagram. The distillation column operates at 4 barg and the temperature ranges from 130^{o}C on top to 160^{o}C at the bottom. The entire inventory of the mixture is 28,000 kg which is distributed among the reboiler and the column bottom (6,000 kg), column trays (10,000 kg) and accumulator drum (12,000kg).

All process equipment and operating conditions are listed in Table 14. To generate releases scenarios, it is assumed that each equipment has the same likelihood of leaking. Thus, a discrete uniform distribution is applied in the program; the number of leak locations was set as 121 following the recommended grid size of 1 m^2 [28]. The releases scenarios are shown in Table 15; it was assumed that all equipment can lead to both continuous and instantaneous release, depending on the failure mode. The failure data was taken from OGP [46] and HSE [47] and are shown in Appendix B.

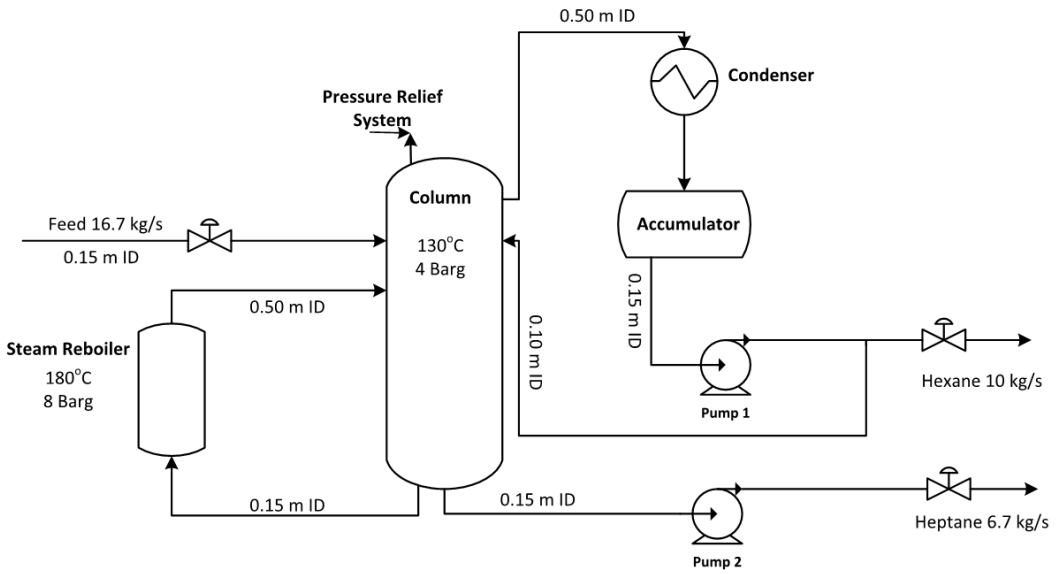

Figure 10: Flow diagram of the distillation unit (modified from [30])

Table 14: List of process equipment and process conditions

Equipment Type	Count	Pressure	Temperature
Process Vessel	3	4 Barg / 8 Barg*	130°C/180 °C*
Valve	3	4 Barg	130°C
Pump	2	4 Barg	130°C
Heat Exchanger	1	4 Barg	130°C
Steel pipe (0.50 ID)	10	8 Barg	180°C
Steel pipe (0.15 ID)	15	4 Barg	130°C
Steel pipe (0.10 ID)	25	4 Barg	130°C

* Conditions at the steam reboiler

If a catastrophic failure occurs, the entire containment is released within a short period. However, if a continuous release takes places, the maximum release time is set to be 10 minutes to account for the emergency response. The bowtie graphs are shown in Figure 4 and Figure 5. Five possible outcomes are considered: BLEVE, VCE, jet fire, flash

fire and pool fire. The toxicity effect is negligible since the unit does not process any toxic chemical. Because the vapors of both hexane and heptane are heavier than the air, the dense gas dispersion model was used.

Table 15: List of release scenarios

Nº	Scenario
1	Release from 100 mm steel pipes
2	Release from 150 mm steel pipes
3	Release from 500 mm steel pipes
4	Release from 150 mm valves
5	Release from 150 mm Hexane pump
6	Release from 150 mm Heptane pump
7	Release from Column (process vessel)
8	Release from Accumulator (process vessel)
9	Release from Steam Reboiler (process vessel)
10	Release from Heat Exchange (process vessel)

Eight wind directions are included and their respective probabilities are listed in Table 16 [30]. All stability classes (A-F) were considered and the wind speed was randomly selected between 1 to 6 m/s. A uniform distribution was addressed to the release height ranging from 0 m (ground source) to 20 m (unit height).

Table 16: Wind directions and their respective probabilities for the plant site

Slice	Direction	Angular degree (deg)	Probability
1	N	0	0.1
2	NE	45	0.1
3	E	90	0.1
4	SE	135	0.1
5	S	180	0.15
6	SW	225	0.2
7	W	270	0.15
8	NW	315	0.1

6.1.1 Layout Information

For the layout study, information was taken from Jung *et al*. [9]. A flat area of 100 m in the east direction and 100 m in the north direction is considered and the expected lifetime of the processing plant is 50 years. The separation unit is located in the middle point (50, 50) and its dimension is 20m x 20m. There are seven facilities to be allocated, the main control room, an office building, a maintenance building, three storage tanks and one utility. Table 17 lists all the parameters for each unit.

Common industrial safety distances between inhabited buildings and hazardous units were applied (see Table 18). These constraints were in the form of Equations (5.12) to (5.15).

Table 17: Description of facilities inside the plant

Nº	Unit	Dimension (m x m)	People Nearby	Equipment Cost ($)	Interconnection cost ($/m/year)
1	Control room	10 x 10	10	1,000,000	10
2	Office	10 x 10	200	300,000	0.1
3	Maintenance Building	10 x 10	10	200,000	2
4	Small storage tank 1	10 x 10	1	100,000	100
5	Small storage tank 2	10 x 10	1	100,000	100
6	Large Storage Tank	10 x 10	-	150,000	1000
7	Utility	10 x10	5	500,000	50
8	Distillation unit	20 x 20	-	-	-

Table 18: Minimum separation distances (from AIChE [1])

Unit	Small storage tanks (U4,U5)	Large Tank (U6)	Utility (U7)	Distillation Unit
Control room (U1)	30 m	76 m	30 m	50 m
Office (U2)	15 m	76 m	30 m	50 m
Maintenance bdg (U3)	15 m	76 m	30 m	50 m

The costs of including fire insulation, fire and blast resistance wall and each reduction factor are listed in Table 19. The decision whether included a mitigation system or not is applicable to all storage tanks given their potential for secondary incidents.

Table 19: Parameters for protective devices (adapted from [58])

Equipment	Protective device costs		
	Fire Insulation	Fire Wall	Barricade
Small Storage Tanks	2,000 $	15,000 $	30,000 $
Large Storage Tank	3,000 $	20,000 $	60,000 $
Reduction Factor	**0.5**	**0.9**	**0.9**

6.2 Results and Discussion

6.2.1 Quantitative Risk Assessment

Risk maps for the distillation unit were calculated following the proposed stochastic approach and are shown in Figure 11 . A set of 10,000 combinations of different random variables was generated; each stochastic variable was selected with respect to its distribution function. Consequently, the outcome values for risk is a distribution rather than single values. From Figure 11, it should be noticed that, at a particular point, risk may assume values with different orders of magnitude depending on the intensity and frequency of a specific scenario. Moreover, it is observed higher values for fatality risks when compared to damage structure risk. This mainly results from the omission of flash fire effects on buildings and equipment. Given the short duration, flash fires usually do not affect nearby units unless it may act as a fuel source such as floating roof tank. However, when it comes to employee vulnerability, flash fires are considered fatal and flammability zones can be extensive in the case of catastrophic failures.

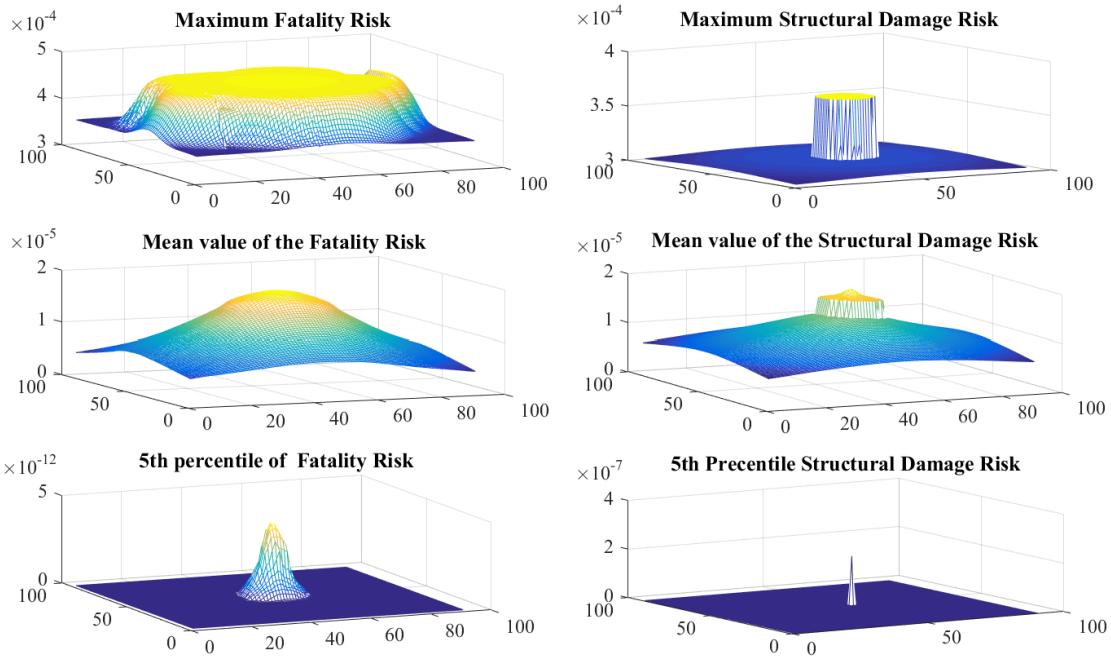

Figure 11: Risk maps for the distillation unit.

To better understand the variation of risk values at certain points, risk curves can be obtained. Figure 12 shows the risk curves at the center line of the facility, moving towards the east. At each point, the final outcome ranges from $1x10^{-15}$ to $1x10^{-4}$ (per year). A challenging task is to decide which values should be applied during the design phase; higher risks requires larger areas to be occupied, increasing layout costs; in contrast, lower risk reduces layout costs but it might underestimate the overall risk resulting hazardous options. This decision with the organization risk perception and risk attitudes and it is the role of designers to identify the values that best represent it. For a conservative approach, the 95^{th} percentile curve can be applied at the same time that, for a risk-neutral perspective, the mean values curve seems to be fittable.

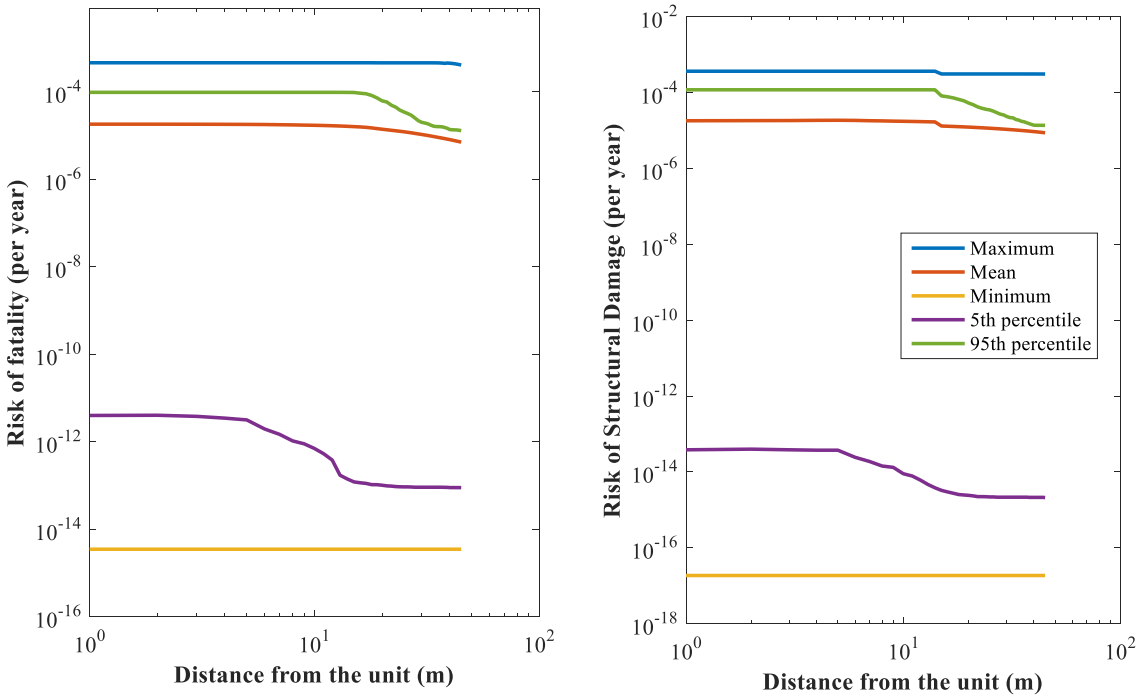

Figure 12: Risk curves at the facility center line in the east direction

Another application for this program is to investigate risk distributions at specific points of interest, which is useful during building vulnerability assessment posterior the layout configuration is defined.

Figure 13 shows boxplots for fatality and structural damage risks at 10m, 50m, and 80m from the distillation unit. The reduction of median values as well as lower and upper quartiles with distance confirms the statement that lower risk values are expected as we move away from the unit. Additionally, at longer distances, risk distributions tend to get wider characterizing a higher variability. A large number of outliers (represented by red points) might be related to catastrophic scenarios, which result in higher risk values. Finally, a non-symmetric shape is observed given the graph is expressed on log-scale.

Thus, a next step would be to investigate which non-symmetric distribution (*e.g.* Weibull, lognormal, exponential) better fits the data. Since is not the scope of this work to validate risk curves, this analysis was not performed.

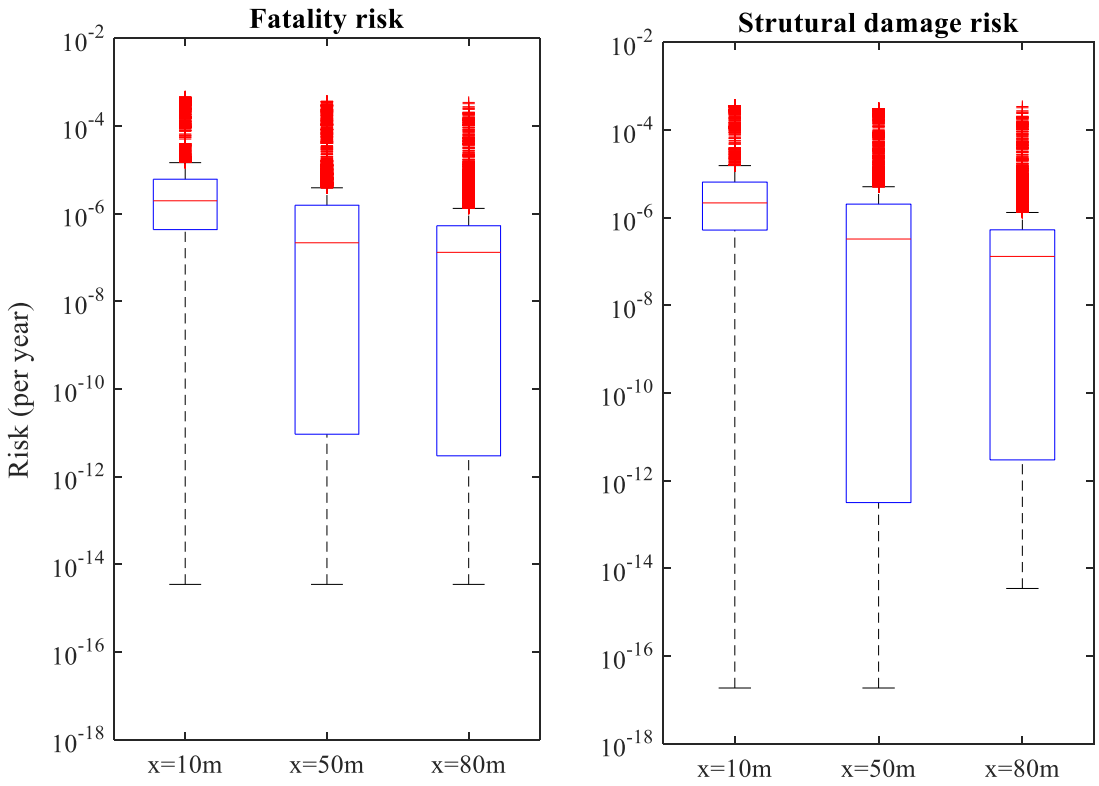

Figure 13: Boxplots of risk values at 10m, 50m and 80m from the distillation unit in the east direction

Safety distances to prevent domino effect can also be determined following the proposed methodology. For this particular example, all atmospheric tanks may be subjected to escalation and minimal distances should be kept between tanks and the

distillation unit. Using damage thresholds for atmospheric tanks (Table 13), frequencies of domino effect are calculated and the distances are chosen based on the risk acceptance criteria. Figure 14 presents two domino effect frequency profiles considering escalation due to overpressure (left side) and fire impingement (right side). Information regarding domino effect frequencies as we move far from the unit center was extracted and listed in Table 20.

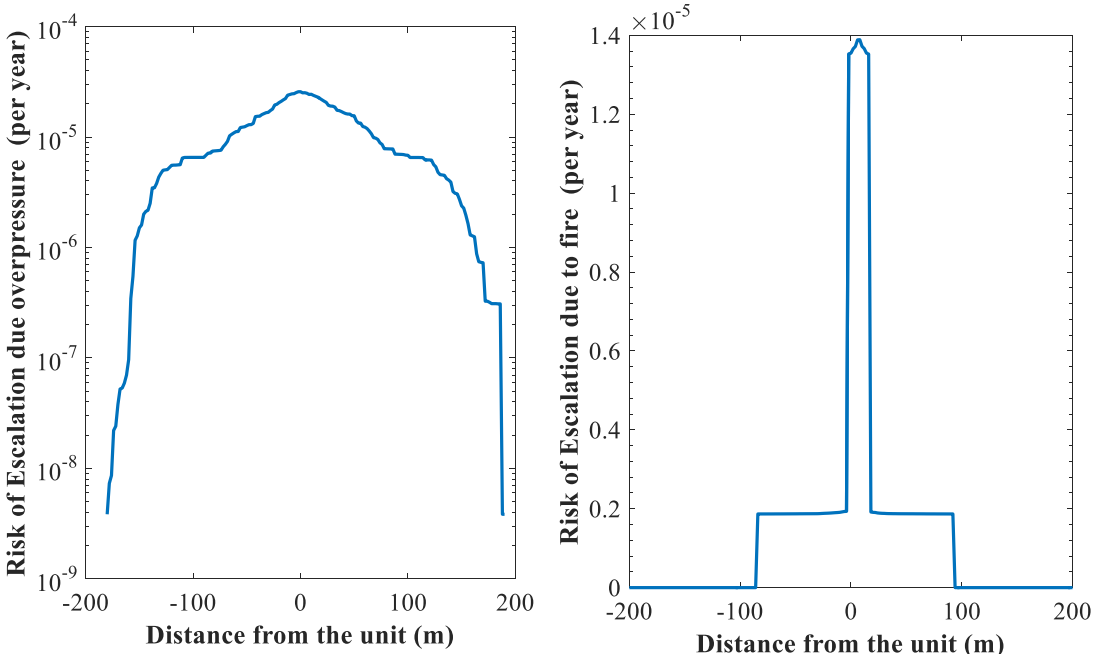

Figure 14: Domino effect frequencies profiles (mean values) according to the distances from the distillation module for storage tanks as target units

Table 20: Distances from the distillation module and its respective frequency of secondary events for a storage tank

Frequency of escalation (per year)	Distance from the distillation unit (m)	
	Overpressure	Fire Impingement
1×10^{-5}	63	16
1×10^{-6}	160	93
1×10^{-7}	187	-

As expected, the occurrence of secondary events reduces as we move far from the distillation module. It is also observed that higher distances are necessary to protect atmospheric tanks from overpressure. For example, if an atmospheric tank is located 63 m away from the distillation unit, one escalation event due to overpressure is likely to occur in 100,000 years; for fire impingement scenarios, this distance is reduced to 16 m. The same procedure was repeated for the largest storage tank and the information is presented in Table 21. Since BLEVE or VCE are not expected to occur in the case of releases from atmosphere tanks, only fire impingement was considered. It is important to notice that those results are applicable for tanks without containment (*e.g.* dikes); if the tank is surrounded by a barrier that prevents the liquid from spreading after spillage, the containment length should be used as a safety distance.

Table 21: Distances from the large storage tank and its respective frequency of secondary events for storage tank

Frequency of escalation (per year)	Distance from the distillation unit (m)
1×10^{-4}	30
1×10^{-5}	84
1×10^{-6}	100

Once safety distances and risk maps are obtained, the next is step is to perform a layout optimization.

6.2.2 Layout Optimization

Including all information mentioned in Section 6.2.2, the MILP model was solved using CPLEX in GAMS software. Four parameters were varied at two levels (risk maps: mean values and 95th percentile; safe distances from the distillation unit; safe distances from each tank; and risk acceptance criteria (RAC): 10^{-3} and 10^{-5} fatality per year. Figure 15 shows the resulting layouts for mean risk values; no difference was observed varying RAC. This behavior is not repeated when the 95th percentile is applied (see Figure 16). Each condition (a-d) refers to a specific combination of safe distances as listed in Table 22.

Table 22: Safe distances applied during layout optimization

Condition	Safe distance from the unit (m)		Safe distance from tanks (m)
	Overpressure	Fire	
(a)	63	16	30
(b)	63	16	84
(c)	160	93	30
(d)	160	93	84

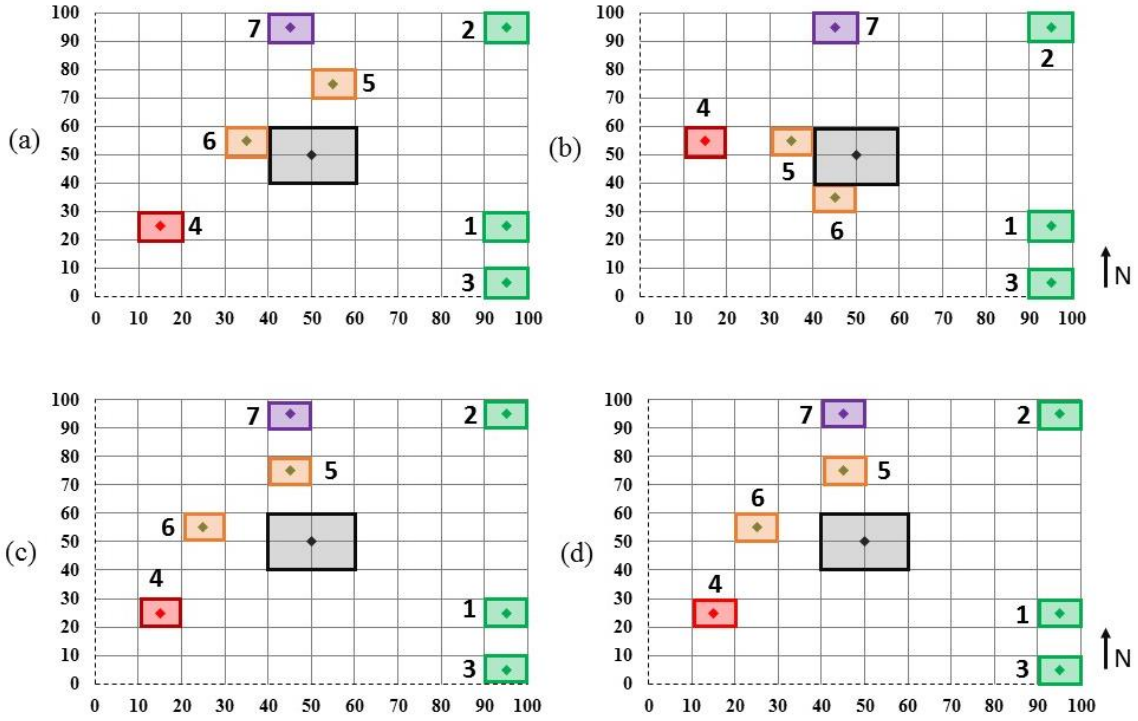

Figure 15: Resulting layouts for mean values of risk maps; each condition (a-d) corresponds to different safe distances combination

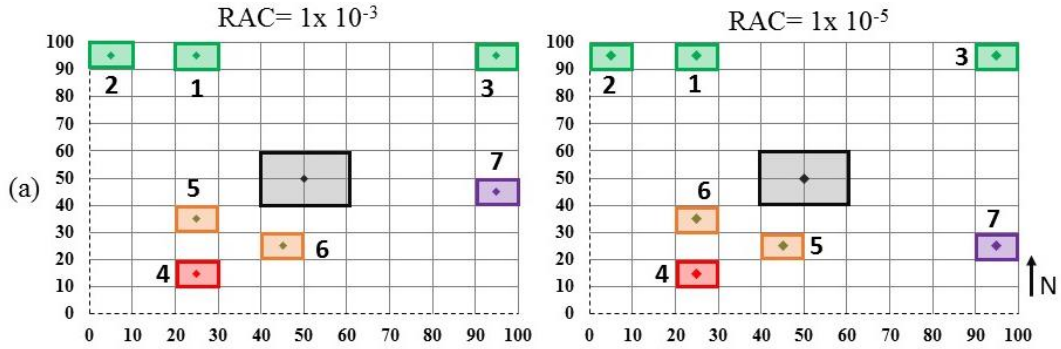

Figure 16: Resulting layouts for the 95th percentile of risk values; each condition (a-d) corresponds to different safe distances combination

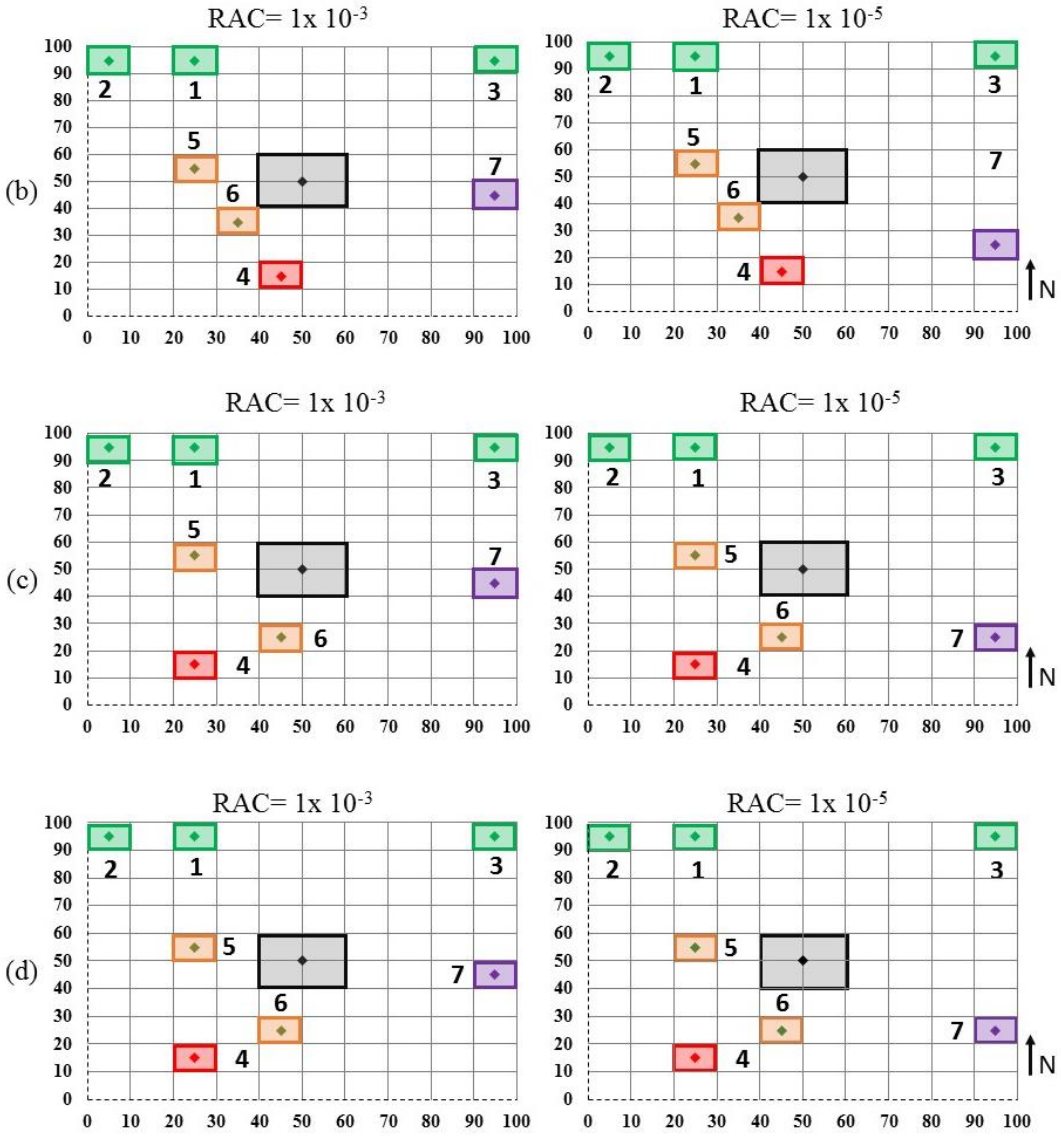

Figure 16: Continued

In the final results, the distillation unit is fixed in the middle point (50, 50) while all the others have their location changed according to the condition applied. Even though several layout options were obtained, there is a trend towards placing the equipment by its

type. For example, high occupancy buildings (units #1, #2 and #3) are fixed in regions with low wind probabilities and, consequently, lower risks. Units #2 and #3 are the most distant from distillation module due to their high number of occupants. Moreover, small storage tanks are in general placed nearby the distillation module and protective devices are necessary to avoid escalation. The largest tank is placed in opposite direction of occupied buildings to respect the minimal safe distance. Finally, unit 7 is positioned close to the facility border and, in case of mean risk values, its final location is invariant. Nevertheless, for the case of 95^{th} percentile, unit 7 assumes two distinct locations according to the RAC; smaller criteria values increase the distance between unit 7 and the central module.

In terms of total costs, mitigation systems are the major contributor factor followed by fatality costs and interconnection costs (see Figures 17 and 18). Potential economic losses due to structural damage have an insignificant affect and it does not influence layout decisions for this particular case. As expected, 95^{th} percentile ranges have a greater impact in fatality costs once the risks are relatively higher than mean values. Moreover, a slight increase in the total cost can be observed as RAC is changed from 10^{-3} to 10^{-5} per year. This is attributed to the longer distant between unit 7 and central module which increases interconnection cost. Finally, condition (a) presented the lowest result for both risk maps while no significant difference was observed between conditions b, c and d. This is consequence of the major contribution of protective device costs. Since there is no space available to allocate all storages tanks (units #4, #5 and #6) in a way that inherently safe distances are respected, mitigation systems are required to protect them from escalation

vectors. For example, each resulting layout requires that all storage tanks must be equipped with blast walls to prevent escalation from overpressure. In addition, with the exception of condition (a) in which only one small tank should be protected by fire insulation, fire walls must be in place for every tank to prevent fire impingement. In cases where bigger facility areas are available, mitigation systems cost might not play a major role and a large variability is expect in the total layout cost as different conditions are applied.

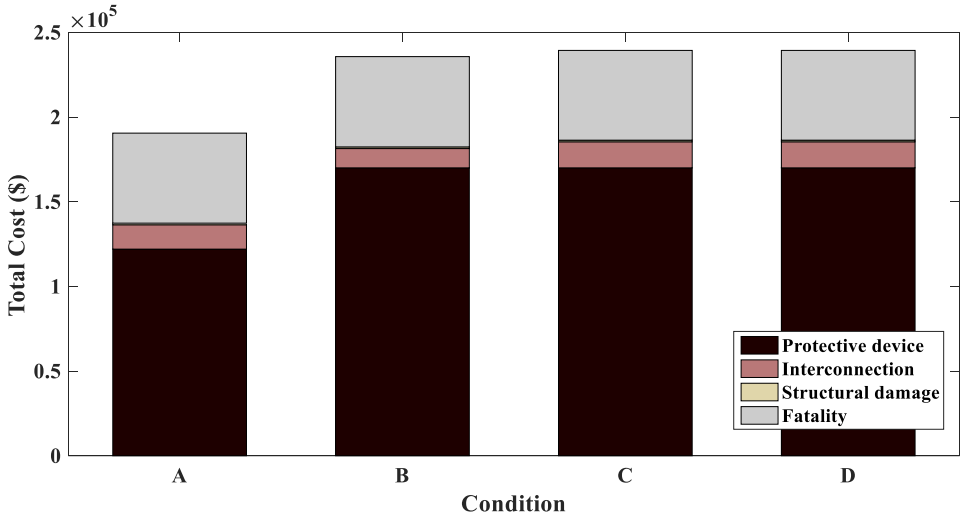

Figure 17: Costs contributions for total layout cost applying mean risk values

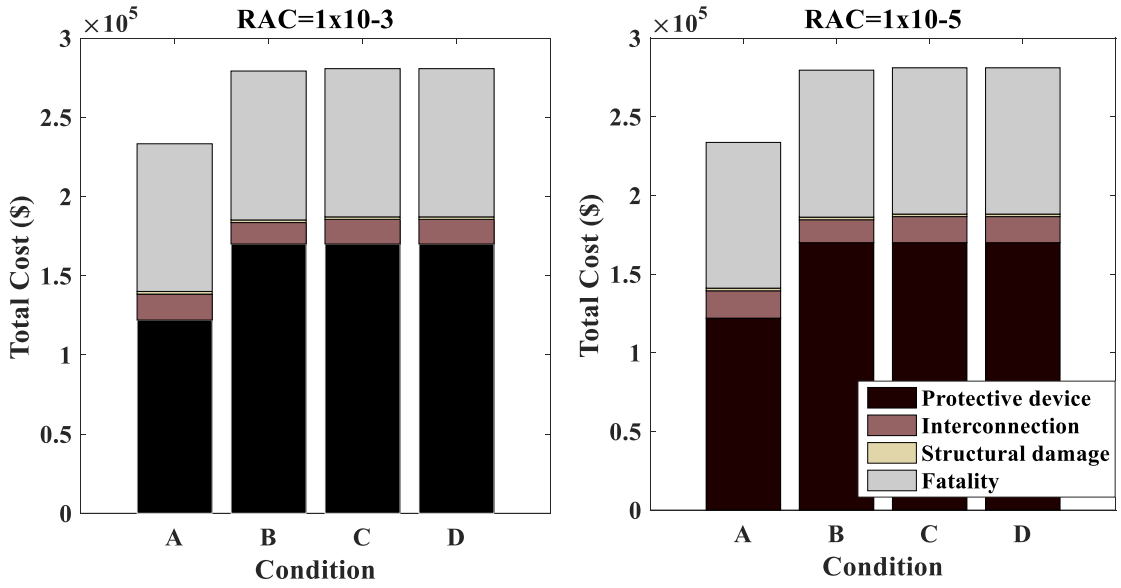

Figure 18: Costs contributions for total layout cost applying the 95th percentile risk values

Figure 19 summarizes the results obtained from both risk maps. Although inhabited buildings, highlighted in green, are located in distinct regions (north direction for the 95th percentile and east direction for the mean values) the distances between each facility and the main hazardous unit remained constant. This is also observed for the larger tank (in red) and the utility (in purple). Nevertheless, small storage tanks were placed closer to the distillation unit when mean values of risk are used.

Figure 19 also shows the result obtained from Jung *et al.* [9]. In this case, following the same pattern as shown previously, occupied buildings and the utility were placed in low-risk regions. However, a major different is observed in the rearrangement of storage tanks. Because the risk of domino effect was not considered in the first place [9], all storage tanks were located in the surroundings of the distillation unit. Contrarily,

in the proposed methodology, the concept of inherently safe distances was introduced during layout optimization and a minimal separation must be maintained between process equipment.

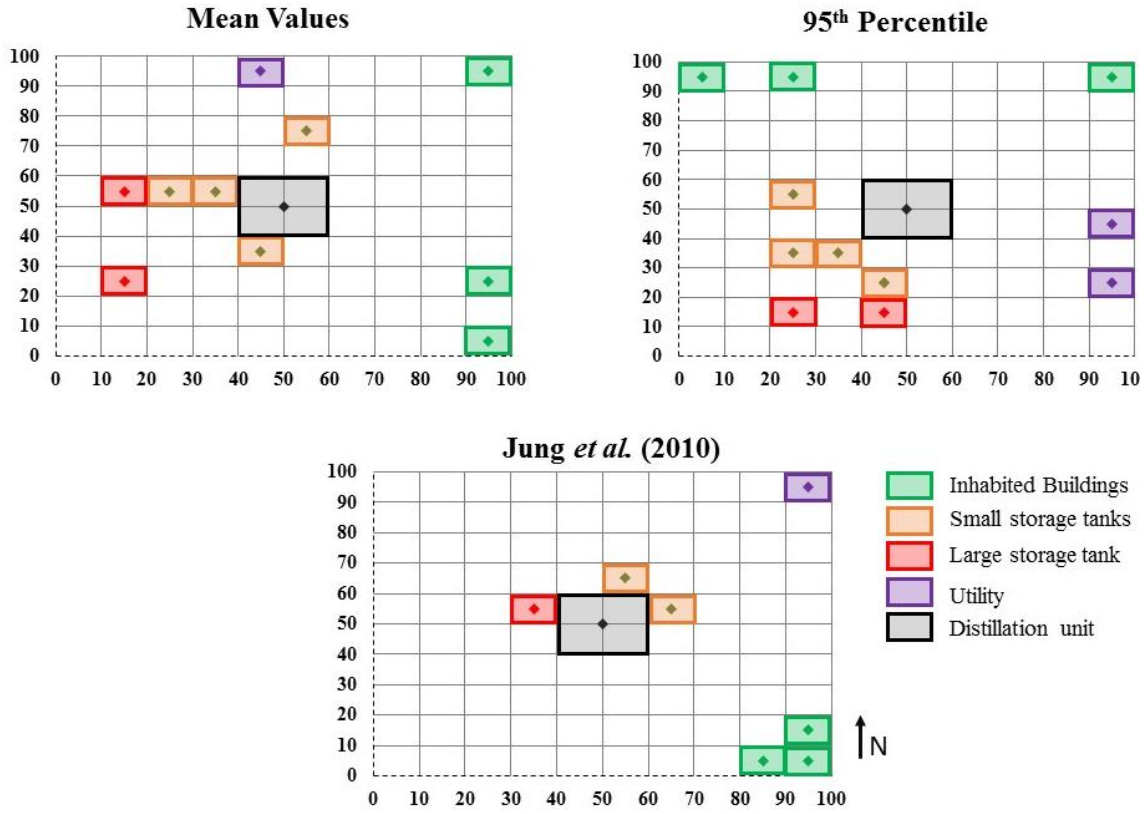

Figure 19: Comparison between the result from Jung et al. (2010) and the proposed methodology

Finally, all problems were solved with a personal computer with an Intel core i5 processor 2.20 GHz. The MILP model for this case involved 1704 binary variables, 200

continuous variables, 3258 constraints, and the solution time was on average 60s, which is relatively a short period.

7. CONCLUSIONS AND FUTURE WORK

7.1 Conclusions

Facility siting and layout configuration are critical factors during design and expansion of any industrial installation. Even though there are several reported studies incorporating safety into the layout optimization, there is still a need for a method that combines layout reformulation and a detailed risk assessment including uncertainties.

In this work, a risk-based layout optimization tool has been developed to support decision-making process during the design phase by providing safer layout options that are also cost-efficient. In the first stage, empirical models for fire and explosion scenarios as well as toxic chemical releases were implemented in Matlab and coupled with Monte Carlo technique to generate risk maps and risk distributions at a particular point of interest. Then, domino effect concepts were introduced into the resulted program to generate minimal separation distances between process units to avoid escalation events. Finally, a MILP formulation is performed to account individual risk acceptance criteria and additional safety features. A grid-based approach was chosen to maintain the linearity of the system.

The main benefit of the proposed methodology is the flexibility given to the user during the layout arrangement. This flexibility is expressed not just in terms of site-specific data but also when it comes to risk acceptance criteria, which is a reflex of the company's safety culture. Other features included in the proposed method are listed as follows:

- The program built in Matlab has an interface with excel spreadsheet, which allows the user to input easily all parameters required to perform risk analysis for a particular processing unit. If a facility has multiple modules, this analysis is carried out for each module separately and then combined;
- The Matlab code can be modified to include extras hazardous scenarios that were not addressed such as dust explosion and criogenic hazards;
- Once the program is running, several risk maps are generated regarding the mean values, maximum values and 95^{th} percentile of the risk. It is role of the user decide wich one better fits the purpose;
- In respect to minimal separation distances, graphics are generated relating the frequency of secondary events with distances from the studied module; then the user should select the distance based on his/her risk criterion;
- Finally, additional constraints were included into the layout optimization code to overcome the problematic when the facility may occupy more than one grid. Moreover, resulting layouts indicate when mitigation systems are required to prevent domino effect.

The applicability of the proposed model was demonstrated through a distillation unit that processes hexane and heptane. Several risk maps were obtained, and overall risk values ranged from $1x10^{-15}$ to $1x10^{-4}$ per year at particular points, representing a considerable variability. To study the layout arrangement, a sensitivity analysis was performed varying risk values, safe distances, and risk acceptance criteria. Even though

several layout options were generated, a trend was observed towards placing the equipment by its type; high occupancy buildings were placed in regions with low wind probabilities and, consequently, lower risks while storage tanks were located nearby the distillation module requiring protective devices to avoid escalation events. In conclusion, the authors believed this risk-based layout optimization tool has a great potential for real-world application; its simple interface combined with the low computational work required facilitate its usage.

7.2 Future Work

Based on the limitations and challenges faced during the execution of this study, there are some areas of improvement that should be explored in the future:

- Even though the Britter and McQuaid model give reasonable results in a relatively short time, a more detailed dense gas dispersion model should be applied to account for air and conservation equations (mass and energy). It would approach more realistic results;
- Results obtained from the program should be validated by available software and large-scale test data;
- In terms of domino effect, this methodology can be combined with the one proposed by Bernechea [27] to conduct a complete risk assessment including the probability of secondary and tertiary events. Additionally, reliability data should be added in the QRA program to predict the ability of protective devices to prevent initiating events. It will enhance the understanding of overall risks.

- Finally, geographic information systems can be coupled with layout optimization technique to focus on reduction of risks to the general public, which would help the decision-making process during land use planning.

REFERENCES

1. AIChE, *Guidelines for facility siting and layout: Center for Chemical Process Safety of the AIChE (CCPS/AIChE), New York, NY*. 2003, Elsevier.

2. Baker, J., et al., *The Report of the BP US Refineries Independent Safety Review Panel*. 2007: CBS.

3. American Petroleum Institute, *Management of Hazards Associated with Location of Process Plant Portable Buildings*. 2007, API Publishing Services: Washington, D.C. .

4. Argo, T. and E. Sandstrom. *Separation Distances in NFPA Codes and Standards*. 2014 [cited 2016 Jan]; Available from: http://www.nfpa.org/Assets/files/AboutTheCodes/59A/RFSeparationDistancesNFPACodesAndStandards.pdf.

5. Vorderbrueggen, J.B., *Imperial sugar refinery combustible dust explosion investigation.* Process Safety Progress, 2011. **30**(1): p. 66-81.

6. Prophet, N., *The benefits of a risk-based approach to facility siting.* Process Safety Progress, 2012. **31**(4): p. 377-380.

7. Jung, S., et al., *New approach to optimizing the facility siting and layout for fire and explosion scenarios.* Industrial & Engineering Chemistry Research, 2011. **50**(7): p. 3928-3937.

8. Dechy, N., et al., *First lessons of the Toulouse ammonium nitrate disaster, 21st September 2001, AZF plant, France.* Journal of Hazardous Materials, 2004. **111**(1): p. 131-138.

9. Jung, S., et al., *A new approach for facility siting using mapping risks on a plant grid area and optimization.* Journal of Loss Prevention in the Process Industries, 2010. **23**(6): p. 824-830.

10. Bowonder, B., *The Bhopal accident.* Technological Forecasting and Social Change, 1987. **32**(2): p. 169-182.

11. Umberto Fortunati, C., *The Seveso accident.* Chemosphere, 1985. **14**(6–7): p. 729-737.

12. Mannan, M.S., H.H. West, and P.C. Berwanger, *Lessons learned from recent incidents: Facility siting, atmospheric venting, and operator information systems.* Journal of Loss Prevention in the Process Industries, 2007. **20**: p. 644-650.

13. Dweck, J., S. Boutillon, and S. Asbill, *Deadly LNG incident holds key lessons for developers, regulators.* Pipeline and Gas Journal 2004. **176**: p. 39-42.

14. Wellman, G.W., et al., *Guidance on risk analysis and safety implications of a large liquefied natural gas (LNG) spill over water*. 2004, Sandia National Laboratories: Albuquerque, NM. p. Medium: ED; Size: [167] p.

15. Dole, E. and G.F. Scannell, *Phillips 66 Company Houston Chemical Complex Explosion and Fire: A Report to the President*. 1990, Occupational Safety and Health Administration.

16. Center for Chemical Process Safety, *Building Siting Evaluation Criteria*, in *Guidelines for Evaluating Process Plant Buildings for External Explosions, Fires, and Toxic Releases*. 2012, John Wiley & Sons, Inc.: Hoboken, NJ. p. 45-69.

17. Vinnem, J.-E., *Offshore risk assessment: principles, modelling and applications of QRA studies*. 2013, London: Springer Science & Business Media.

18. Georgiadis, M.C. and S. Macchietto, *Layout of process plants: A novel approach.* Computers & Chemical Engineering, 1997. **21, Supplement**: p. S337-S342.

19. Patsiatzis, D.I., G. Knight, and L.G. Papageorgiou, *An MILP approach to safe process plant layout.* Chemical Engineering Research and Design, 2004. **82**(5): p. 579-586.

20. Penteado, F.D. and A.R. Ciric, *An MINLP Approach for Safe Process Plant Layout.* Industrial & Engineering Chemistry Research, 1996. **35**(4): p. 1354-1361.

21. Vázquez-Román, R., et al., *Optimal facility layout under toxic release in process facilities: A stochastic approach.* Computers & Chemical Engineering, 2010. **34**(1): p. 122-133.

22. Díaz-Ovalle, C., et al., *A model to optimize facility layouts with toxic releases and mitigation systems.* Computers & Chemical Engineering, 2013. **56**: p. 218-227.

23. Medina-Herrera, N., A. Jiménez-Gutiérrez, and I.E. Grossmann, *A mathematical programming model for optimal layout considering quantitative risk analysis.* Computers & Chemical Engineering, 2014. **68**: p. 165-181.

24. Han, K., S. Cho, and E.S. Yoon, *Optimal layout of a chemical process plant to minimize the risk to humans.* Procedia Computer Science, 2013. **22**: p. 1146-1155.

25. López-Molina, A., et al., *An approach for domino effect reduction based on optimal layouts.* Journal of Loss Prevention in the Process Industries, 2013. **26**(5): p. 887-894.

26. Alileche, N., et al., *Thresholds for domino effects and safety distances in the process industry: A review of approaches and regulations.* Reliability Engineering & System Safety, 2015. **143**: p. 74-84.

27. Bernechea, E.J. and J. Arnaldos, *Optimizing the design of storage facilities through the application of ISD and QRA.* Process Safety and Environmental Protection, 2014. **92**(6): p. 598-615.

28. Alghamdi, S., *Developmental of a vapor cloud explosion risk analysis tool using exceedance methodology*, 2011. Texas A&M University: College Station, TX.

29. Ramírez-Marengo, C., et al., *A stochastic approach for risk analysis in vapor cloud explosion.* Journal of Loss Prevention in the Process Industries, 2015. **35**: p. 249-256.

30. Center for Chemical Process Safety, *Guidelines for Chemical Process Quantitative Risk Analysis*. Center for Chemical Process Safety/AIChE: New York, NY.

31. Crowl, D.A. and J.F. Louvar, *Chemical process safety : fundamentals with applications*. 3rd ed. ed. Prentice Hall international series in the physical and chemical engineering sciences. 2011, Upper Saddle River, NJ: Prentice Hall.

32. TNO Yellow Book, *Methods for Calculation of Physical Effects due to Releases of Hazardous Materials.* Gevaarlijke Stoffen, Netherland, 2005.

33. Jung, S., *Facility siting and layout optimization based on process safety* in *Chemical Engineering*. 2011, Texas A&M University: College Station, TX.

34. International Association of Oil & Gas Producers, *Consequence Modeling* in *Risk Assessment Data Directory*. 2010, OGP: OGP. p. 40.

35. Woodward, J.L., *Estimating the Flammable Mass of a Vapor Cloud*. 1998, New York, NY: Center for Chemical Process Safety/AIChE.

36. Mannan, S. and F.P. Lees, *Lees' loss prevention in the process industries : hazard identification, assessment, and control*. 3rd ed. ed. 2005, Boston, MA: Elsevier.

37. Moosemiller, M., *Development of algorithms for predicting ignition probabilities and explosion frequencies.* Journal of Loss Prevention in the Process Industries, 2011. **24**(3): p. 259-265.

38. American Institute of Chemical Engineers and Center for Chemical Process Safety, *Guidelines for vapor cloud explosion, pressure vessel burst, BLEVE, and flash fire hazards*. 2nd ed. ed. CCPS concept book. 2010, Hoboken, NJ: Wiley.

39. Díaz Alonso, F., et al., *Characteristic overpressure–impulse–distance curves for the detonation of explosives, pyrotechnics or unstable substances.* Journal of Loss Prevention in the Process Industries, 2006. **19**(6): p. 724-728.

40. Kinsella, K.G., *A rapid assessment methodology for the prediction of vapour cloud explosion overpressure*, in *International Conference and Exhibition on Safety, Health, and Loss Prevention in the Oil, Chemical, and Process Industries*. 1993: Singapore.

41. Rew, P., H. Spencer, and T. Maddison. *The sensitivity of risk assessment of flash fire events to modelling assumptions*. in *Institution of Chemical Engineers Symposium Series*. 1999. Hemspehre Publishing Corporation

42. Abbasi, T. and S.A. Abbasi, *The boiling liquid expanding vapour explosion (BLEVE): Mechanism, consequence assessment, management.* Journal of Hazardous Materials, 2007. **141**(3): p. 489-519.

43. Planas-Cuchi, E., J.M. Salla, and J. Casal, *Calculating overpressure from BLEVE explosions.* Journal of Loss Prevention in the Process Industries, 2004. **17**(6): p. 431-436.

44. Pula, R., et al., *Revised fire consequence models for offshore quantitative risk assessment.* Journal of Loss Prevention in the Process Industries, 2005. **18**(4): p. 443-454.

45. Casal, J., et al., *Jet fires: a "minor" fire hazard.* Chemical Engineering Transactions, 2012. **26**: p. 13-20.

46. International Association of Oil and Gas Producers, *Risk Assessment Data Directory, Process Release Frequencies*. 2010, OGP.

47. Health and Safety Executive, *Failure Rate and Event Data use within Risk Assessments*. 2012, HSE p. 96.

48. Khan, F.I. and S.A. Abbasi, *DOMIFFECT (DOMIno eFFECT): User-friendly software for domino effect analysis.* Environmental Modelling & Software, 1998. **13**(2): p. 163-177.

49. Rad, A., et al., *FREEDOM II: An improved methodology to assess domino effect frequency using simulation techniques.* Process Safety and Environmental Protection, 2014. **92**(6): p. 714-722.

50. Cozzani, V., et al., *The assessment of risk caused by domino effect in quantitative area risk analysis.* Journal of Hazardous Materials, 2005. **127**(1–3): p. 14-30.

51. Necci, A., et al., *Assessment of domino effect: State of the art and research Needs.* Reliability Engineering & System Safety, 2015. **143**: p. 3-18.

52. Cozzani, V., G. Gubinelli, and E. Salzano, *Escalation thresholds in the assessment of domino accidental events.* Journal of Hazardous Materials, 2006. **129**(1–3): p. 1-21.

53. Cozzani, V., A. Tugnoli, and E. Salzano, *The development of an inherent safety approach to the prevention of domino accidents.* Accident Analysis & Prevention, 2009. **41**(6): p. 1216-1227.

54. Rojas, E.J.B., *Design optimization of storage terminals through the application of QRA,* 2013. Universitat Politècnica de Catalunya.

55. Özyurt, D.B. and M.J. Realff, *Geographic and process information for chemical plant layout problems.* AIChE journal, 1999. **45**(10): p. 2161-2174.

56. Health and Safety Executive, *Reducing Risk, Protecting People*, in *Discussion Document. HSE DDE11 C*. 2001, HSE. p. 5.

57. Mine Safety and Health Administration. *Cost of Accidents* 1998 [cited 2016; Available from: http://arlweb.msha.gov/s&hinfo/costgenerator/costgenerator.htm.

58. de Lira-Flores, J., et al., *A MINLP approach for layout designs based on the domino hazard index.* Journal of Loss Prevention in the Process Industries, 2014. **30**: p. 219-227.

APPENDIX A

COEFFICIENTS FOR TNO MULTI-ENERGY METHOD CURVES

A-1: Values for parameters c and b to estimate scaled overpressure [39]

Explosion level	Scaled distance	c	b	Scaled distance	B	d
1	$0.23 \leq R < 0.6$	0.01	0	$0.6 \leq R \leq 7$	$6.40 \times 10{-}3$	−0.97
2	$0.23 \leq R < 0.7$	2.00×10^{-2}	0	$0.7 \leq R \leq 12$	$1.32 \times 10{-}2$	−0.98
3	$0.23 \leq R < 0.6$	5.00×10^{-2}	0	$0.6 \leq R \leq 30$	$6.05 \times 10{-}2$	−0.99
4	$0.23 \leq R < 0.5$	1.00×10^{-1}	0	$0.5 \leq R \leq 70$	$6.44 \times 10{-}2$	−0.99
5	$0.23 \leq R < 0.6$	2.00×10^{-1}	0	$0.6 \leq R \leq 90$	$1.17 \times 10{-}1$	−0.99
6	$0.23 \leq R < 0.6$	5.00×10^{-1}	0	$0.6 \leq R \leq 100$	$3.01 \times 10{-}1$	−1.11
7	$0.23 \leq R < 0.5$	1.00	0	$0.5 \leq R \leq 100$	$4.06 \times 10{-}1$	−1.20
8	$0.23 \leq R < 0.5$	2.00	0	$0.5 \leq R < 1$	$4.76 \times 10{-}1$	−2.08
	$1 \leq R < 2$	4.67×10^{-1}	−1.58	$2 \leq R \leq 100$	$3.18 \times 10{-}1$	−1.13
9	$0.23 \leq R < 0.35$	5.00	0	$0.35 \leq R < 1$	$4.87 \times 10{-}1$	−2.03
	$1 \leq R < 2$	4.67×10^{-1}	−1.58	$2 \leq R \leq 100$	$3.18 \times 10{-}1$	−1.13
10	$0.23 \leq R < 1$	4.41×10^{-1}	−2.39	$1 \leq R < 2$	$4.67 \times 10{-}1$	−1.58
	$2 \leq R \leq 100$	3.18×10^{-1}	−1.13			

A-2: Values for parameters c and b to estimate impulse [39]

Explosion level	Scaled distance	c	d	Scaled distance	c	d
1	$0.23 \leq R < 0.6$	4.41×10^{-2}	−0.20	$0.6 \leq R \leq 7$	2.96×10^{-2}	−0.94
2	$0.23 \leq R < 0.7$	5.22×10^{-2}	−0.27	$0.7 \leq R \leq 12$	4.03×10^{-2}	−1.05
3	$0.23 \leq R < 0.6$	8.74×10^{-2}	−0.20	$0.6 \leq R \leq 30$	6.05×10^{-2}	−0.99
4	$0.23 \leq R < 0.5$	1.4×10^{-1}	0	$0.5 \leq R \leq 70$	6.77×10^{-2}	−0.97
5	$0.23 \leq R < 0.6$	1.25×10^{-1}	−0.26	$0.6 \leq R \leq 90$	8.46×10^{-2}	−1.00
6	$0.23 \leq R < 0.8$	1.28×10^{-1}	−0.45	$0.8 \leq R \leq 100$	1.14×10^{-1}	−1.03
7	$0.23 \leq R < 0.6$	1.98×10^{-1}	−0.49	$0.6 \leq R \leq 100$	1.14×10^{-1}	−1. 03
8	$0.23 \leq R < 0.6$	1.66×10^{-1}	−0.90	$0.6 \leq R \leq 100$	1.14×10^{-1}	−1. 03
9	$0.23 \leq R < 0.3$	1.11	0.89	$0.3 \leq R < 0.4$	3.08×10^{-1}	−1.08
	$0.4 \leq R < 0.8$	8.08×10^{-2}	−2.26	$0.8 \leq R \leq 100$	1.14×10^{-1}	−1.03
10	$0.23 \leq R < 0.3$	10.82	1.14	$0.3 \leq R < 0.4$	3.15×10^{-1}	−1.79
	$0.4 \leq R < 0.5$	1.30×10^{-3}	−7.52	$0.5 \leq R \leq 100$	1.14×10^{-1}	−1.03

Data obtained from: Díaz Alonso, F., et al., *Characteristic overpressure–impulse–distance curves for the detonation of explosives, pyrotechnics or unstable substances.* Journal of Loss Prevention in the Process Industries, 2006. **19**(6): p. 724-728.

APPENDIX B

FAILURE DATA

Hole diameter range (mm)	**Centrifugal pump**	**Process vessel**	**Heat exchanger**	**Valve (0.150m ID)**	**Steel pipe (0.10m ID)**	**Steel pipe (0.15m ID)**	**Steel pipe (0.50m ID)**
1 to 3	3.4E-03	3.9E-04	1.2E-03	3.1E-05	2.0E-06[b]	2.6E-05	2.3E-05
3 to 10	1.0E-03	2.0E-04	4.1E-04	1.2E-06	2.0E-06[b]	8.5E-06	7.5E-06
10 to 50	2.9E-04	1.0E-04	1.4E-04	4.7E-06	1.0E-06[b]	2.7E-06	2.4E-06
50 to 150	5.4E-04	2.7E-05	2.4E-05	2.4E-06	5.0E-07[b]	6.0E-07	3.6E-07
>150	-	2.4E-05	1.2E-05	-	-	-	1.6E-07
Catastrophic Failure	5.4E-04	2.4E-05	1.2E-05	2.4E-06	5.0E-07[b]	6.0E-07	1.6E-07

Data obtained from: International Association of Oil and Gas Producers, Risk Assessment Data Directory, Process release frequencies. 2010, OGP.

[b] Health and Safety Executive, Failure Rate and Event Data use within Risk Assessments. 2012, HSE p. 96.

APPENDIX C

CODE FOR THE RISK ASSESSMENT TOOL

```
%Case study, distillation column
clear all

module= xlsread('input_data.xlsx','Module_export');
failure_data=xlsread('input_data.xlsx','Failure data');
chem_data=xlsread('input_data.xlsx','data_export');
scenarios=xlsread('input_data.xlsx','consequence_modeling_export');
m_size=xlsread('input_data.xlsx','module_size');

n=10000; % number of trials

%Vectors
inst=zeros(1,n);

% Number of scenarios
ns=length(module(:,1));

% Input data
ting=180; %Ignition time
ds=[45 45 1]; %Site dimension
hg=1;
d=0:hg:2*ds(1);


% Environmental Conditions
rh=20;
spaw = 15.08;
spbw = 5514;
Ta=298; %K
rhoa=1.1477e00; %Kg/m3
T=298;% Gas constant
Pa=101.315; % Ambient pressure (kPa)
R=8.314;
stab_vector=['A' 'B' 'C' 'D' 'F'];

% Source condition
dso=[0 0 0];
trmax=600; %(s) maximum release time

%Cloud center
xc=zeros(n,1);

%% Virtual Number of leaks (nvl)
hx=m_size(4);
hy=m_size(5);
nvl=m_size(6);

if (nvl~=0)
    % Unit size
```

```
    ux=-m_size(2)/2:hx:m_size(2)/2;
    uy=-m_size(3)/2:hy:m_size(3)/2;

    % Leak point and its position [number xi yi]
    lp=zeros(length(ux)*length(uy),3);
    lp(:,1)=[1:length(ux)*length(uy)];
    for j=1:length(uy)
    lp((j-1)*length(ux)+1:j*length(ux),2)=ux;
    lp((j-1)*length(ux)+1:j*length(ux),3)=uy(j);
    end
else
    lp=zeros(1,3);
    lp(1,1)=1;
    nvl=1;
end

%% Frequency release

for j=1:n
    i2(j)=randi([1,ns]); %selection of the scenario
    %selection of hole size
    f_hole_size(j)=0;
    while f_hole_size(j)==0
      hole_size(j)=randi([2 500]);
      c=find_column(hole_size(j),failure_data(:,1));
      f_hole_size(j)=failure_data(c,module(i2(j),2)+1)*module(i2(j),3);
    end
    c=length(failure_data(:,1));
    fcat(j)=failure_data(c,module(i2(j),2)+1)*module(i2(j),3);

[mg(j),ml(j),ftype(j),MW(j)]=mass_release(i2(j),hole_size(j),module,che
m_data);
end


%% Stochastic Variables
for j=1:n
ua(j)=randi([1 6]);
tr(j)=module(i2(j),8)/(mg(j)+ml(j));
if (tr(j)>trmax)
        tr(j)=trmax;
end
stab(j)=stab_vector(randi([1,5]));
c1(j)=randi([1,8]);
h(j)=randi([0,20]); %release height
theta(j)=randi([0,8])*45;
vli(j)=randi([1,nvl]); %leak position
end

%Coordinates N:270 E:0 S:90 W:180

theta= randsample([0:7],n,true,[0.1 0.1 0.15 0.2 0.15 0.1 0.1 0.1])*45;
```

```
%% Continuous Release

[Pe1,Psd1,Pvce_I,Pjf]=continuous(mg(1),ml(1),d,ua(1),i2(1),stab(1),ting
,hole_size(1),tr(1),ds,module(i2(1),8),c1(1),h(1),hg,module,chem_data);
l=imrotate(Pe1,45);
Pe=zeros(length(l),length(l),n);
Psd=zeros(length(l),length(l),n);

pos=-hg*(round(length(l)/2)-1):hg:(round(length(l)/2)-1)*hg;


d=0:hg:2*ds(1);


for j=1:n
if (f_hole_size(j)~=fcat(j))
    ting=randi([9 18])*10;

[Pjf,Pff,Pvce_fat,Pvce_sd,Psd_pf,P_pf]=continuous(mg(j),ml(j),d,ua(j),i
2(j),stab(j),ting,hole_size(j),tr(j),ds,module(i2(j),8),c1(j),h(j),hg,m
odule,chem_data);

    %% Leak position
    xi=find(pos==lp(vli(j),2),1);
    yi=find(pos==lp(vli(j),3),1);

    %% Jef Fire
    JF=myinsertMatrix(Pe(:,:,j),Pjf/6,xi,yi)*scenarios(2,2);
    %% Flash Fire
    FF1=imrotate(Pff,theta(j));
    FF2=myinsertMatrix(Pe(:,:,j),FF1,xi,yi)*scenarios(3,2);

    %% VCE
    % fatalities
    VCE_fat1=imrotate(Pvce_fat,theta(j));
    VCE_fat2=myinsertMatrix(Pe(:,:,j),VCE_fat1,xi,yi)*scenarios(4,2);

    % Structural Damage
    VCE_sd1=imrotate(Pvce_sd,theta(j));
    VCE_sd2=myinsertMatrix(Pe(:,:,j),VCE_sd1,xi,yi)*scenarios(4,2);
    VCE_sd3=insertMatrix(Pe(:,:,j),VCE_sd1)*scenarios(4,2);

    %% Pool Fire
    %center position
    [Q,P]=size(Pe(:,:,j));
    xi=round(Q/2);
    yi=round(Q/2);

    % fatalities
    PF_fat=insertMatrix(Pe(:,:,j),P_pf)*scenarios(5,2);
```

```
    % Structural Damage
    PF_sd=insertMatrix(Pe(:,:,j),Psd_pf)*scenarios(5,2);

    %% Total Pobability
    % Fatalities
    Pe(:,:,j)=(1-(1-JF).*(1-FF2).*(1-VCE_fat2).*(1-
PF_fat)).*f_hole_size(j);
    Pe(:,:,j)=preve_nan(Pe(:,:,j));
    % Structural Damage
    Psd(:,:,j)=(1-(1-JF).*(1-FF2).*(1-VCE_sd2).*(1-
PF_sd))*f_hole_size(j);
    Psd(:,:,j)=preve_nan(Psd(:,:,j));



%% Clear
    clear JF FF2 VCE_sd2 VCE_sd1 VCE_fat2 VCE_fat1 PF_fat PF_sd FF1
end
end



%% CATASTROPHIC SCENARIO

mliq=scenarios(2,4);
mvapor=scenarios(1,4);

for j=1:n
if (f_hole_size(j)==fcat(j))
    ting=randi([9 18])*10;

[Pbleve_sd,Pvce_sd,Pbleve_fat,Pvce_fat,Pff,P_pf,Psd_pf]=catastrophic(mv
apor,mliq,d,ua(j),i2(j),stab(j),ting,hg,module,chem_data,scenarios);
%% Leak position
    xi=find(pos==lp(vli(j),2),1);
    yi=find(pos==lp(vli(j),3),1);

    %% BLEVE
    BLEVE_sd=insertMatrix(Psd(:,:,j),Pbleve_sd);
    BLEVE_fat=insertMatrix(Psd(:,:,j),Pbleve_fat);

    %% VCE
    % fatalities
    VCE_fat1=imrotate(Pvce_fat,theta(j))*scenarios(4,2);
    VCE_fat2=myinsertMatrix(Pe(:,:,j),VCE_fat1,xi,yi)*scenarios(4,2);

    % Structural Damage
    VCE_sd1=imrotate(Pvce_sd,theta(j))*scenarios(4,2);
    VCE_sd2=myinsertMatrix(Pe(:,:,j),VCE_sd1,xi,yi);

    %% Pool Fire
    % fatalities
```

```
    PF_fat=insertMatrix(Pe(:,:,j),P_pf)*scenarios(5,2);

    % Structural Damage
    PF_sd=insertMatrix(Pe(:,:,j),Psd_pf)*scenarios(5,2);

    %% Flash Fire
    FF1=imrotate(Pff,theta(j))*scenarios(3,2);
    FF2=myinsertMatrix(Pe(:,:,j),FF1,xi,yi)*scenarios(3,2);

    % Fatalities
Pe(:,:,j)=Pe(:,:,j) + (1-(1-BLEVE_fat).*(1-FF2).*(1-VCE_fat2).*(1-
PF_fat)).*fcat(i2(j));
    Pe(:,:,j)=preve_nan(Pe(:,:,j));
    % Structural Damage
    Psd(:,:,j)=Psd(:,:,j)+ (1-(1-BLEVE_sd).*(1-PF_sd).*(1-
VCE_sd2)).*fcat(i2(j));
    Psd(:,:,j)=preve_nan(Psd(:,:,j));
    %% Clear
    clear BLEVE_fat BLEVE_sd  FF1 FF2 VCE_sd2 VCE_sd1 VCE_fat2 VCE_fat1
PF_fat PF_sd
end
end

%% Statistical Analysis

save data.mat Pe Psd ds hg -v7.3

index=find(d==ds(1),1);
index2=round(length(Pe(:,:,1))/2)-index;
index3=round(length(Pe(:,:,1))/2)+index;

x=-ds(1):hg:ds(1);

for i=1:length(x);
for  j=1:length(x)
    Pemax(i,j)=max(Pe(i+index2-1,j+index2-1,:));
    Pemin(i,j)=min(Pe(i+index2-1,j+index2-1,:));
    Pemean(i,j)=mean(Pe(i+index2-1,j+index2-1,:));

    if (Pemean(i,j)==NaN)
        Pemean=Pemean(i-1,j-1);
    end


    Pe5th(i,j)=prctile(Pe(i+index2-1,j+index2-1,:),5);
    Pe95th(i,j)=prctile(Pe(i+index2-1,j+index2-1,:),95);

    Psd_max(i,j)=max(Psd(i+index2-1,j+index2-1,:));
    Psd_min(i,j)=min(Psd(i+index2-1,j+index2-1,:));
    Psd_mean(i,j)=mean(Psd(i+index2-1,j+index2-1,:));
    Psd5th(i,j)=prctile(Psd(i+index2-1,j+index2-1,:),5);
    Psd95th(i,j)=prctile(Psd(i+index2-1,j+index2-1,:),95);
```

```
end
end

size(Pemax)
x=-ds(1):hg:ds(1);
[X,Y]=meshgrid(x,x);

figure
subplot(1,2,1)
loglog(x,Pemax(index,:))
hold on
loglog(x,Pemean(index,:))
loglog(x,Pemin(index,:))
loglog(x,Pe5th(index,:))
loglog(x,Pe95th(index,:))
xlabel('Distance from the unit (m)')
ylabel('Risk of fatality (per year)');
legend('Maximum','Mean','Minimum','5th percentile', '95th percentile')

legend('Maximum','Mean','Minimum','5th percentile', '95th percentile')
subplot(1,2,2)
loglog(x,Psd_max(index,:))
hold on
loglog(x,Psd_mean(index,:))
loglog(x,Psd_min(index,:))
loglog(x,Psd5th(index,:))
loglog(x,Psd95th(index,:))
xlabel('Distance from the unit (m)')
ylabel('Risk of Structural Damage (per year)');
legend('Maximum','Mean','Minimum','5th percentile', '95th percentile')
hold off

figure
subplot(3,2,1)
mesh(Pemax)
title('Maximum Fatality Risk')

subplot(3,2,2)
mesh(Psd_max)
title('Maximum Structural Damage Risk')

subplot(3,2,3)
mesh(Pemean)
title('Mean value of the Fatality Risk')

subplot(3,2,4)
mesh(Psd_mean)
title('Mean value of the Structural Damage Risk')

subplot(3,2,5)
mesh(Pe5th)
title('5th percentile of  Fatality Risk')
```

```
subplot(3,2,6)
mesh(Psd5th)
title('5th Precentile Structural Damage Risk')

hold off


%% Histogram
i10=find(pos==10,1);
i50=find(pos==50,1);
i80=find(pos==80,1);


n0=round(length(Pe(:,:,1))/2);

for j=1:n
risk10_Pe(j)=Pe(n0,i10,j);
risk10_SD(j)=Psd(n0,i10,j);
risk50_Pe(j)=Pe(n0,i50,j);
risk50_SD(j)=Psd(n0,i50,j);
risk100_Pe(j)=Pe(n0,i80,j);
risk100_SD(j)=Psd(n0,i80,j);
end


bp(1:n,1)=risk10_Pe;
bp(n+1:2*n,1)=risk50_Pe;
bp(2*n+1:3*n,1)=risk100_Pe;
bp(1:n,2)=risk10_SD;
bp(n+1:2*n,2)=risk50_SD;
bp(2*n+1:3*n,2)=risk100_Pe;


bp(1:n,3)=risk10_Pe;
bp(n+1:2*n,3)=risk50_Pe;
bp(2*n+1:3*n,3)=risk100_Pe;




a = ['x=10m';'x=50m';'x=80m']
celldata = cellstr(a)

for j=1:n
bc(j,1)=celldata(1);
bc(j+n,1)=celldata(2);
bc(j+2*n,1)=celldata(3);
end

figure
subplot(1,2,1)
title('Fatality Risk');
boxplot(bp(:,1),bc(:,1))
```

```
subplot(1,2,2)
title('Strutural Damage Risk');
boxplot(bp(:,2),bc(:,1))



%%  Exporting to Excel
    %v=export_excel(d0,d1,d,risk)
    %d0= vector the facility dimensions
    d0=[45 45];
    %d1= distance bewteen the center of each grid
    d1=10;

    vector(1,:)=export_excel(d0,d1,x,Pemax);
    vector(2,:)=export_excel(d0,d1,x,Pemin);
    vector(3,:)=export_excel(d0,d1,x,Pemean);
    vector(4,:)=export_excel(d0,d1,x,Pe5th);
    vector(5,:)=export_excel(d0,d1,x,Pe95th);

    xlswrite('results.xls',vector','Fatality Risk','B2');

    vector2(1,:)=export_excel(d0,d1,x,Psd_max);
    vector2(2,:)=export_excel(d0,d1,x,Psd_min);
    vector2(3,:)=export_excel(d0,d1,x,Psd_mean);
    vector2(4,:)=export_excel(d0,d1,x,Psd5th);
    vector2(5,:)=export_excel(d0,d1,x,Psd95th);

    xlswrite('results.xls',vector2','Structural Risk','B2');

    %Positions
    y=-d0(2):d1:d0(2);
    %X positions;
    x=-d0(1):d1:d0(1);

 for i=1:length(y)
    dt2(1,(i-1)*length(y)+1:(i)*length(y))=x;
    dt2(2,(i-1)*length(y)+1:(i)*length(y))=y(i)*ones(1,length(y));
 end
    dt2(3,:)=abs(dt2(1,:))+abs(dt2(2,:));

    xlswrite('results.xls',dt2','Distances100','B2');



%%%%%%%%%%%%%%%%%%%%%%%%%%%% Main Functions %%%%%%%%%%%%%%%%%%%%%%%%%%%%


%%%%%%%%%%%%% continuous %%%%%%%%%%
```

```
function
[Pjf,Pff,Pvce_fat,Pvce_sd,Psd_pf,P_pf]=continuous(mg,ml,d,ua,i2,stab,ti
ng,hole_size,tr,ds,mt,c1,h,hg,module,chem_data)


% Environmental Conditions
[rh,spaw,spbw,Ta,rhoa,g,Pa]=env_cond();

% Component Characteristics
[T,P,ftype,phi]=scen_type(i2,module);
[AIT,MIE,lfl,ufl,M,k,Tb,Psat,thermo_data,hc,cp,hv]=component(ftype,chem
_data,P);

%% Gas dispersion (Section 2.2)

rho=1/thermo_data(1,5);

if (rho>rhoa) % Heavy gas
    vol=mg*thermo_data(1,5);
    [v,xc,Lb]=bm_plume(vol,ua,lfl,rho,hole_size,ting);
    if(tr<0.6*xc/ua)||(tr<300)
        vol=mg*tr*thermo_data(1,5);
        [v,xc]=bm_puff(vol,ua,lfl,rho,ting);
    end
else

[mf,xc,conc,inst,sigmay,sigmaz]=gpm(mg,ua,dso,c1,h,stab,ufl,lfl,ds,ting
,tr,MW);
   mf=subplus(mf);
   v=zeros(n,1);
    if (mf>=0)

[v,iu,il]=volume_light_gas(xc,inst,conc,d,sigmay,sigmaz,h,lfl,ufl,M);
     end
   v=max(v,0);
end

%% Probability of Ignition

[Pimm_ign,Pdel_ign,Pexp]=Prob(ml+mg,tr,T,AIT,MIE,P);

%% VCE Modeling

    % Input
    %Stochastic Variable
    s=randi([1,4]); % Severity Level
    eff=randi([15,40])/100; % Efficiency

   [Psvce,Ivce]=vce(v,eff,d,s,xc,hg);

   % Probability
    Pvce_ign=(1-Pimm_ign).*(Pdel_ign).*(Pexp);
    %Death from Impact
```

```
     Y_vce=max(-46.1+4.82*log(Ivce),0);
     Pvce_I=50*(1+(Y_vce-5)./abs((Y_vce-5)).*erf(abs((Y_vce-
5)/sqrt(2))))/100*Pvce_ign;

     %Death from Overpressure
    Y_vce=max(-77.1+6.91*log(Ivce),0);
    Pvce_fat=50*(1+(Y_vce-5)./abs((Y_vce-5)).*erf(abs((Y_vce-
5)/sqrt(2))))/100*Pvce_ign;

    %Probability of fatality (Union of prob from impact and prob from
     %overpressure
    Pvce_fat=1-(1-Pvce_fat).*(1-Pvce_I);

   % Structural Damage
    Y_vce=max(-23.8 +2.92*log(Psvce),0);
    Pvce_sd=50*(1+(Y_vce-5)./abs((Y_vce-5)).*erf(abs((Y_vce-
5)/sqrt(2))))/100*Pvce_ign;


%%  Jet Fire
yjf=zeros(length(d));
thetajv=100;
dia=hole_size/1000;
[W1,W2,rl]=jetfire(mg,dia,ua,thetajv,thermo_data,T,M,k,hc);
rl=min(rl,max(d));

rl=min(rl,max(d));

% Damage radius
d1=-max(d):hg:max(d);
[X,Y]=meshgrid(d1,d1);
Pjf=max(rl^2-X.^2-Y.^2,0);
Pjf=min(Pjf,1)*Pimm_ign;


%% Flash Fire
Pff=zeros(length(d));
if (rho>rhoa) % Heavy gas
    ylfl=zeros(1,length(d));
    cont=1;
    j2=[];

    vol=mg*thermo_data(1,5);
    [v,xc,Lb]=bm_plume(vol,ua,lfl/2,rho,hole_size,ting);
    xlfl=xc*2;

    % LFL/2 Contour
    b0=hole_size/2/1000;

    for i=1:length(d)
        if (d(i)<=xlfl)
            ylfl(i)=(2*b0+8*Lb+2.5*(Lb^(1/3))*(d(i)^(2/3)))/2;
        else
```

```
            continue
        end
    end

    if(tr<2.5*xc/ua)||(tr<=300)||(Lb>=100)

        vol=mg*thermo_data(1,5)*ting
[v,xc,bt]=bm_puff(vol,ua,lfl/2,rho,ting);
        cont=cont+1;
        ylfl=real(sqrt((bt^2-(d-xc).^2)));

    end

% Probability of Death
    if (v>0)
    for k=1:length(d)
         for i=1:length(d)
           if (round(ylfl(k))>=d(i))&&(round(ylfl(k))>0)
                Pff(k,i)=1;
           end
         end
    end

    end


else

% Finding the burning zone (between xufl and xlfl/2)
      clfl=lfl*Pa*MW/Ta/R;
      cufl=ufl*Pa*MW/Ta/R;
       [cmax,imax]=max(conc(:,1));
       [cmin,imin]=min(conc(imax:length(d),1));
       imin=imin+imax-1;

       if (inst==1)
           ixufl=xc;
         % finding xlfl

         if(cmin>=clfl/2)&&(cmin<xufl)
             xlfl=d(imin);
         else
             for i=1:imax
                 if (conc(i,1)<=clfl/2)
                     xlfl1=d(i);
                 else
                     xlfl1=0;
                     continue
                 end
             end

             for i=imax:length(d)
                 if (conc(i,1)>=clfl/2)
```

```
                xlfl2=d(i);
            else
                continue
            end
        end
     end
    % Cloud radius
    rb=max(abs(xlfl1-xufl),abs(xlfl2-xufl));
    ylfl=real(sqrt((bt^2-(d-xufl).^2)));

   else
if(cmax<clfl)
    v=0;
    ixufl=1;
    ixlfl=1;
else
     % finding xufl

     if (cmax<cufl)
         ixufl=1;
         for i=1:imax
             if (conc(i,1)<=clfl/2)
                 ixufl=i;
             else
                 continue
             end
         end
      else
         for i=imax:imin
             if (conc(i,1)>=cufl)
                 ixufl=i;
             else
                 continue
             end
         end
     end

     % finding xlfl

     [cmin,imin]=min(conc(ixufl:length(d),1));
     imin=ixufl+imin-1;
     if(cmin>=clfl/2)
         ixlfl=imin;
     else

         for i=(ixufl):imin
             if (conc(i,1)>=clfl/2)
                 ixlfl=i;
             else
                 continue
             end
         end
```

```
        end

    end
       for i=ixufl:ixlfl
       ylfl(i)=round(sigmay(i).*sqrt(2*conc(i,1)./clfl*2));
       end

       %Probability of death
       if (cmax>clfl/2)

       for k=ixufl:ixlfl
         if  (round(ylfl(k)) >0)
             for i=1:round(ylfl(k))
                    Pff(k,i)=1;
             end
         end
       end
       end

   end

end

Pff_ign=(1-Pimm_ign).*(Pdel_ign).*(1-Pexp);
Pff=Pff_ign*Pff;
Pff=rot(d,0,Pff,hg);

%% Pool Fire
Ppf_ign=Pff_ign;
eff=randi([6 8])/10;
[P_pf,Psd_pf]=poolfire(ml,eff,d,hg,Tb,thermo_data,hc,cp,hv);
P_pf=P_pf*Pff_ign;
Psd_pf=Psd_pf*Pff_ign;
end

%%%%%%%%%%%%% catastrophic %%%%%%%%%%

function
[Pbleve_sd,Pvce_sd,Pbleve_fat,Pvce_fat,Pff,P_pf,Psd_pf]=catastrophic(mv
0,ml0,d,ua,i2,stab,ting,hg,module,chem_data,scenarios)
% Return the effects of a catastrophic event

% Environmental Conditions
[rh,spaw,spbw,Ta,rhoa,g,Pa]=env_cond();

% Component Characteristics
[T,P,ftype,phi]=scen_type(i2,module);
[AIT,MIE,lfl,ufl,M,k,Tb,Psat,thermo_data,hc,cp,hv]=component(ftype,chem
_data,P);

%% Flashing Liquids
    if (T>Tb)
    fv=min(2*cp*(T-Tb)/hv,1);
```

```
    % Droplets consideration (fraction = fv)
    mv=mv0+fv*ml0;
    ml=(1-fv)*ml0;
    else
    mv=mv0;
    ml=ml0;
    end
 %% Gas Dispersion
rho=1/thermo_data(1,5);
if (rho>rhoa) % Heavy gas
    vol=mv*thermo_data(1,5);
    [v,xc,bt]=bm_puff(vol,ua,lfl,rho,ting);
else

[mf,xc,c,inst,sigmay,sigmaz]=gpm_puff(q,ua,dso,c1,h,stab,ufl,lfl,ds,te,
MW);
      mf=subplus(mf);

[v,iu,il]=volume_light_gas(xc,inst,conc,d,sigmay,sigmaz,h,lfl,ufl,M);
     v=max(v,0);
end

%% Probability of Ignition

[Pimm_ign,Pdel_ign,Pexp]=Prob(ml+mv,60,T,AIT,MIE,P);

prob=[Pimm_ign,Pdel_ign,Pexp];

%% BLEVE Modeling
   if (scenarios(1,2)==1)
   % Input data
    mawp=1.10; %MPa
    po=1.2; % failure overpressure
    psv=(P+1.013)*100e3; %Pa


[delta_p,q,t,I]=BLEVE(mawp,po,ml0,mv0,psv,cp,hc,hv,thermo_data,d,hg);
    ps=delta_p*Pa*1e3;

    % Probability
    % Burn death from fireball
    V=t*q.^(4/3)*1e-04;
    Y_bleve=-14.6+2.56*log(V);
    Pbleve_fb=50*(1+(Y_bleve-5)./abs((Y_bleve-5)).*erf(abs((Y_bleve-
5)/sqrt(2))))/100*Pimm_ign;

    %Death from Impact
    Y_bleve=-46.1+4.82*log(I);
    Pbleve_I=50*(1+(Y_bleve-5)./abs((Y_bleve-5)).*erf(abs((Y_bleve-
5)/sqrt(2))))/100*Pimm_ign;

    %Death from Overpressure
    Y_bleve=-77.1+6.91*log(ps);
```

```
    Pbleve_fat=50*(1+(Y_bleve-5)./abs((Y_bleve-5)).*erf(abs((Y_bleve-
5)/sqrt(2))))/100*Pimm_ign;


%Total probability of fatalities
    Pbleve_fat=1-(1-Pbleve_I).*(1-Pbleve_fat).*(1-Pbleve_fb);

    %Structural Damage
    Y_bleve=-23.8+2.92*log(ps);
    Pbleve_sd=50*(1+(Y_bleve-5)./abs((Y_bleve-5)).*erf(abs((Y_bleve-
5)/sqrt(2))))/100*Pimm_ign;
   else
   Pbleve_sd=zeros(length(d));
   Pbleve_fat=zeros(length(d));
   end
    %% VCE Modeling
if(scenarios(4,2)==1)
    % Input
    %Stochastic Variable
    s=randi([1,4]); % Severity Level
    eff=randi([15,40])/100; % Efficiency
    [Psvce,Ivce]=vce(v,eff,d,s,xc,hg);

   % Probability
    Pvce_ign=(1-Pimm_ign).*(Pdel_ign).*(Pexp);
    %Death from Impact
    Y_vce=max(-46.1+4.82*log(Ivce),0);
    Pvce_I=50*(1+(Y_vce-5)./abs((Y_vce-5)).*erf(abs((Y_vce-
5)/sqrt(2))))/100*Pvce_ign;
    %Death from Overpressure
    Y_vce=max(-77.1+6.91*log(Psvce),0);
    Pvce_fat=50*(1+(Y_vce-5)./abs((Y_vce-5)).*erf(abs((Y_vce-
5)/sqrt(2))))/100*Pvce_ign;

    %Total probability of fatalities
    Pvce_fat=1-(1-Pvce_I).*(1-Pvce_fat);

   % Structural Damage
         Y_vce=max(-23.8 +2.92*log(Psvce),0);
         Pvce_sd=50*(1+(Y_vce-5)./abs((Y_vce-5)).*erf(abs((Y_vce-
5)/sqrt(2))))/100*Pvce_ign;
else
 Pvce_sd=zeros(length(d));
 Pvce_fat=Pvce_sd;
end

%% Flash Fire
Pff=zeros(length(d),length(d));
if (rho>rhoa) % Heavy gas
   [v,xc,bt]=bm_puff(vol,ua,lfl/2,rho,ting);
    ylfl=real(sqrt((bt^2-(d-xc).^2)));
    % Probability of Death
    if (v>0)
```

```
    for k=1:length(d)
            for i=1:length(d)
                if (round(ylfl(k))>=d(i))&&(round(ylfl(k))>0)
                Pff(k,i)=1;
                end
            end
    end
    end

else

% Finding the burning zone (between xufl and xlfl/2)
       clfl=lfl*Pa*MW/Ta/R;
       cufl=ufl*Pa*MW/Ta/R;
       [cmax,imax]=max(conc(:,1));
       [cmin,imin]=min(conc(imax:length(d),1));
       imin=imin+imax-1;
       ixufl=xc;
         % finding xlfl
         if(cmin>=clfl/2)&&(cmin<xufl)
             xlfl=d(imin);
         else
             for i=1:imax
                 if (conc(i,1,j)<=clfl/2)
                     xlfl1=d(i);
                 else
                     xlfl1=0;
                     continue
                 end
             end

             for i=imax:length(d)
                 if (conc(i,1)>=clfl/2)
                     xlfl2=d(i);
                 else
                     continue
                 end
             end
         end
        % Cloud radius
        rb=max(abs(xlfl1-xufl),abs(xlfl2-xufl));
        ylfl=real(sqrt((rb^2-(d-xufl).^2)));


 %Probability of death
     if (cmax>clfl/2)
       for k=ixufl:ixlfl
         if  (round(ylfl(k))>0)
             for i=1:round(ylfl(k))
                    Pff(k,i)=1;
             end
         end
      end
```

```
    end

 end

Pff_ign=(1-Pimm_ign).*(Pdel_ign).*(1-Pexp);
Pff=Pff*Pff_ign;
Pff=rot(d,0,Pff,hg);


%% Pool Fire
eff=randi([6 8])/10;
Ppf_ign=Pff_ign;
[P_pf,Psd_pf] =poolfire_cat(ml,eff,d,hg,Tb,thermo_data,hc,cp,hv);
P_pf=P_pf*Ppf_ign;
Psd_pf=Psd_pf*Ppf_ign;
End

%%%%%%%%%%%%% Prob %%%%%%%%%%

function [Pimm_ign,Pdel_ign,Pexp]=Prob(FR,time,T,AIT,MIE,P)
% Return the values for probabilities (immediate, delayed and
explosion)

%Unit conversion

%T = Process Temperature (F)
T=(T-273.15)*9/5 +32;
AIT=(AIT-273.15)*9/5 +32;
%P= Process pressure (psig)
P=P*14.5;
% Release Rate
FR=2.2*FR;

%% Immediate Ignition
Pai=1-5000*exp(-9.5*T/AIT);

if (T/AIT<0.9)
    Pai=0;
elseif (T/AIT>1.2)
    Pai=1;
end
Pimm_ign= Pai + 0.0024*P^(1/3)/(MIE)^(2/3);
if (Pimm_ign>1)
    Pimm_ign=1;
end

%% Delayed Ignition

% Modifiers
% Material Released
M1=min(0.6-.85*log10(MIE),3);
if (M1<=0.1)
    M1=0.1;
```

```
end

% Magnitude Of release
M2=min(7*exp(0.42*log(FR)-4.67),2);

%Duration of the release
s_vector=[0.5 0.25 0.1]; % depends on the equipment density
s=s_vector(randi([1 3]));
M3=(1-(1-s^2)*exp(-0.015*s*time))/0.3;

Mp=M1*M3*M2;

if (Mp>1)
    Pdel_ign=1-(0.7/Mp);
else
    Pdel_ign=0.3*Mp;
end

%% Delayed Ignition resulting in an explosion
Pexp=min(0.024*FR^0.435,.7);

end

%%%%%%%%%%%%% VCE %%%%%%%%%%
function [Ps,I]=vce(V,eff,d,s,xc,hg)
% Input
% V= volume of the gas cloud
% eff= efficiency (random variable 0.15-0.40)
% d=Distances from the centre of explosion
% s= Severity level
d1=-max(d):hg:max(d);
% Grid
     xc=min(xc,10);
    [X,Y]=meshgrid(d1-xc,d1);

 %Parameters
  % Hc= Heat of combustion (J/m3)
    Hc=3.6e6;
  % Atmospheric pressure(Pa)
    p0=101.315e3;
  % Sound Speed
  c0=343; %m/s

%Energy Released
E=Hc*V*eff;

%Sachs-Scale Distance
R=sqrt(X.^2+Y.^2)./(E/p0)^(1/3);

c=[0.0065 0.015 0.035 0.075 0.12 0.35];
ps1=[0.01 0.02 0.05 0.1 0.2 0.4];

Ps=c(s).*p0./R;
```

```
% Estimation of the Impulse
coeff=[-5 -5 -2.5 -4/3 -7/6 -0.6];
b0=[6 4 2.5 1.7 .95 .4];
tsf=[5 3 2 1.3 .6 0];
zf=[.5 .5 .5 .6 .6 .5];
cont=1;
ts=tsf(s)+zeros(length(R));
ts(1:cont,1:cont)=10.^(log10(b0(s))+coeff(s).*(R(1:cont,1:cont)-0.3));

if (s==6)
ts=10.^(.35+.001368.*(R-0.5));
ts(1:cont,1:cont)=10.^(log10(b0(s))+coeff(s).*(R(1:cont,1:cont)-0.3));
      for j=cont:length(d)
        if (R(1,j)<=5)
            cont1=j;
        else
          continue
        end
      end

ts(cont+1:cont1,cont+1:cont1)=10.^(log10(.28)+.015556.*(R(cont+1:cont1,
cont+1:cont1)-0.5));
    end

    ts=(E/p0)^(1/3)*ts/c0;
    I=ts.*Ps/2;

end


%%%%%%%%%%%%% Pool Fire %%%%%%%%%%
unction [prob,psd]=poolfire(m,n,d,hg,Tb,thermo_data,hc,cp,hv)

%Input parameters
% ftype=fluid type
% Hc=heat cof combustion
% Hv= heat of vaporisation
% n= fraction of combustion
% m= mass released rate
% Cp= specific heat
% Tbp = Boiling point
% rho= density
% r= Position vector
% theta-wind direction
r1=-max(d):hg:max(d);
if (m>0)
    [X,Y]=meshgrid(r1,r1);
    rho=1/thermo_data(1,4);

    % Environmental Conditions
    rh=20;
    spaw = 15.08;
```

```
spbw = 5514;
Ta=298; %K
rhoa=1.1477e00; %Kg/m3
g=9.8; %m/s2


%Vertical rate of liquid level decrease
Hmod=hv+cp*(Tb-Ta);
y=1.27*1e-6*hc/Hmod;

% Mass burning rate
mbr=rho*y;

% Pool diameter
D=sqrt(4*m/pi/mbr);

%Flame Height
H=42*D*(mbr/rhoa/sqrt(g*D))^0.61;

% Burning time
tbeq=m/mbr/(pi*(D^2)/4);
tbemp=20; %s

%Actual path length
x= sqrt(H^2/4 + sqrt(X.^2+Y.^2));

%Partial vapour pressure of water and absorption factor
rpwa = .01*rh*exp(spaw-spbw/Ta)*.133e3;

for i=1:length(x)
    for j=1:length(x)
        if(rpwa*x(i,j)>=1e4) && (rpw*x(i,j)<=1e5)
            ta=2.02/(rpwa*x(i))^0.09;
        else

        %absortion factor from figure 6.2 (linear estimation)
        aw=5.746e-2*log10(rpwa*x(i,j))-.148;
        aco=8.503e-3*log10(rpwa*x(i,j))-7.005e-3;

        %Transmissivity
        ta=1-aw-aco;
        end
        %Heat flux
        q(i,j)=ta*n*mbr*hc/16/pi/(x(i,j)./D).^2;
    end
end

% Probit function
Ypf= max(-36.38 +2.56.*log(tbemp.*q),0);
prob=50*(1 +(Ypf-5)./abs(Ypf-5).*erf(abs(Ypf-5)/sqrt(2)))/100;

% Structural Damage
psd=max(D.^2-(X-3).^2-(Y.^2),0);
```

```
    psd=min(psd,1);
else
    prob=zeros(length(r1));
    psd=prob;
end

end


%%%%%%%%%%%%% Jet Fire  %%%%%%%%%%
%Jet fire modeling (Chamberlain Model: horizontal and vertical release)
function [W1,W2,Lb0]=jetfire(m,d0,v,thetajv,thermo_data,T0,M,k,Q )
%v=wind velocity (m/s)
%d0=diameter of the role (m)
%m=mass release rate (Kg/s)
%x=equipment type
% Thermodynamic data


%% Parameter to be calculated
%ua=wind speed in the release direction
%wa=wind speed perpendicular to the release

%% Input parameters
Ta=298; %K
pa=101.3e3; %N/m2;
P0=5.013*101.3e3; %N/m2;
R=8.314; %J/mole/K
wmae=2.8835e-2; %Kg/mol;
g=9.8; %m/s



%% Calculations

rhoj=thermo_data(2,5);
wg=M/1000; %Kg/mol
%Mass fraction
W=wg/(15.816*wg+0.0395);
%Temperature of expanding jet
Tj=T0*((pa/P0)^((k-1)/k));
%Static pressure
Pc=P0*(2/(k+1))^(k/(k-1));

%Mach-Number
if (Pc>pa)
    Mj=sqrt(k+1)*sqrt(((Pc/pa)^((k-1)/k) -1)/(k-1));
else
    F=(3.6233e-5)*m*sqrt(Tj/k/wg)/(d0^2);
    Mj=sqrt(sqrt(1 +2*(k-1)*F^2 -1)/(k-1));
end

% Exit velocity of the expading jet
```

```
  u=Mj*sqrt(k*R*Tj/wg);
%Ratio of wind speed to jet velocity
  r=v/u;
% Density of air
  rhoa = wmae*pa/(R*Ta);
% Density of the gas
  rhoj= rhoj*298/Tj;

% Combustion effective source diameter
  Ds=sqrt(4*m/pi()/rhoa/u);

  if (Pc>pa)
      dj=sqrt(4*m/pi/u/rhoj);
%       rhoj=Pc*wg/R/Tj;
      Ds=dj*sqrt(rhoj/rhoa);
  end
 % Auxiliary variable Y (dimensionless)
 ca=0.024*(g*Ds/(u^2))^(1/3);
 cb=0.2;
 beta= sqrt(wmae*2250/wg/Ta);
 cc=(beta/W)^(2/3);

 % finding f
 syms y
 f=ca*y^(5/3) +cb*y^(2/3)-cc == 0;
 %Y = solve(f,y)
 % Newton-Raphson method
    x=1;
    x_old=0;
    it=1;
    while (abs(x_old-x)>1e-3)
        x_old=x;
        x=x_old-(0.2*(cb*x_old^(2/3))+ca*(x_old^(5/3))-
cc)/(2/3*x_old^(-1/3)+(ca*5/3*x_old^(2/3)));
        it=it+1;
    end
    Y=x;

 %Length of the jet flame in still air
 Lb0=Y*Ds;

 %Length of the jet flame measured from the tip of the flame to the
centre of the exit plane:
 Lb=Lb0*0.51*(exp(-0.4*u)+ 0.49)*(1 -6.07e-3*(thetajv-90));

 % Richardson Number (Ri)
 Ri=(g/(Ds^2)/(u^2))^(1/3)*Lb0;

 if (r<0.05)
     alpha=(thetajv-90)*(1-exp(-25.6*r)) +8000*r/Ri;
 else
     alpha=(thetajv-90)*(1-exp(-25.6*r)) + (134+1726*sqrt(r-0.026))/Ri;
 end
```

```
% Lift-off of the flame
if (alpha==0)
    b=0.2*Lb;
else
    if (alpha==180)
        b=0.015*Lb;
    else
       K=0.185*exp(-20*r)+0.015;
       b=Lb*sin(K*alpha)/sin(alpha);
    end
end

%Length of frustum (rl)
rl=sqrt((Lb^2)-(b^2)*(sin(alpha))^2)-b*cos(alpha);

%density ratio (pair/pj)
rrho=Tj*wmae/Ta/wg;

%Richardson number based on combustion source
Rids=(g/(Ds^2)/(u^2))^(1/3)*Ds;
C=1000*exp(-100*R)+0.8;

%frustum base width
W1=Ds*(13.5*exp(-6*r)+1.5)*(1-1-1/15*sqrt(rrho))*exp(-
70*(Rids)^(C*r));

%Frustum tip width
W2=Lb*(0.18*exp(-1.5*r)+0.31)*(1-0.47*exp(-25*r));

%Surface area of frustum (m2)
A=pi()/4*(W1^2+W2^2) +pi()/2*(W1+W2)*sqrt(rl^2+((W2-W1)/2)^2);

%Suface emissive power
Fs=0.21*exp(-0.00323*u)+0.11;
SEP=m*Q*Fs/A;


%% Horizontal release Johnson, Brightwell and Carsley Model

%Momentum flux
pj=rhoa/rrho;
G=pi()*pj*(u^2)*(dj^2)/4;
%Ds=dj*sqrt(rhoj/rhoa);
%Fiding Lb0
ca=(pi*rhoa*g/4/G)^(1/3);
cb=(2.85*Ds/W)^(2/3);
f2(y)=0.2*(y^(2/3))+0.024*ca*(y^(5/3))-cb;
%Yh=solve(f2,y,'Real',true);
x=1;
x_old=0;
it=1;
while (abs(x_old-x)>1e-3)
```

```
    x_old=x;
    x=x_old-(0.2*(x_old^(2/3))+0.024*ca*(x_old^(5/3))-
cb)/(.4/3*x_old^(-1/3)+(.024*5/3*ca*x_old^(2/3)));
    it=it+1;
end
Lb0=x;

%Richardson Number
Ri=(pi*rhoa*g/4/G)^(1/3)*Lb0;
%Mometum fluxes
    gammax=sqrt(pi*rhoa/4/G)*Lb0*v;
    %gammaz=sqrt(pi()*pa/4/G)*Lb0*wa; (neglected);

%Position of the flame
    if (Ri<5.11)
        fe=0.55*(1-0.55)*exp(-0.168*Ri);
    else
        fe=0.55+(1-0.55)*exp(-.168*Ri-0.3*(Ri-5.11)^2);
    end

    if(Ri<3)
        re=0;
    else
        re=0.82*(1-exp(-.5*(Ri-3.3)));
    end
    X=Lb0*fe*(1+re*gammax);

% y position of the flame
    he=(1+1/Ri)^(-8.78);
    ce=0.02*Ri;
    Y=Lb0*he*(1-ce*gammax);
    if (Y/Lb0>1)
        Y=Lb0;
    end
    Lbxy=sqrt(X^2+Y^2);
% Maximum Diameter
    W2=(-0.004 +0.039*Ri-gammax*(0.0094+9.5e-7*(Ri^5)))*Lbxy;

%Lift-off
    b=0.141*sqrt(G*rhoa);
%Minimum diameter of the flame
    W1= (-.18+.081*Ri)*b;
    if (W1/b<0.12)
        W1=0.12*b;
    end
    if (W2<W1)||(W2>Lbxy)
        W2=(W1+Lbxy)/2;
    end

%Z position of the flame
    %Z=(X-b)*0.178*gammaz;

%Surface area of frustum (m2)
```

```
 A=pi()/4*(W1^2+W2^2) +pi()/2*(W1+W2)*sqrt(rl^2+((W2-W1)/2)^2);

 %Suface emissive power
 Fs=0.21*exp(-0.00323*u)+0.14;
 SEP=m*Q*Fs/A;

end



%%%%%%%%%%%% BLEVE %%%%%%%%%%
BLEVE Estimation Acording to CCPS guidelines and TNT model

%% Input Data
% mawp= maximum allowable work pressure
% po= failure overpressure
% Ta= room temperature (K)
% mf= liquid mass (Kg)
% mg= gas mass (Kg)
% d= distance vector (m)
% f_type= fluid type in case of more than one chemical or mixture

% Chemical Properties of the component
% psv= operation pressure (Pa)
% hc=heat of combustion;
% cp=specific heat;
% hv=heat of vaporisation ;
% thermo_data= Thermodynamic data in both states



%% Environmental Conditions
rh=20;
spaw = 15.08;
spbw = 5514;
ta=300;

d1=-max(d):hg:max(d);
% Grid
[X,Y]=meshgrid(d1,d1);

%Step 1: Data Collection
p1=po*(mawp+0.1);

%Step 3: Calculate internal energy in expanded state, u2.
%For saturated liquid
x=(thermo_data(1,6) -thermo_data(2,6))/(thermo_data(2,7) -
thermo_data(2,6));
u2f=(1-x)*thermo_data(2,2) +x*thermo_data(2,3);
% For saturated vapor
x=(thermo_data(1,7) -thermo_data(2,7))/(thermo_data(2,7) -
thermo_data(2,6));
```

```
u2g=(x)*thermo_data(2,2) +(1-x)*thermo_data(2,3);

%Step 4: Calculate Specific work
ef= thermo_data(1,2)-u2f;
eg= thermo_data(1,3)-u2g;
beta=0.8;

%Step 5: Calculate the explosion energy
Eexf=2*ef*mf;% Saturated liquid
Eexg=2*eg*mg;% Saturated vapor
Et= Eexf+Eexg; %kJ
wtnt=beta*0.214*Et/1000; %Kg
z=sqrt(Y.^2+X.^2)/(wtnt^(1/3));
delta_p=1616*(1+(z./4.5).^2)./sqrt(1+(z./0.048).^2)./sqrt(1+(z./0.32).^
2)./sqrt(1+(z./1.35).^2);

% Finding Impulse J
cont=1;
for i=1:length(d)-2
    if(X(1,i)<=10)
        cont=cont+1;
    else
        continue
    end
end

I(:,:)=335*z.^(-1.06);
I(1:cont,1:cont)=203.*z(1:cont,1:cont).^(-0.91);
I=wtnt^(1/3)*I;




%% Fireball from TNO "yellow book"
mt=mg+mf;
% Radius of the fireball
rfb=3.24*mt^0.324; %mt=considering that all material will be relased (I
should improve that)

%Duration of the fireball
t=.852*mt^0.26; %seconds

%the lift-off height of the fireball
hb=2*rfb;

%Distance from the centre fo the fireball
Xt=sqrt(X.^2+Y.^2+hb^2);

%Maximum value of the view factor
Fv=(rfb./Xt).^2;

%Fraction of the generated heat radiated
```

```
Fs=0.00325*psv^0.32;

%Net available heat for radiation
T=1700; %k
delta_h=hc-hv-cp*T;

%Surface Emissive Power SEP
SEP=delta_h*mt*Fs/(4*pi()*(rfb^2)*t);
%Actual path length
xa=Xt-rfb;

%Partial vapour pressure of water and absorption factor
rpwa = .01*rh*exp(spaw-spbw/ta)*.133e3;

for i=1:length(xa)
    for j=1:length(xa)
        if(rpwa*xa(i,j)>=1e4) && (rpwa*xa(i,j)<=1e5)
            tau=2.02/(rpwa*xa(i,j))^0.09;
        else

        %absortion factor from figure 6.2 (linear estimation)
        aw=5.746e-2*log10(rpwa*xa(i,j))-.148;
        aco=8.503e-3*log10(rpwa*xa(i,j))-7.005e-3;

        %Transmissivity
        tau=1-aw-aco;
        end
        %Heat flux
        q(i,j)=SEP*Fv(i,j)*tau;
    end
 end
end
```